Reliability Analysis of Oil and Gas Pipelines Subjected to Dent and Corrosion Defects

By

Ahmed Abdelmoety

A thesis submitted in partial fulfillment of the requirements for the degree of

Doctor of Philosophy

in

Structural Engineering

Department of Civil and Environmental Engineering

University of Alberta

Abstract

Pipelines are considered one of the most efficient ways of transferring oil and gas from the extraction sites to refineries, and finally to consumers. However, leakage or loss of containment of pipelines in the transmitting grid can be caused by several factors such as overpressure, cracking, and corrosion defects. Goals are set to ensure the pipelines safety while managing to minimize the maintenance expenses. To achieve these goals, this thesis focuses on the reliability analysis on different aspects of the design and defect assessment of pipelines.

Assessment of reliability levels associated with the design and safety factors (DFs and SFs) by evaluating the probabilities of failure (POFs) for different pipe configurations, corrosion defects, and DF/SFs in conducted in this thesis. Two limit states are considered: yielding of intact pipes based on the Barlow's equation and failure of corroded pipes based on the RSTRENG model under internal pressure. The POFs associated with different DF/SFs are calculated and discussed; the safety levels (e.g., safety class) of pipes based on the different DF/SFs are also determined. The DFs commonly used for the yielding of intact pipes are found to be in the highest safety class. The SFs used for corroded pipes based on the RSTRENG model is also found to be in the highest safety class for long corrosion defects, but in the lowest safety class for short corrosion defects.

Dent defects can decrease the life span of oil and gas pipelines. Subsequently, this thesis performs a strain-based reliability analysis on pipe dent defects using a response surface method (RSM) and the first order reliability method (FORM). Two different limit states are used for the reliability analysis, which are the exceedance of the strain capacity of the pipe material by the maximum equivalent plastic strain (MEPS) generated in the pipe and the exceedance of the unity by the ductile strain damage generated in the dented region. The ductile strain damage in the dented region is calculated using the ductile failure damage indicator (DFDI) and strain limit damage (SLD) damage models. Different pipe configurations, pipe lengths, indenter sizes, and dent depths are considered. A suitable finite element (FE) model for the reliability analysis was developed for this study using the FE analysis software ABAQUS. The uncertainties in the pipe wall thickness, the dent depth, the yield strength of the pipe material, and the strain capacity are considered for the reliability analysis. The POFs of several dent defects were calculated. For the strain capacity limit state, it has been found that the POF, which is highly related to the nominal value of the MEPSs generated in the dent defect, is not only related to the indentation depth or the size of the indenter. Thus, the dent depth criterion used in the engineering practice can lead to inconsistent reliability levels in dented pipes. For the ductile strain damage limit state, The SLD and DFDI damage model-based POF were also found to increase with the increase of the dent depth and the decrease of the indenter size. Also, the SLD and DFDI strain damage criterion are found to be more sensitive to the change of indentation depth and the indenter size than the MEPS criterion.

The interaction of the dent and corrosion defects is also investigated at the final part of this thesis using strain-based reliability analyses based on the MEPS. A finite element (FE) model is developed and validated to calculate the strains in the DCCD region. The same reliability technique used in the plain dent problem is used to calculate the PoF for the DCCD. A combination of two pipes with different outside diameter to wall thickness ratios, different dent depths, and different corrosion depths and lengths within the dent depth are considered to investigate the effect of the corrosion defect on the pipe dent defect. From the obtained results, it is found that in the case of the overlap of the corrosion edge with the plastically strained region under the indenter, the probability of failure increases significantly. Otherwise, from a strain-based reliability analysis approach, for corrosion depth up to 60% of the pipe wall thickness defects within dent defects, the corrosion defect does not influence the probability of failure of the DCCD.

Preface

This thesis is an original work by Ahmed Khaled Abdelmoety under the supervision of Dr. Samer Adeeb and the co-supervision of Dr. Yong Li. It is presented in a paper format and consists of seven chapters.

Chapter 1 is a general introduction to the study's background, scope, and objectives.

Chapter 2 is the literature review on the pipe dent and corrosion defects, strain limits in dent defects, and reliability analysis.

Chapters 3 to 6 are the main contents of this thesis.

Chapter 3 was published as: Ahmed K. Abdelmoety, Qian Zheng, Yong Li, Muntaseer Kainat, Nader Yoosef-Ghodsi, Samer Adeeb (2021). Probability of Failure Associated with Design and Safety Factors for Intact and Corroded Pipes under Internal Pressure. Journal of Pipeline Systems Engineering and Practice. Volume 12, Issue 3. https://doi.org/10.1061/(ASCE)PS.1949-1204.0000544

Chapter 4 was published as: Ahmed K. Abdelmoety, Muntaseer Kainat, Nader Yoosef-Ghodsi, Yong Li, Samer Adeeb (2022). Strain-based reliability analysis of dented pipelines using a response surface method. Journal of Pipeline Science and Engineering, Volume 2, Issue 1, Pages 29-38. ISSN 2667-1433. https://doi.org/10.1016/j.jpse.2021.11.002

Chapter 5 is prepared as a journal manuscript titled "Reliability Analysis of Pipelines Containing Plain Dent Defects Using Different Strain Damage Criteria" to be submitted to peer-reviewed journal for publication.

Chapter 6 is prepared as a journal manuscript titled "Strain-Based Reliability Analysis of Pipelines Containing Dent Combined with Corrosion Defects Using Response Surface Method" to be submitted to a peer-reviewed journal for publication.

Chapter 7 contains the general conclusions of this thesis and suggestions for future research on the reliability analysis of dents and corrosion defects in pipelines.

I also contributed to the following publications:

- Qian Zheng, Ahmed Khaled Abdelmoety, Yong Li, Muntaseer Kainat, Nader Yoosef-Ghodsi, Samer Adeeb (2021). Reliability analysis of intact and defected pipes for internal pressure related limit states specified in CSA Z622:19. Volume 192, 104411, ISSN 0308-0161, https://doi.org/10.1016/j.ijpvp.2021.104411.
- Ahmed Khaled Abdelmoety, Qian Zheng, Muntaseer Kainat, Nader Yoosef-Ghodsi, Yong Li, Samer Adeeb (2022). Reliability Assessment of Dented Steel Pipes using Response Surface Method with Improved Meta-model Form. Conference proceedings of the technology for future and ageing pipeline conference, Gent, Belgium, March 29-31.

Acknowledgement

I would like to express my sincere gratitude to my supervisor Dr. Samer Adeeb for his constant support, encouragement, his patient guidance, and patience during my Ph.D. journey and also for creating several opportunities for my career. I would like also to thank my co-supervisor Dr. Yong Li for sharing his knowledge, his valuable comments and suggestions, and for always encouraging me to bring my true potential.

I would like to express my love and gratitude to my parents Nagwa ElCherif and Khaled Abdelmoety for dedicating their life to raise me and build my values, my intelligence, and my intellect so I can reach this point in my life. I would like to also thank my sister and friend Noha Khaled for her constant emotional and intellectual support. I would like also to thank all my teachers and my professors at faculty of engineering, Cairo University that helped forging my mind to be able to pursue this study and reach this point in my life. And, above all, thank Allah for everything.

I would like to thank MITACS and Enbridge Pipeline Inc. for providing partial funding for my Ph.D. journey to make it possible and helping me reach this level of knowledge.

I would like to thank Digital Research Alliance of Canada, as this research was enabled in part by support provided by them.

Table of contents

List of tables

List of figures

1. General Introduction

1.1. Research background and motivation

Pipelines are an essential component of Canada's vast transportation network in the oil and gas industry. They are an economical and efficient way of transporting oil and gas from the refineries to consumers on land and offshore. If designed well with appropriate material selected and maintained following good practices, pipelines should operate well and safely during their lifetime. However, like any structure, failures can possibly occur to pipelines due to many influencing factors. These factors can be natural such as ground movements that can over-strain, ripple, wrinkle, buckle the pipes and potentially cause their failure. Also, these influences can be mechanical such as the impact of construction equipment or the removal of the corrosion protection layer that can cause external corrosions, dents, cracks, gouges, and grooves in the pipelines. Moreover, operational mistakes like over-pressuring the pipeline can cause internal corrosion defects or yielding or bursting of the pipes. The loss of pipeline integrity can cause environmental damages resulting from leaks in case of oil pipelines or explosions in case of gas pipelines. Therefore, many researchers have studied pipeline defects and different ways to assess them, because the safety of the pipelines has to be ensured with a certain level of confidence during their lifetime.

Several defect types can reduce the safety levels of pipelines. One type of defect is the over-straining of the pipe material beyond its yield capacity [1] from over-pressuring the pipe or from pipe dents, which will be one of the defects to be studied in this study. Dent defects cause the development of high stress and strain regions in the pipe material, which can be a weak point for the development of cracks leading to the failure of the pipe after several internal pressure loading cycles. The assessment of the dent defects and the evaluation of their integrity and suitability for operation is an important task for the pipeline operators to ensure the pipeline safety and to reduce maintaining costs, therefore, a major part of this study will focus on the assessment of plain dent defects. Several methods exist for the assessment and determining the safe limitations

of dent defects in the literature and in different oil and gas design and assessment standards, which are presented in the literature review chapter.

Another important pipeline defect is the corrosion defect that can cause the burst of the pipes [2], as the metal loss from the pipe's inner or outer layers reduce the amount of metal resisting the internal pressure stresses causing the reduction of its burst pressure. Failure of the pipe subjected to corrosion is highly probable to occur if the burst pressure of the pipe is lower than the maximum allowable operating pressure (MAOP) of the pipe. Typically, design factors incorporated into intact pipe design provide a safety margin that enables pipelines to withstand corrosion defects up to a certain limit without failure [1]. Nevertheless, corrosion defects must be regularly monitored and evaluated to guarantee that they are not compromising the pipeline's integrity. Several analytical, empirical, and numerical-models-based criteria [3–9] have been provided in the literature and in the pipeline assessment standards to calculate and evaluate the remaining strength or the failure pressure of the pipes subjected to corrosion defects, which are presented in literature review section. Another type of defects can also develop which is the dent combined corrosion defect (DCCD). After the indentation of the pipe, the indented part is more susceptible to corrosion defect due to the removal of corrosion protection coating on the pipe giving a high possibility of the generation of a corrosion defect within the dent defect region. The information and assessment methods of the DCCD is further discussed in the literature review chapter.

As a result of all these hazards, different procedures for assessing pipelines were developed to make sure that the pipeline is fit for its purpose, which is to transport liquid and gas safely and efficiently without jeopardizing humans or the environment from pipeline burst or leakage. The "Fitness-for-purpose" assessment also helps determine if the defected pipeline needs repair or can operate safely under its current condition, which will help pipeline companies allocate the appropriate resources to safely rehabilitate any defects. Several efforts investigating different pipe defects are found in the literature. For example, Cosham and Hopkins [10,11] prepared a Pipeline

Defect Assessment Manual (PDAM), a joint industry project sponsored by 15 international oil and gas companies to specify the best methods for assessing defects in pipelines. Another project sponsored by the American Petroleum Institute (API) to determine the effect of the smooth and kinked dents on pipelines is conducted by Alexander and Keifner [12].

In order to perform pipeline defect assessments, operators can perform a deterministic or a probabilistic engineering assessment. Using the deterministic approach, equations containing different variables or parameters (characterized by determined values depending on each assessment or design case) can be used, for example, to calculate the capacity of a pipeline containing a specific defect. If the demand exceeds the predicted capacity, the pipe is assumed to be unsafe for operation. A safety factor is usually used with the deterministic equations to account for any unconsidered factors or any uncertainty in predicting the real behaviour predicted by the equation. On the other hand, for the probabilistic analysis (reliability analysis) or design, the statistical uncertainty of the different parameters, or random variables (RVs), of the equation is taken into account. The probabilistic, or reliability, analysis results will be a probability that the demand will exceed the capacity. By setting a target reliability or probability of failure, the safe operation of the pipeline can be assessed.

Generally, for the convenience of engineering practice, the pipe design is typically using a deterministic design format with the design or safety factor (DF or SF). The DF or SF in some design equations are provided without mentioning their associated probability of failure, therefore, they typically require rigorous reliability-based calibration that can provide more information for, or quantify, the choice of the safety level. Different reliability methods and techniques are developed in the literature and will be discussed in more details in the literature review chapter.

The main objective of this research is to assess the reliability levels of pressurized oil and gas pipelines with and without corrosion and dent defects using efficient and practical structural reliability assessment procedures. The assessment of the design

and safety factors of intact and corroded pipelines would be used for designing new pipes and assessing in-service pipes aiming to improve the safety and integrity of pipelines while avoiding overdesign. The assessment of plain dent and dent combined with corrosion defects will help improve the safety of pipelines and reduce repairing costs for pipeline companies. This research will help reduce the gap between academic research and practical applications by providing guidelines towards using reliability methods in the design and assessment of pipelines in practice compared to using the design and safety factors and the assessment guidelines specified by the design standards. Using reliability analysis in the design and assessment of pipelines will result in economical design without undue conservatism and cost-effective maintenance plans without inappropriate mitigation actions on defected pipes because reliability analysis is more appropriate than the design and safety factors used to determine pipe safety. To specific, the following objectives, linked to the four core chapters of this thesis, are presented as follows.

Objective 1

Investigation of the safety levels of the design and safety factors provided by pipeline standards using appropriate reliability techniques. The following are the specific tasks for this objective:

1. Determine the safety levels measured by the probability of failure of intact pipes designed according to the safety factors provided in CSA Z662:19, ASME B31.4-2019, and ASME B31.8-2018.

2. Perform reliability analysis on corroded pipes to check the safety levels of the safety factors against corrosion given in the ASME B31G-2012 standard for determining the remaining strength of the corroded pipelines.

Objective 2

Assessment of plain dent defects using a strain-based reliability procedure. The following are the specific tasks for this objective:

1. Develop and validate a suitable finite element model for reliability analysis to model the dent defect.

2. Investigate a suitable reliability method to calculate the POF of a dent defect accurately and time-efficiently.

3. Validate the chosen reliability method.

4. Investigate the main factors controlling the POF of a dent defect.

5. Investigate the safety and validity of the limits given by the pipelines' standards for dent defects.

Objective 3

Assessment of plain dent defects using a damage-based reliability procedure. The following are the specific goals for this objective:

1. Perform reliability analysis on the same study cases used in the previous objective using a damage-based criterion instead of the strain-based criterion.

2. Compare between damage-based and strain-based reliability results.

Objective 4

Assessment of dent combined with corrosion defects (DCCD) using a strain-based reliability procedure. The following are the specific goals for this objective:

1. Develop and validate a suitable finite element model for reliability analysis to model the dent combined with corrosion defect.

2. Adjust the reliability method developed in objective 2 to determine the POF of a dent defect combined with a corrosion defect.

3. Investigate the effect of corrosion defect on the dent defects POF.

4. Investigate the safety and validity of the limits given by the pipelines' standards for dent combined with corrosion defects.

1.2. Thesis outline

This thesis is consistent of a general introduction chapter and a literature review chapter followed by four main chapters constituting the body of this study. Lastly, a conclusion chapter is provided at the end before the references.

Chapter 2 presents a literature review on the main topics needed in this thesis such as, the design and safety factors for design and assessment of pipelines, the corrosion and dent defect assessment studies and limitations, the strain limits and calculation of the pipe material, and reliability analysis methods.

Chapter 3 presents a reliability-based study on the design factors against yielding provided in the design standards and on the safety factors provided in the corrosion assessment US standard (ASME B31G) to determine their safety levels.

Chapter 4 presents reliability analyses on different pipe sizes using the response surface method (RSM) and the first order reliability method (FORM) as a reliability analysis method together with finite element (FE) modeling to determine the main parameters affecting the probability of failure of plain dent defects. The pipe material strain capacity is used as the strain limit in the limit state function of the problem.

Chapter 5 presents reliability analyses on different pipe sizes using the RSM and FORM as reliability analysis methods together with FE modeling of the pipe. However, the limit state function is based on the strain damage of the pipe material. The ductile failure damage indicator (DFDI) and the strain limit damage (SLD) are used as ductile strain damage models to calculate the damage in the pipe dented region.

Chapter 6 presents reliability analyses on different pipe sizes using the RSM and the FORM as reliability analysis method together with FE modeling to investigate the interaction of corrosion defect with the dent defect and quantitively assess the interaction of the two defects on the probability of failure of the pipe.

Chapter 7 concludes the thesis. It provides an overall research summary and finding for chapter 3, 4, 5, and 6 in the thesis.

2. Literature Review

2.1. Intact pipeline design

The Canadian standard, CSA Z662:19 [13], and the US standards, ASME B31.4-2019 for liquids and slurries [14] and ASME B31.8-2018 [15], for oil and gas pipelines provide pressure design equations that ensure that steel pipelines operate within the elastic regime without yielding. The Canadian and the US pipelines standards, CSA Z662:19, ASME B31.4, and ASME B31.8, provide almost the same equation, based on Barlow's equation for calculating hoop stresses, for the calculation of design pressure of pipelines. The equation provided in the CSA Z662:19 (section 4.3.5.1) is presented in Eq. (2.1).

$$P = \frac{2 \times S \times t}{D} \times F \times L \times J \times T \tag{2.1}$$

Here, P is the internal design pressure in MPa, S is the Specified Minimum Yield Strength (SMYS) for the pipe material, t is the pipe Wall Thickness (WT), D is the pipe Outside Diameter (OD), F is the design factor, L is the location factor, J is the joint factor, and T is the temperature factor.

This equation is used in the design stage by setting the maximum operating pressure of the pipe, the specified minimum yield strength of the pipe, and all the factors. Then, a pipe geometry is selected satisfying the condition that the pressure (P) in the pipe is equal to or higher than the maximum operating pressure (MOP) applied to the pipe. Later in the thesis, this equation will be used in an opposite way for an existing pipe with known geometry, design factor, and pipe material to calculate the MOP, which will be equal to the pressure (P) in the equation.

Almost the same equation is provided in the ASME B31.8-2018 (section 841.1), but without using the location factor L in the equation. The ASME B31.4-2019 (section 403.2) provides an allowable pipe wall thickness equation, which is similar to the CSA Z662:19 and the ASME B31.8-2018, but reformed to calculate pipe wall thickness, not

the internal pressure. Only the design and joint factors are included in the ASME B31.4-2019 equation.

In this study, the temperature and joint factors are ignored, and their values are assumed to be equal to 1 in the reliability analysis considering limit states related to the internal pressure applied on pipe bodies. The CSA Z662:19 states the design factor shall be taken equal to 0.8 instead of 0.72 in the previous versions of the standard, and the location factor (ranging from 1 to 0.55) was introduced to alter the design factor based on the location and the type of the pipeline making the design factor vary from 0.8 to 0.44.

In contrast, the ASME B31.8-2018 states that the design factor has values of 0.8, 0.72, 0.6, 0.5, or 0.4 based on the location class of the pipeline, and the ASME B31.4-2019 states that the design factor should be taken less than 0.72.

As a result, in this study, Eq. (2.1) will be used with a design factor ranging from 0.8 to 0.4 to evaluate the safety levels associated with these design factors while ignoring the effect of the joint and temperature factors in the design equation.

2.2. Pipelines defects

This subsection presents the different pipe defects considered in this study and the relevant research done on these defects in the literature. This study will consider two primary pipe defects: the pipe's external corrosion and the pipe plain dents, as well as the combination of these two defects.

2.2.1. Corrosion defects problem

Pipes can be subjected to internal and external corrosion defects. Internal corrosion is metal loss mostly caused by the presences of electrolytes, such as water, and species, such as CO_2, H_2S, pH, and O_2, and influenced by the flow parameters, such as temperature, pressure, and velocity [16]. External corrosion is a metal loss in the pipe outer layer caused by damage or disbanding to the pipe coating. Corrosion defects can impact the burst pressure of pipes [17]. Usually, the safety margin gained by the

design factors included in the intact pipe design enable pipelines to resist corrosion defects up to a certain limit without failing. However, corrosion defects have to be monitored and assessed frequently to ensure that they are not affecting the pipeline's integrity.

Several analytical equations and criteria [2] have been provided in the literature and in the pipelines assessment standards to calculate the remaining strength or the failure pressure of the pipes subjected to corrosion defects. One of first methods to predict the failure pressure of a corroded pipeline is the NG-18 criterion set by Maxey *et al*. [18] in 1971. In the NG-18 criterion, the predicted hoop stress at failure is calculated as a percentage of the so called "flow stress" depending on the ratio of the through thickness corroded area to the through thickness intact area and on the Folias factor. The flow stress is used to describe the stress level applied to a material to bring it to plastic deformation (or flowing), and it is between the yield and the ultimate stresses of the material [19]. The Folias factor M is a stress concentration factor accounting for the bulging effect of a notch in pressurized pipes [3]. The corrosion shape in the NG-18 criterion models the corrosion bed shape with a parabolic shape for short corrosion defects, as shown in Figure 2.1(a), and with a rectangular shape for long corrosion defects [3], as shown in Figure 2.1(b). ASME B31G-1991 [20], the manual for determining the strength of corroded pipelines, provided the *original* ASME B31G equations for the assessment of corrosion defects, which is similar to the NG-18 equation. However, in the original ASME B31G equations, a modified Folias factor was used for long corrosion defects to overcome the excessive conservatism of the original NG-18 equations in the reported failure pressure for long corrosion defects [21]. The newest version of the manual for determining the strength of corroded pipelines, ASME B31G-2012 [17], provides a *modified* set of ASME B31G equations, also called the 0.85 dL method, having the same form of the original equations, but with changes in the approximation of the corrosion bed shape assuming that 55% of the corrosion depth is rectangular and the remaining 45% of the depth is parabolic, as shown in Figure 2.1(c). ASME B31G-2012 also provides a method for calculating the remaining

strength of corroded pipes based on the effective area method developed by Keifner and Vieth [3], also known as the RSTRENG method. The RSTRENG method considers the actual area of the metal loss and divides it into a grid of cells with different depths. Then through an iterative process, the failure pressure is calculated through each meridian of the grid, and the lowest calculated failure pressure governs.

Other equations and methods were also found in the literature. Cronin *et al.* [7] presented a method called the Corroded Pipe Strength (CPS) that predict the failure pressure using a weighted depth difference method. The European Fitness for Service Network developed a model based on Tresca failure criterion and Hollomon strain-hardening model to predict the failure pressure of corroded pipes [9]. Zhang *et al.* proposed a burst model using regression analysis on 27 Finite Element (FE) models of X65 girth welded pipes [8]. Choi *et al.* [5], Chen *et al.* [4], and Shuai et al. [6] also provided methods based on the FE simulations for the prediction of the failure pressure of corroded pipes.

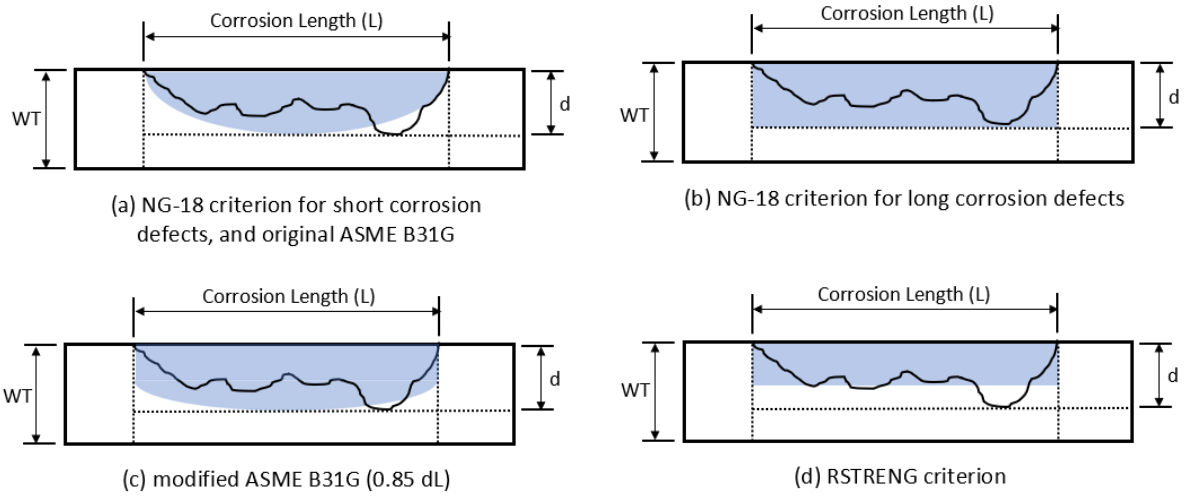

Figure 2.1. *Corrosion defects showing the corrosion approximation for each failure pressure criterion.*

Zhou and Huang [21] and Bai *et al*. [3] showed, based on experimental models, that the RSTRENG model is the best model among the original and modified ASME B31G to accurately predict the burst pressure of corroded pipes, which made the RSTRENG model the main model to be used in our study. Zhou and Huang [21] also compared the RSTRENG model results to experimental tests data and came up with a Model Error (ME), a probabilistic variable that characterizes the deviation and scattering of the RSTRENG model results from the actual experimental test data. They separated the defects into long and short defects by a normalized length value of 2.25 and provided two different ME variables for long and short defects.

In the following, the limitation given by the different design standards for the corrosion defects is presented. According to CSA Z662:19, any pipe having combined internal and external corrosion defects, each having any length, with the sum of their maximum depths less than (1) 10% of the pipe wall thickness or (2) the wall thickness presented as corrosion allowance in the pipe design are assumed to be acceptable and do not require repair. Corrosion areas are considered defects for pipes that need repair or replacement, if they contain cracks, are concentrated in the seams of electric resistance welded or flash welded pipe or are located in material likely to exhibit brittle fracture initiation.

According to ASME B31.4-2019, corroded areas with depth up to 20% of wall thickness are acceptable but need to be treated to avoid further corrosion. Corroded areas with maximum depths between 20% and 80% of the pipe wall thickness are permitted to remain unrepaired if the Maximum Allowable Operating Pressure (MAOP) of the pipe is less than the failure pressure of the corroded pipe calculated using the ASME B31G original or modified or the effective area method (RSTRENG method). ASME B31.8-2018 simply states that gas pipes should be replaced or repaired if the failure pressure of the corroded pipe is less than the MAOP of the pipe.

In this study, the RSTRENG model will be used as the failure pressure predicting model for corroded pipes. The study will consider corrosion defects ranging from 10% to 80% of the pipe wall thickness.

2.2.2. Plain dent defects

Plain dent defects are defined as permanent plastic deformation of the pipe circular cross-section without any reduction, caused by metal loss, in the wall thickness and without any other stress concentrators such as gouges and arc burns [10,13], as shown in Figure 2.2. Plain dents cause a concentration of stresses and strains at the dent location, which can possibly cause localized pipeline wall failure.

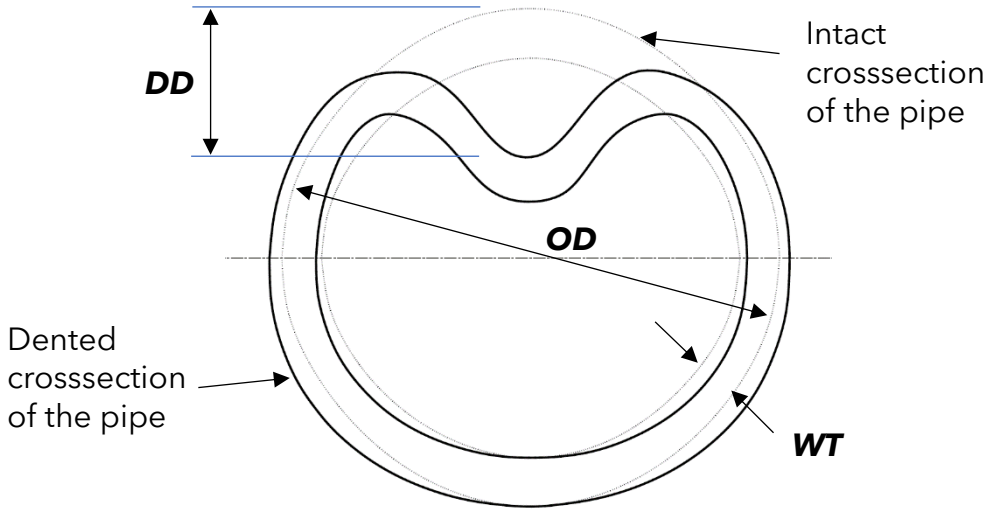

Figure 2.2. *Dent defect deformation in a pipe section showing the pipe's intact section in dash lines.*

Plain dents can be divided into either smooth or kinked dents depending on the radius of curvature of the sharpest part in the dented part of the profile. Kinked dents are those dents whose radius of curvature of the sharpest part is less than five times the wall thickness of the pipe [10].

Dents can be combined with other pipe defects, like internal and external corrosion, gouges, grooves, arc burn, and cracks, which can occur at a mill or weld location. Our study considers dents that do not occur at a mill or weld location and that are not

associated with stress-concentrators, like gouges, grooves, arc burns, and cracks. However, dents combined with external corrosion defects are considered.

The failure of the gas pipelines subjected to plain dent defects is attributed, in the majority of cases, to excessive strain or fatigue failure of the over-stressed material at the dent location. Several researches [22–24] have studied the effect of fatigue failure on the life of pipelines. However, only a limited number of studies were found on the strain assessment of pipe dents, ignoring the fact that reaching the strain capacity of the overstrained pipe material at the dent location plays an important role in pipe failure.

Rosenfeld *et al*. [25] suggested that the severity of the dent defect should be determined by its strain level and that two (one gas and one liquid) pipeline operators had adopted strain-based criteria for assessing pipe dents. The ASME B31.8-2018 provided equations for estimation of the strains at the dent location in Appendix R. However, Okoloekwe et *al*. [26] reported the inaccuracy of the ASME B31.8-2018 Appendix R equations at predicting the maximum strains generated at the dent location and provided a new method based on the dent profile for predicting the maximum strains generated at the dent location. Zhao *et al*. [27] also reported the inaccuracy of the ASME B31.8-2018 Appendix R strain prediction equations and provided a new technique based on the Finite Element Method (FEM) to accurately predict the maximum dent strains.

In the following, the acceptance criteria for dents provided by the different design standards for plain dent defects is presented. According to CSA Z662:19, plain Dent Depth (DD) should be limited to 2% of the pipe outside diameter. However, for plain dents having

(1) dent depths exceeding 6 mm for 101.6 mm OD or smaller,

(2) dent depths exceeding 6% of the OD for pipes with OD larger than 101.6 mm, or

(3) dent length less than 20 times the dent depth,

unless their measured curvature strain is less than 6%, they are to be cut and replaced unless considered acceptable by an engineering assessment. CSA Z662:19 points out that the strain in a dent can be calculated by the equations provided in Appendix R in the ASME B31.8 standard for gas transmission and distribution pipeline systems or any other engineering methodology, which opens the door for using the FE analysis to calculate the strains. Some dents that are safe to operate under the maximum operating pressure, however, have to be cut and replaced to permit the passage of the internal inspection and cleaning device [15].

According to ASME B31.8-2018, plain dent depths should not exceed 6% of the pipe OD to be safe. However, plain dents can have any depth without being unsafe if the strain level within the dent does not exceed

(1) half of the minimum elongation of the pipe material manufacturing specifications,

(2) 40% of the average elongation from pipe manufacturer mill test reports,

(3) the maximum strain level of 6% if no data about the used steel is available.

According to ASME B31.4-2019, only the condition that the dent depth should not exceed 6% of the pipe OD is mentioned for the safety of the dent defect.

The acceptance criteria for plane dents in the above regulations are based on the dent depth (which should not exceed 6% of pipe OD) and the strain level in the dent (which should not exceed 6%). Zhao and Cheng [27], however, have reported that the 6% limit is excessively conservative. Also, Adeeb and Horsley [28] used a 20% principal strain limit instead of the 6% in their study investigating the effect of internal pressure on the possibility of rupturing high pressure gas pipes due to the punctures resulting from impact of falling rocks.

2.2.3. Dents combined with corrosion defects (DCCD)

DCCD is plain dent defects combined with corrosion, metal loss, defects within the dented area where the pipe is plastically deformed.

Many research papers have been found on dents combined with gouges [29–31] and dents combined with cracks [32–34] defects, but to the best of the author's knowledge, there are currently no studies investigating the assessment of dents combined with corrosion.

According to CSA Z662:19 (section 10.10.4.2), dents that (1) contain corroded area with a maximum corrosion depth more than 40% of the nominal wall thickness, (2) contain corroded areas having a depth greater than 10%, up to and including 40%, of the nominal wall thickness of the pipe and a depth and length that exceed the maximum allowable longitudinal extent determined as specified in ASME B31G (Level 0 evaluation) should be considered as a defect and have to but cut and replaced.

According to ASME B31.8 for gas pipes, dents combined with corrosion with depth more than 6% of pipe OD or corrosion reducing the pipe's failure pressure to less than the MOP is considered injurious and should be repaired or replaced.

According to ASME B31.4 for liquid pipes, dents with corrosion having a minimum thickness less than the minimum thickness allowed by the corrosion defect alone should be cut and replaced.

The API assessment and management of pipeline dents standard, the API 1183-2020 [35], states that a generalized dent-corrosion feature interaction has not been developed and that for corrosion interacting with dent defects, the three following different assessment criteria can be applied separately:

(1) The same procedures stated by ASME B31.8 for dents combined with corrosion (presented above).

(2) The evaluation of the corrosion defect as the only defect according to the ASME B31G to make sure that the failure pressure is more than the MOP.

(3) For dents with corrosion having a depth less than 30% of the pipe WT in the interaction zone of the dent, given in Figure 2.3, their fatigue life should be reduced by a fatigue life reduction factor depending on the corrosion thickness. Fatigue life

reduction of dents with corrosion having depth more than 30% of the pipe WT should be evaluated using detailed dent response based on finite element modelling and fracture mechanics techniques.

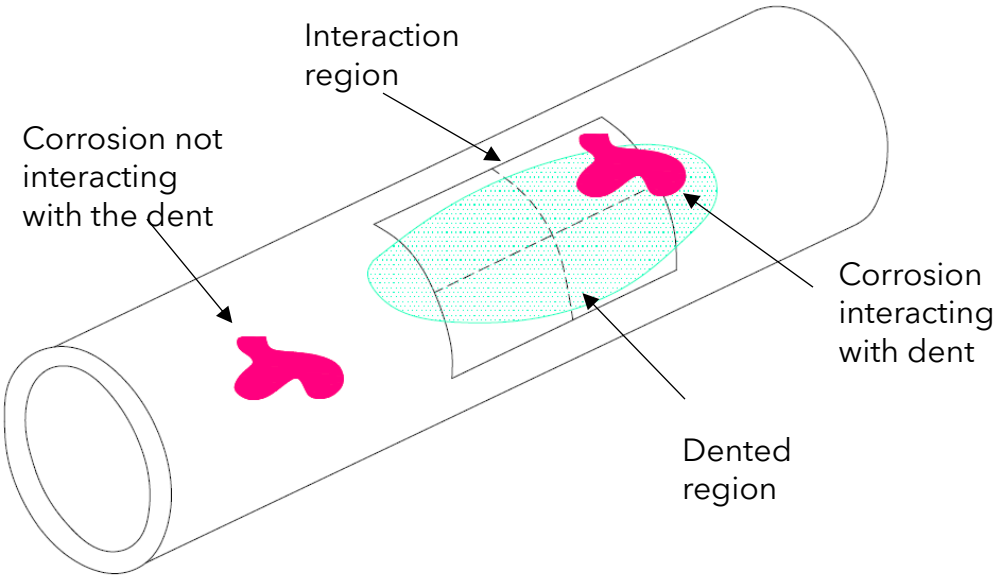

Figure 2.3. *Interaction zone for the dent defect, given by* [35].

There is an obvious lack in research investigating the interaction between the dent and corrosion defects, as most of the design and assessment standards treat it as a plain dent or a plain corrosion defect. The DCCD is treated similarly to different interacting defects or unsafe and needs replacement. Therefore, in this study, the reliability strain-based assessment will be performed for the DCCD to provide quantitative data on the assessment of this type of defect.

2.2.4. Strains in dent defects

Accurate prediction of the maximum strains and the strains profile in the plain dent area is crucial in any study related to the strain failure of pipes subjected to defects. The evaluation of the strains in plain dents can be performed either experimentally or numerically by creating FE models. Each approach has its advantages and disadvantages. The experimental approach is more realistic than the numerical one,

but it is relatively expensive. On the other hand, the numerical approach is way less expensive and easier to adjust, but its accuracy must always be checked. Going through the literature, several researchers [36–41] performed experimental tests and developed numerical models for analyzing pipes subjected to dent defects. Also, several researchers [27,42,43] created FE models for predicting the internal stresses and the strains in pipe dents.

In this study, efficient and suitable FE models will be created to calculate the strains in dent defects. The numerical models previously presented from the literature will be considered the basis for building the new model. Also, the results of the experimental models will be used to check and validate the developed FE models.

In a dent strain assessment, the pipeline strains calculated from the analytical models based on the profile, or from FEA are compared with the Tensile Strain Capacity (TSC) to assess the safety level of operating the pipe with the dent. Different TSC limits exist depending on the type of pipe defect. TSC of pipe with girth weld defects is different from the TSC of pipes subjected to dent defects [14]. Several researchers investigated the pipes TSC of different pipes with girth weld defects steel grades. Abdulhameed et *al*. [44] experimentally tested eight different pipes to check the effect of the internal pressure on the TSC of pipes with girth weld defects and compare it to the TSC values provided by CSA Z662:11; Elyasi et *al*. [45] simulated eight full-scale pipes, tested experimentally by [44], made of API 5L X52 steel using the extended FEM to predict the pipes tensile capacity and to show the efficiency of the extended FEM in predicting the experimental results; Lin [46] performed research on the tensile properties of the X52 steel pipes, where a complete section is provided on the prediction of the tensile strain capacity of the vintage X52 steel pipes. The range of the strain capacity in the above-mentioned studies is usually between 1 to 2% depending on the material ductility, any previous plastic strain. According to the ASME B31.4-2019, Section 451.12, a maximum of 2% strain limit is set for the conditions of non-cyclic support movement, such as fault movement. However, this strain limit is not applied in the case

of localized strain, such as in dents. Therefore, in this study, the strain capacity will be taken as the strain capacity of the pipe base material.

The API SPEC 5L (2018), Section 9.3 [47] provides an equation for the calculation of the specific minimum elongation of the different steel grades depending on the Specified Minimum Tensile Strength (SMTS) of the steel grade and the full crossectional area of the steel pipe. The CSA Z662:19, appendix O for the reliability design and assessment of pipeline provides statistical data for the ultimate tensile strain of the API 5L X60 with a mean of 36% and 6% Coefficient Of Variation (COV) and the API 5L X65 steels with a mean of 36% and a COV of 7%. Also, Lin [46] provided the tensile properties of the vintage Enbridge Norman Wells X52 pipelines by taking six test specimens from the base metal of the pipe at different locations on the pipe in the longitudinal and in the circumferential directions. The range of the elongation percentage of the different specimens ranged from 27.9% to 33%.

Another method that can be used to assess the dent defects by assessing the strain concentrations developed in the dented region is the ductile damage models. To avoid determining the limiting strain that is considered safe and not to be exceeded, Zhao and Cheng [48] suggested a different strain assessment criterion which is the strain damage models that take into consideration the stress tri-axiality to determine the strains that will lead to the cracking of the pipe material and the accumulation of the strain damage at each point of the pipe material. Several studies have been conducted on the use of different damage criterion for the prediction of pipelines cracking and damage. Arumugam et al. [49] provided a study on the quantification of the plastic strain limit of dent defects using the Strain Limit Damage (SLD), given in the the ASME boiler and pressure vessels code (ASME BPVC.VIII.3-2021 [50]), and the Ductile Failure Damage Indicator (DFDI) damage models, given in the standard for the assessment and management of pipeline dents (API 1183-2020 [35]), and the minimum elongation limit criterion for dented pipes showing that the experimental information highly favours the DFDI and SLD strain damage models to be used as a mean to assess the severity of dent defects. Li and Dang [51] used the DFDI to analyze the ductile damage

of the pipes subjected to constrained and unconstrained dents to show that the plastic damage is higher on the inside walls of the pipe than on the outside wall and that the dent depth and the pipe internal pressure has significant effect on the constrained dent damage. Gao et al. [52] predicted dent defect cracking using the DFDI criterion and finite element modeling and demonstrated that the DFDI with the inline inspection magnetic flux leakage can effectively identify the potential risk of dent with cracking. Wu et al. used Oyane's damage criterion with finite element modeling to assess oil and gas pipelines [53] and natural gas pipelines [54] instead of using the dent depth-based failure criterion that does not account for several parameter such as, the internal pressure, the loading order, and the geometry of the pipe. Moreover, in [55] Wu et al. performed the damage analysis using an ellipsoidal indenter to indent the pipe in the longitudinal and circumferential directions showing that the longitudinal dent produced higher damage in the pipe material. Wu et al. also showed that the with the amount of damage positively correlates with the indentation depth and negatively corelates with the indenter size.

2.3. Reliability analysis methods

The main aim of the reliability analysis is to calculate the probability that a system or a component will violate a certain condition. This condition, defined as a Limit State that is mathematically described by a Limit State Function (LSF) $g(X)$, is presented by a point (threshold value) in one-dimensional problems when X is a scalar, a curve in a two-dimensional problem (as shown in Figure 2.4), a surface in the three-dimensional problems, or, generally, a hypersurface in a multidimensional problem when X is a vector. The LSF equation, $g(X) = 0$, represents the boundary between the safe region, where all function values are greater than zero $g(X) > 0$, and the failure region, where all function values are less than zero $g(X) < 0$.

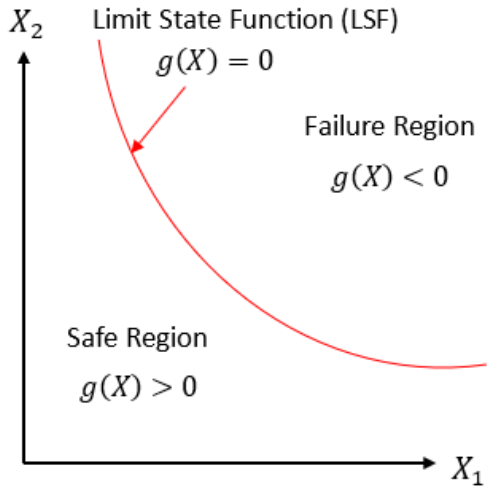

Figure 2.4. *Two-dimensional problem showing the LSF with the safe and unsafe zones.*

The probability that the LSF value is less than zero is known as the Probability of Failure (PoF) in the reliability analysis context. However, it does not necessarily mean the physical failure of a component or the system, depending on how the LSF is defined.

Several reliability analysis techniques have and are still being developed to calculate this probability of failure. In a two-dimensional problem, as shown in Figure 2.5, the probability of failure is the integration of the joint probability distribution over the failure side of the LSF. This general integration is represented in Eq. (2.2).

$$POF = P(g(X) < 0) = \int_{g(X)<0} p(X)dX \tag{2.2}$$

where POF is the probability of failure, $g(X)$ is the LSF, and $p(X)$ is the joint probability density function of random vector X.

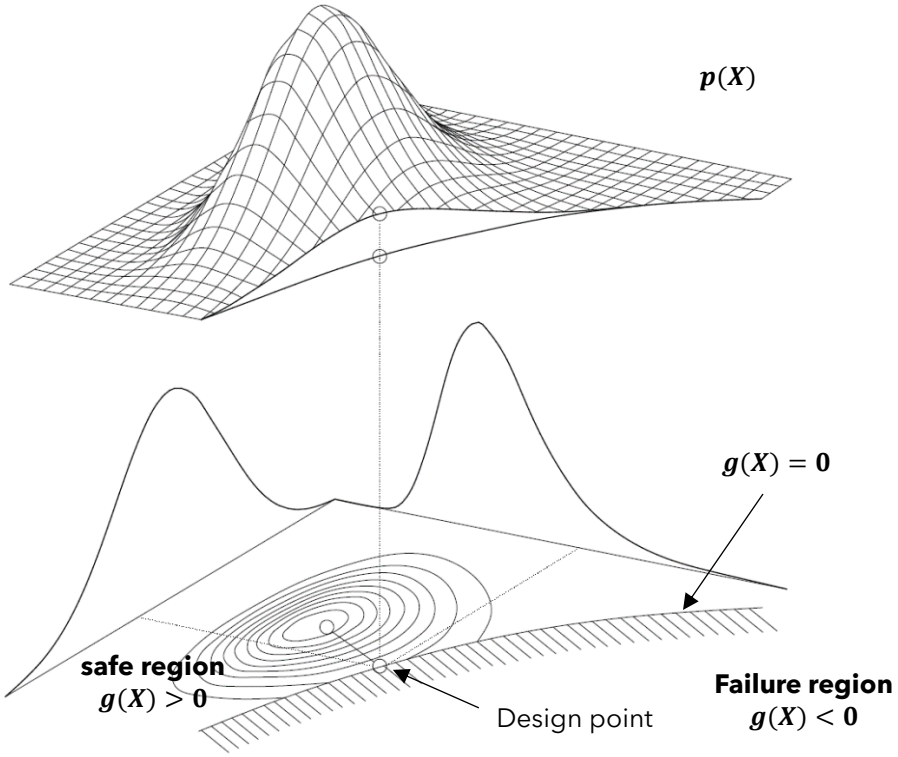

Figure 2.5. *Two-dimensional problem showing the LSF, the joint probability density function.*

Direct integration can be used to get the POF, knowing that the integration of the total volume under the $p(X)$ is going to be equal to 1. However, evaluating the integral becomes computationally expensive when the problem dimension increases, and using other reliability analysis techniques becomes more practical and convenient. Also, the complexity in the integration domain, sometimes implicit, also increases the challenges in direct integration for the POF.

The Monte Carlo Simulation (MCS) method [56] is considered one of the easiest and most accurate reliability methods, if a sufficient number of samples are generated, to use for reliability analysis. The MCS calculates the POF by randomly generating numerous simulations or sample points and calculating the ratio of the number of simulations in the failure zone to the total number of simulations. The accuracy of the method increases with the increase of the number of generated simulations. The MCS

main drawback is its inefficiency in accurately evaluating extremely low ($<10^{-6}$) POF due to the extremely large number of simulations needed for the analysis, which demands high computational processing capacity, particularly when the LSF evaluation is computationally expensive (e.g., based on large finite-element models). One alternative method to the MCS is the Weighted Monte Carlo (WMC) method developed by Rashki et al. [57], which is more efficient than the MCS at predicting the extremely low POF at a significantly lower number of simulations.

Additionally, several approximate analytical methods, such as the First-Order Reliability Method (FORM) [58], were developed to evaluate the POF. The FORM transforms the joint probability distribution and the LSF to a standard normal space, where the reliability index (β), which is the shortest distance from the origin to the hypersurface defined by LSF = 0 in the normal standard space. The Design Point (DP) or the Most Probable Point (MPP), which is the point on the hypersurface LSF = 0 with gives the shortest distance from the origin to the hypersurface LSF = 0, are obtained by approximating the LSF as a linear function at each analysis iteration in FORM. The main drawback of the FORM is that its approximation is dependent on the nonlinearity in the LSF and the closeness of the problem random variables to the Gaussian (normal) distribution. A modification to the FORM is the Second-Order Reliability Method (SORM) [59] that approximates the LSF as a second-order polynomial function at each analysis iteration instead of a first-order polynomial function in FORM.

Another reliability technique is the response surface method (RSM) [60]. Many researchers have used and modified the classical RSM [61–66] to improve its performance for reliability analysis. The RSM is based on the iterative process of generating and performing reliability analysis on a Response Surface (RS) generated to locally approximate the original LSF of the problem. The RS is constructed from discrete points from the system, under investigation, response observations, and the determination of these points is based on the Design of Experiment (DOE) [67]. Depending on the number of problem parameters or independent variables (predictors or regressors) and the analysis duration, different DOE methods, such as

the full and the fractional factorial method, can be chosen to generate the response observations to construct the RS using the least-squares method.

The reliability analyses have been applied in many areas of structural engineering, such as nonlinear [68] and ageing concrete structures [69,70]. Also, reliability analysis has been applied in assessing steel bridges [71,72]. Moreover, the reliability analysis has been applied to the pipeline assessment as probabilistic analysis subjected to corrosion defects has been performed by several researchers [6,73–77]. Garbatov and Soares [23] and He and Zhou [22] performed fatigue reliability analysis for dented pipelines. Also, Hassanien et al. [78] used surrogate models, or the RSM, to perform reliability analysis on dented pipelines.

Many other reliability methods exist in the literature, and each reliability method has its strengths and drawbacks. The challenge is always to choose the reliability analysis techniques that suit the problem at hand. In this thesis, different reliability methods will be used in different problems depending on their suitability for the problem from a practical perspective.

3. Probability of Failure Associated with Design and Safety Factors for Intact and Corroded Pipes Under Internal Pressure

3.1. Introduction

Pipelines are considered the safest method for the transportation of oil and gas products from the extraction sites to refineries, and finally to consumers [77,79]. However, leakage or loss of containment of pipelines in the transmitting grid can be caused by several factors such as overpressure, cracking, and corrosion [80]. The associated environmental risk due to a damaged pipeline can be very high in addition to the cost due to failure to supply fluids [81]. Consequently, the safe design and integrity assessment of pipes is crucial for proper operation of pipelines.

To ensure a safe and economic design, probabilistic analysis offers a rigorous approach to perform reliability-based design for engineering problems with uncertainties. This approach involves defining a limit state function (LSF) and a target probability of failure (POF) predefined for a specific design situation. However, for the convenience of engineering practice, the pipe design is typically using a deterministic design format with the design or safety factor (DF or SF). The DF or SF in some design equations are provided without mentioning the associated POFs [13–15,17]. As such, this paper aims to assess the POFs associated with (1) the DFs used in the design against yielding of intact pipes given in the US and the Canadian standards of oil and gas pipeline systems (ASME B31.4 [14], ASME B31.8 [15], and CSA Z662:19 [13]), and (2) the SFs used for checking the remaining strength of corroded pipelines against failure in the US standard [17].

To facilitate the probabilistic design of pipelines, some research was devoted to the reliability assessment of intact and corroded pipes. For example, [82] provided a guide on using the reliability methods to increase the design factors provided by ASME B31.8 and BS8010 [83] without significant impact on the pipeline safety. [84] provided a

justification on the increase of the design factors of intact pipes from 72% SMYS to 80% using reliability analyses results. [85] estimated the reliability levels of pressurised pipelines subject to localised corrosion defects using FORM, based on an equation close to original ASME B31G equation, but reliability analysis was not linked to the DFs used in their analysis. [77] provided a reliability assessment of corroded pipes under internal pressure based on the failure equation provided by [86] and on the DF provided by ASME B31G. However, no research has provided a comprehensive reliability assessment of the DFs and SFs provided in the Canadian and US standards against yielding of intact pipes and burst failure of corroded pipes based on the RSTRENG equation with its modelling error considered.

Several methods can be used for reliability analysis. One of the most notable method is the Crude Monte Carlo (CMC) sampling method [56] because of its ease of use and its accuracy with sufficient number of samples. However, as will be explained later in the paper, CMC is inefficient with the calculation of the extremely low POF (e.g., less than 10^{-6}) due to the large number of simulations required. Other simulation methods were developed to overcome the deficiency of the CMC like the stratified sampling [87], Latin Hypercube sampling [88], importance sampling [89], subset simulation [90], and Weighted Monte Carlo (WMC) method [57]. Among these methods, the WMC as a straightforward generalization of CMC, is very easy for implementation and found to be very efficient in calculating low POFs and thus will be used in this paper.

Additionally, several approximate analytical methods, such as the first-order reliability method (FORM) [58], were developed to calculate the POF. In comparison with the sampling methods, FORM is a very efficient method in calculating the extremely low POF. Nevertheless, the approximation error in FORM depends on the nonlinearity in the LSF and the closeness to Gaussian distribution of basic random variables. In this paper, FORM will be used to calculate the POF, and a sampling method (i.e., WMC) will be used to cross-check and validate the results obtained by FORM.

In this paper the POFs associated with the DFs for yielding of intact pipes and the SFs for the burst of corroded pipes are calculated. Firstly, the LSFs used for calculating the POF are presented, followed by the description of the design variables and their statistical properties considered for reliability analysis. Secondly, a brief review of the two reliability methods used to calculate the POFs is presented. Finally, the reliability analysis results are presented and discussed in depth to shed lights on the current pipeline engineering practice from the perspective of probability-based design and integrity assessment.

3.2. Limit state functions

Two limit states are considered for the calculation of POFs. The first one is concerned with yielding of intact pipes due to internal pressure, and the second one is concerned with failure of corroded pipes due to internal pressure. Note that the nominal or characteristic values, which are deterministic and used in the design process, of the corresponding random variables (RV) are differentiated by adding a bar over the deterministic variables.

Yielding of intact pipes

The yielding limit state of pipes is based on the Barlow's equation used to calculate the circumferential (hoop) stress in pipes given in CSA Z662:19. Specifically, the limit state function used to characterize the yielding limit state is presented in Eq. (3.1).

$$g_y = \sigma_y - \sigma \tag{3.1}$$

where σ_y is the yield strength of the pipe steel, and σ is the circumferential (hoop) stress in the pipe due to internal pressure or the maximum operating pressure (*MOP*), as in this paper the pipe is in operation with its full capacity designed, i.e., the *MOP* is considered the same as the design pressure P. The internal circumferential stress σ in a pipe due to internal pressure is calculated from the following Barlow's equation [2], see Eq. (3.2).

$$\sigma = \frac{PD}{2t} \tag{3.2}$$

where D is the pipe outside diameter, t is the pipe wall thickness, and P is the design pressure calculated by Eq. (3.3), from CSA Z662:19.

$$P = \frac{2\,\sigma_y t}{D} \times F \times L \tag{3.3}$$

where F is the design factor that is typically less than 1.0, and L is the location factor. It has to be mentioned that in ASME B31.4 and in ASME B31.8 the design and location factors are combined into one factor considered as the design factor, and that the joint, and temperature factors in this equation are all assumed to be equal to 1 as they are out of this study scope.

Failure of the corroded pipes

The limit state function for the burst of pipes with corrosion defects due to internal pressure is presented in Eq. (3.4).

$$g_c = ME \times P_f - MOP \tag{3.4}$$

where P_f is the failure pressure of the pipe with corrosion defects, and ME is a RV to characterize the model error in predicting P_f by means of the test-to-prediction ratio. Note that many models exist for the calculation of the failure pressure of the corroded pipes. One of the first models developed is the NG-18 criterion, which appeared as early as 1971 [18]. Following the NG-18 criterion, the original ASME B31G equation assumes that the corrosion defect shape is parabolic. Later on, the modified B31G equation uses the same criterion, but the corrosion defect is assumed to be a combination of rectangular and parabolic shapes to give a more accurate modelling of the corrosion defect shape. However, one of the most significant drawbacks of the B31G equations is their overestimation of the failure pressure for long irregular corrosion shapes [3]. As such, the RSTRENG equation was proposed by [91] to improve

the estimation of failure pressure for long corrosion defects by taking the complete profile of the corrosion into consideration when calculating the corroded effective area, which makes the results more accurate than the B31G equations. The RSTRENG criterion proved to be one of the most efficient methods to predict the closest values to the actual failure pressure [21]. In this paper, the RSTRENG method is used in the LSF for the burst of corroded pipes, as given by the Eq. (3.5):

$$P_f = 2\sigma_{flow}\left(\frac{t}{D}\right)\left(\frac{1-X_d}{1-\frac{X_d}{M}}\right) \tag{3.5}$$

where X_d is the normalized depth of the corrosion defect, σ_{flow} is the flow stress, and M is the Folias factor, and they are given by equations (3.6) – (3.8), respectively:

$$X_d = \frac{d}{t} \tag{3.6}$$

$$\sigma_{flow} = \sigma_y + 10{,}000 \text{ psi} \tag{3.7}$$

$$M = \begin{cases} \sqrt{1 + 0.6275 * X_L - 0.003375 * {X_L}^2}, & X_L < 50 \\ 3.3 + 0.032 * X_L, & X_L > 50 \end{cases} \tag{3.8}$$

where d is the corrosion defect depth, X_L is the normalized length of the corrosion defect given by Eq. (3.9),

$$X_L = \frac{L^2}{Dt} \tag{3.9}$$

where L is the corrosion defect length.

As studied in [21], the RSTRENG model is not accurate, and a test-to-prediction variable, *ME*, is applied to the model as a multiplication factor in the LSF to consider the model uncertainty.

3.3. Design cases and statistical data

To assess the POFs associated with different design cases for pipes, seven different steel grades and sixteen different pipe geometry configurations are considered. The probabilistic characteristics (e.g., distribution types and relevant statistics) for the uncertain design variables are provided in this section.

Design cases

For intact pipes, the steel grades and the designation to be used in this study are obtained from [47]. The specified minimum yield strength ($SMYS$) for the steel grades is summarized in Table 3.1, and the designation is summarized in Table 3.2, with the dimensions of the pipes considered. The pipe characteristics are shown in Figure 3.1.

Table 3.1. *Specified minimum yield strength (SMYS) for pipe steel grades considered.*

Steel Grades	*SMYS* (psi)
X42	42100
X46	46400
X52	52200
X60	60200
X65	65300
X70	70300
X80	80500

Table 3.2. *Nominal dimensions of the pipes for the cases studied.*

Pipe designation	Pipe outside diameter $\overline{D}$ (in)	Pipe wall thickness $\bar{t}$ (in)
NPS 12 (300)	12.75	0.172; 0.250; 0.500
NPS 22 (550)	22.00	0.219; 0.406; 0.812
NPS 30 (750)	30.00	0.281; 0.406; 0.562; 1.188
NPS 36 (900)	36.00	0.344; 0.500; 0.688
NPS 44 (1100)	44.00	0.438; 0.562; 0.812

According to the practical range of 25 to 110 for $\overline{D/t}$, pipe dimensions considered were selected from [92] to approximately cover that range (Table 3.2).

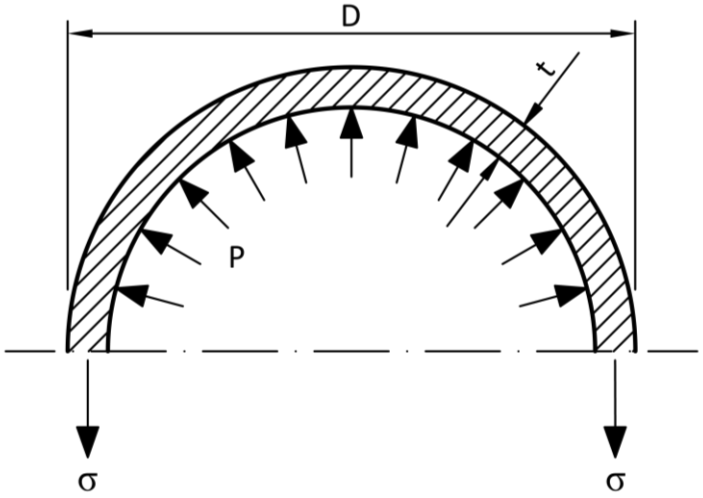

Figure 3.1. *Cross section of the pipe showing pipe geometry, internal pressure and hoop stresses.*

With the pipe geometry and the steel grades assumed, the design pressure is calculated according to Eq. (3.3) by replacing the yield strength σ_y with *SMYS* and the

other RVs with their deterministic characteristic or nominal values. According to CSA Z662:19 (table 4.2), for the natural gas and liquid pipelines, the DF is generally set to 0.8 and the location factor is varying from 1 to 0.5 (1, 0.9, 0.75, 0.7, 0.625, 0.55, 0.5) depending on location class and the surroundings of the pipeline, which make the product of the design and location factors range from 0.8 to 0.4 (0.8, 0.72, 0.6, 0.56, 0.5, 0.44, 0.4). According to ASME B31.4, for liquids and slurries pipeline systems, the design and location factors are combined into one factor having a maximum value of 0.72 (ignoring the weld joint factor). According to ASME B31.8, for gas pipeline systems, the design and location factors are also combined into one factor ranging from 0.8 to 0.4 (0.8, 0.72, 0.6, 0.5, 0.4) dependent on location classes. In this paper, the POF associated with the design factor of 0.72 is calculated, then compared with the POFs associated with the other design factors ranging from 0.8 to 0.4. With the design pressure determined, the *MOP* considered is assumed to be the same as the design pressure of each pipe in this study.

As in the intact pipes, the same pipe geometry and steel grades are assumed for corroded pipes considered in this study. The design pressure or the *MOP* for the defect-free condition is calculated according to Eq. (3.3), by replacing the yield strength σ_y with *SMYS* and the other random variables with their deterministic characteristic or nominal values and using DF of 0.72. According to ASME B31G the minimum SF (ratio of failure pressure to *MOP*) is 1.25, hence this SF will be considered in this study to get the maximum POF. Knowing the SF and the MOP, the failure pressure can be calculated. The RSTRENG equation can then be used to calculate the defect length $\bar{L}$ and depth $\bar{d}$ after assuming a ratio between $\bar{L}$ and $\bar{d}$. Furthermore, since ASME B31G states that the SF could be higher than 1.25, a graph showing the relation between the POF and higher SFs, for example, greater than 1.25 up to 1.4 for short and long corrosion defects, will be presented.

Statistical data

The yield strength σ_y of the pipe steel for a given grade follows a lognormal distribution having a mean of 1.08**SMYS* and a coefficient of variation (COV) of 4% [93]. The

statistical data for pipe outside diameter D and wall thickness t are obtained from [94] and [95], respectively. The pipe outside diameter D is assumed to follow a normal (Gaussian) distribution having a mean of the nominal value of the diameter $\overline{D}$ and COV of 0.06%. Similarly, the pipe thickness t is assumed to follow a normal (Gaussian) distribution, where the mean is determined by the bias factor 1.1, i.e., mean = 1.1*the nominal value of the thickness $\bar{t}$, and the COV is 3.3%.

The statistical data for the maximum operating pressure MOP is obtained from CSA Z662:19. The MOP RV follows a Gumbel distribution with 1.07*$\overline{MOP}$, and COV 2%. It must be noted that there is a range for the mean and the COV in CSA Z662:19 from 1.05*$\overline{MOP}$ to 1.07*$\overline{MOP}$ for the mean and from 1 to 2% for the COV. The upper bounds are considered to maximize the POF.

The statistical data for the normalized depth and length of corrosion defects are obtained from [3]. The normalized depth X_d follows a lognormal distribution having a mean of 0.8*$\overline{X_d}$ and a COV of 8%, while the normalized length X_L follows normal (Gaussian) distribution, having a mean of 0.9*$\overline{X_L}$ and a COV of 5%.

For the corroded pipes, the RSTRENG model is used to determine the failure pressure. In [21], it was found that the RSTRENG model tends to underpredict and overpredict the failure pressure for relatively long and short corrosion defects, respectively. A RV, ME, defined as the ratio between the actual and predicted failure pressure of the pipes, is used to quantify such model inaccuracy. Since the short defects are separated from the long defects using a threshold value of 2.25 for the normalized corrosion length in [21], two different probabilistic distributions were correspondingly used to represent model uncertainty. The distribution for ME given by [21] is used in this work. The statistical data for the basic random variables considered are summarized in the Table 3.3, together with the sources used for such information. Note all RVs are assumed to be statistically independent here.

Table 3.3. *Summary of statistical data of the basic random variables.*

Random Variable (RV)	Distribution	Bias factor	COV (%)	References
Yield strength (σ_y)	Lognormal	1.08	4.00	[93]
Pipe outside diameter (D)	Normal	1.00	0.06	[94]
Pipe thickness (t)	Normal	1.10	3.30	[95]
Max. operating pressure (MOP)	Gumbel	1.07	2.00	[13]
Normalized depth (X_d)	Lognormal	0.80	8.00	[3]
Normalized length (X_L)	Normal	0.90	5.00	[3]
ME (Short Corrosion)	Normal	0.936	13.3	[21]
ME (Long Corrosion)	Normal	1.149	13.3	[21]

3.4. Reliability methods

In this paper, the CMC method can be potentially used for calculating the POF due to its simplicity and accuracy. However, if the POF values will be less than 10^{-6}, this will require more than 10^8 simulation for CMC to calculate an accurate POF. As a result, FORM will be used instead because of its ability to calculate the extremely low POFs without a lot of computational efforts. The drawback of FORM is that its accuracy due to its nature of first-order approximation of the LSF. Therefore, to check the POFs estimated using FORM, Weighted Monte Carlo (WMC) method proposed by [57] is used for cross-checking. As follows, these two reliability methods used in this study are briefly reviewed.

First Order Reliability Method (FORM)

FORM is considered a semi-analytical reliability analysis method, and it's suitable for the calculation of the extremely low POFs. In FORM the POF is calculated using Eq. (3.10).

$$POF = \Phi(-\beta_{HL}) \tag{3.10}$$

where Φ is the cumulative standard normal (Gaussian) distribution function, and β_{HL} is the reliability index as proposed by Hasofer & Lind [58]. The β_{HL} is the minimum distance from the origin to the limit state surface in the standard normal space, which is transformed from the original probability space of the basic random variables. Thus, the β_{HL} is calculated by solving a nonlinear equality-constraint optimization problem. Readers of interest are referred to in [58] for more details about this method.

Weighted Monte Carlo Methods (WMC)

The WMC method is a new simulation method proposed recently by [57] for calculating extremely low POFs with proved efficiency. In the WMC, uniformly distributed samples are generated within a properly chosen interval for all RVs, and a weight index defined based on probability density value at any sample is applied to the indicator function when calculating the POF. Thus, the POF is estimated by taking the weighted sample average of the indicator function. For each sample point a weight is calculated using Eq. (3.11).

$$W_i = \prod_{j=1}^{S} f_j(i) \tag{3.11}$$

where S is the number of basic RVs, i is the sample point index, f_j is the probability density function of the j^{th} RV. The POF is calculated by Eq. (3.12),

$$POF = \frac{\sum_{i=1}^{N} I.W_i}{\sum_{i=1}^{N} W_i} \tag{3.12}$$

where, I is the indicator function, which equals to 1 for all the samples violating the LSF and 0 otherwise. For more accurate estimation, many iterations (i.e., $N_{oi} > 1$) can be done to calculate the final POF as the average of the POFs obtained from Eq. (3.12), as shown in Eq. (3.13).

$$POF = \frac{1}{N_{oi}} \sum_{k=1}^{N_{oi}} \frac{\sum_{i=1}^{N} I.W_i}{\sum_{i=1}^{N} W_i} \tag{3.13}$$

3.5. Reliability analysis results and discussion

3.5.1. Intact pipes

Figure 3.2 illustrates the relationship between POF and $\overline{D/t}$ ratios for the combined design factor of 0.72. The POF is shown by the flat curve independent of $\overline{D/t}$ and the steel grade. Note WMC is only applied to the pipes with X42 and X80 (as the results are independent of the steel grade, only the upper and lower grades are plotted). Using FORM, the POF for a design factor of 0.72 was around $2*10^{-11}$. The values calculated by WMC are slightly higher than the values calculated by FORM but they are both of the same order. Figure 3.3 illustrates the relation between the POF and the different combined design and location factors using FORM and WMC, and very close POFs are obtained for most of the cases studied.

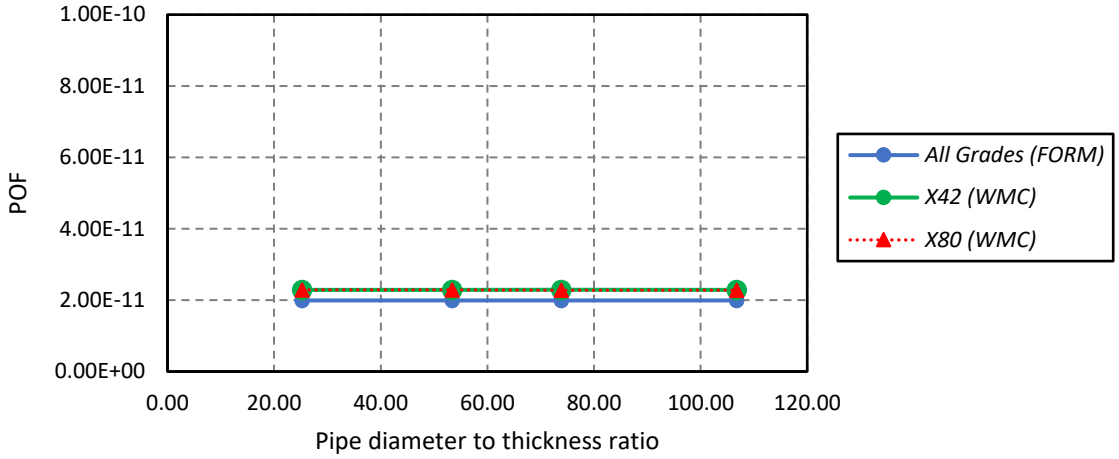

Figure 3.2. *POF associated with the 0.72 design factor for different* $\overline{D/t}$ *ratios and highest and lowest steel grades.*

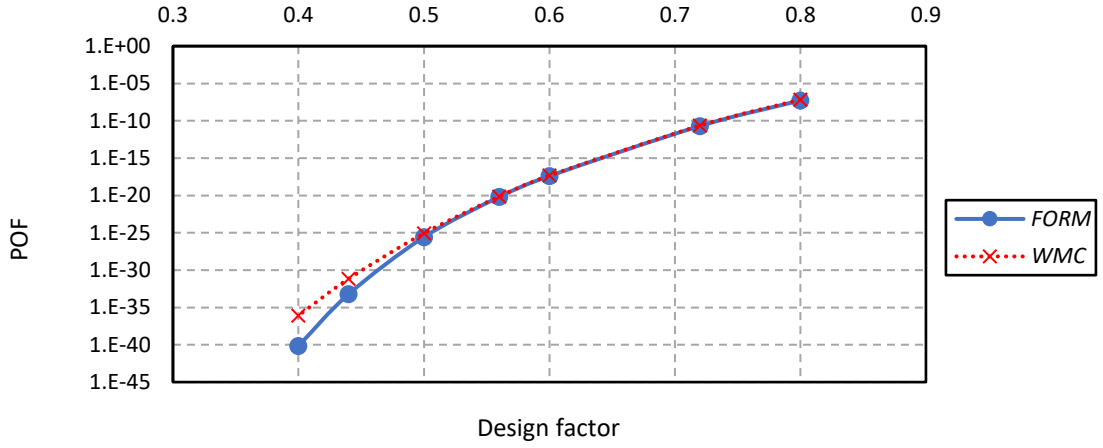

Figure 3.3. *POF associated with different design factors.*

3.5.2. Pipes with corrosion defects

The corrosion defect length and depth for different pipes mentioned in Table 3.2 has been calculated for different $\overline{L/d}$ ratios. It was observed that for a certain $\overline{D/t}$, for different $\overline{L/d}$ ratios, the normalized length $\overline{X_L}$ and depth $\overline{X_d}$ is not changing despite the change of the diameter and thickness. This indicates, according to Eq. (3.5), that the

POF will be a factor of D/t, not a factor of the diameter or the thickness alone. Consequently, the results of the NPS 30 (750) will only be considered as it covers a wide $\overline{D/t}$ range (25.25 to 106.76).

Calculated POFs without including ME

Figure 3.4 and Figure 3.5 illustrate the relationship between POF, calculated using FORM, and $\overline{L/d}$ ratio for different steel grades, and different $\overline{D/t}$ ratios, respectively, for a SF of 1.25. The results show that the maximum POF is associated with the highest steel grade X80 and the lowest $\overline{D/t}$ ratio. Figure 3.6 shows that the results of FORM and WMC are of the same order of accuracy and following the same trend, which provide a validation to our results. It can be concluded that the maximum POF associated with the 1.25 SF without considering ME is approximately $2*10^{-9}$.

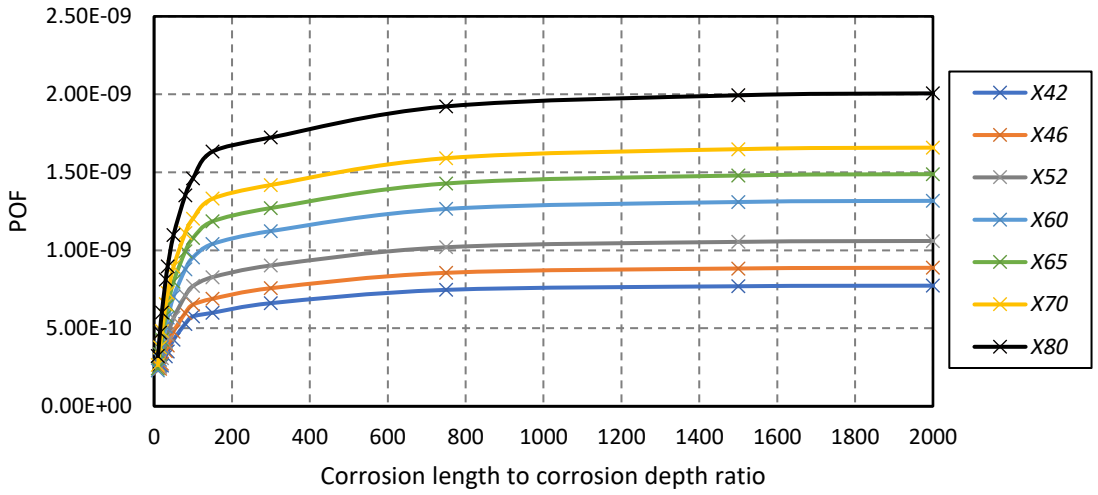

Figure 3.4. *POFs associated with SF=1.25 for corroded pipes with different $\overline{L/d}$ and different steel grades without considering ME: $\overline{D/t}$ =25.25.*

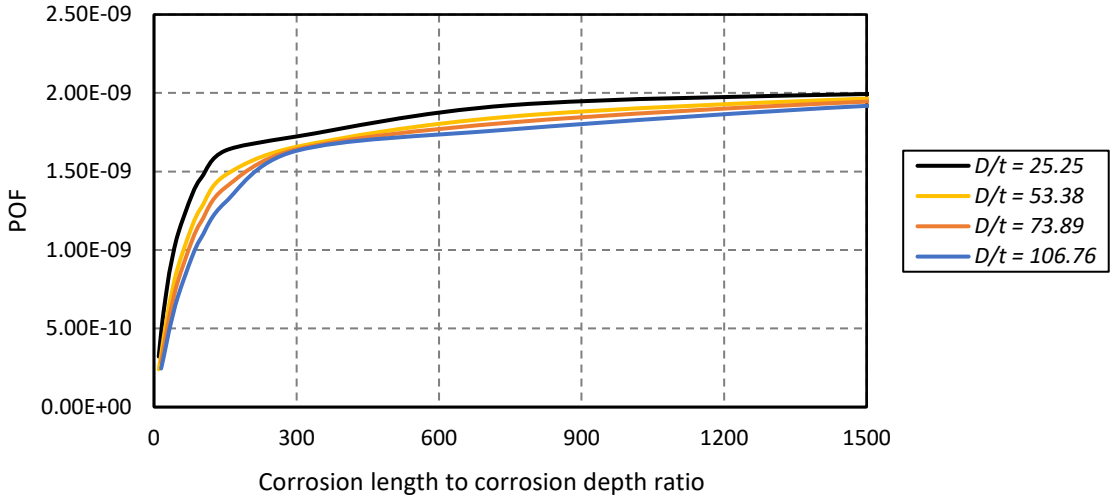

Figure 3.5. *POFs associated with SF = 1.25 for corroded pipes with different* $\overline{L/d}$ *and different* $\overline{D/t}$ *without including* ME*: X80 steel grade.*

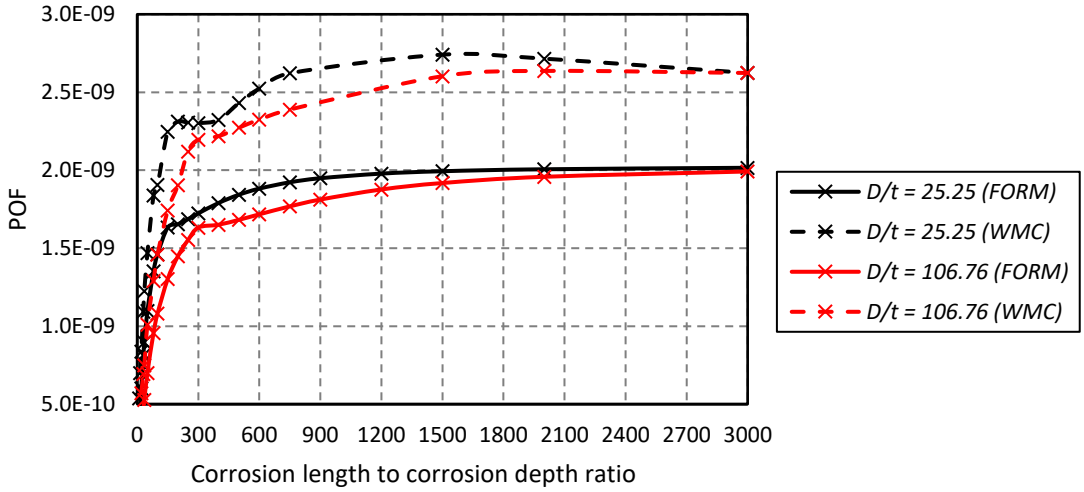

Figure 3.6. *Comparison of the predicted POFs associated with SF = 1.25 using FORM and WMC for corroded pipes without including* ME*.*

According to [21], the normalized length 2.25 is the limit between relatively short and long corrosion defects for the RSTRENG equation. From the calculated corrosion

lengths and depths, it was found that for the pipes used in practice, the normalized length is around 2.25 when the length to depth ratio of the corrosion defect is around 30. Thus, $\overline{L/d}$ of 30 is assumed to be the limit between short and long corrosion defects. Consequently, the model error ME for short corrosion defects will be applied to the cases of $\overline{L/d}$ < 30 and ME for long corrosion defects will be applied to the cases of $\overline{L/d}$ > 30 .

Calculated POFs for short deep corrosion defect including ME

Figure 3.7 and Figure 3.8 illustrate the relationship between POF and $\overline{L/d}$ ratio for different steel grades, and different $\overline{D/t}$ ratios, respectively, for a SF of 1.25 for pipes with short corrosion defects considering ME. The results show that the maximum POF is associated with the highest steel grade X80 and the lowest $\overline{D/t}$ ratio. Figure 3.9 shows that the results of FORM and WMC are of the same order of accuracy and following the same trend. It can be concluded that the maximum POF associated with the SF = 1.25 for pipes with short corrosion defects is approximately $3.12*10^{-2}$. In Figure 3.10 the maximum POFs associated with the SFs are plotted.

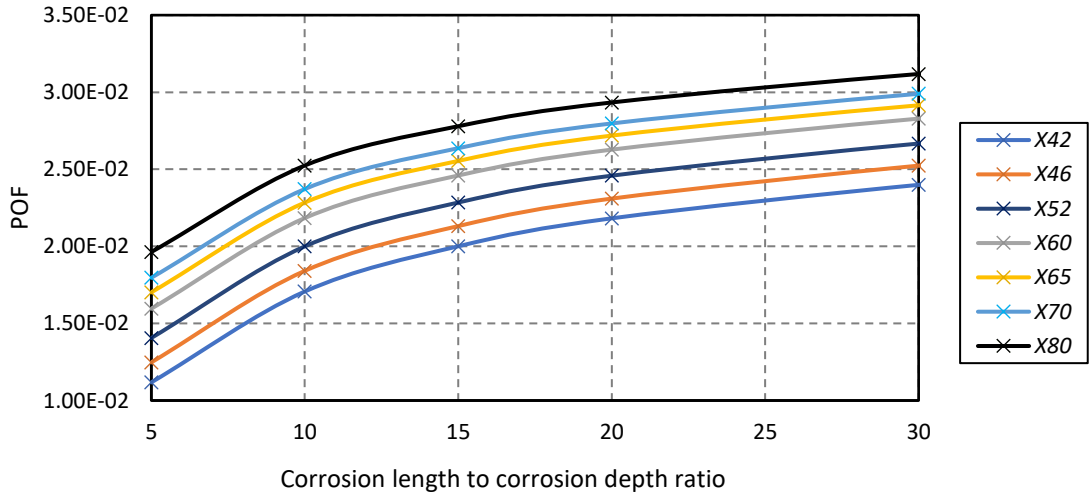

Figure 3.7. *POFs associated with SF = 1.25 for pipes with short deep corrosion defects considering different $\overline{L/d}$ and different $\overline{D/t}$ including ME: $\overline{D/t}$=25.25.*

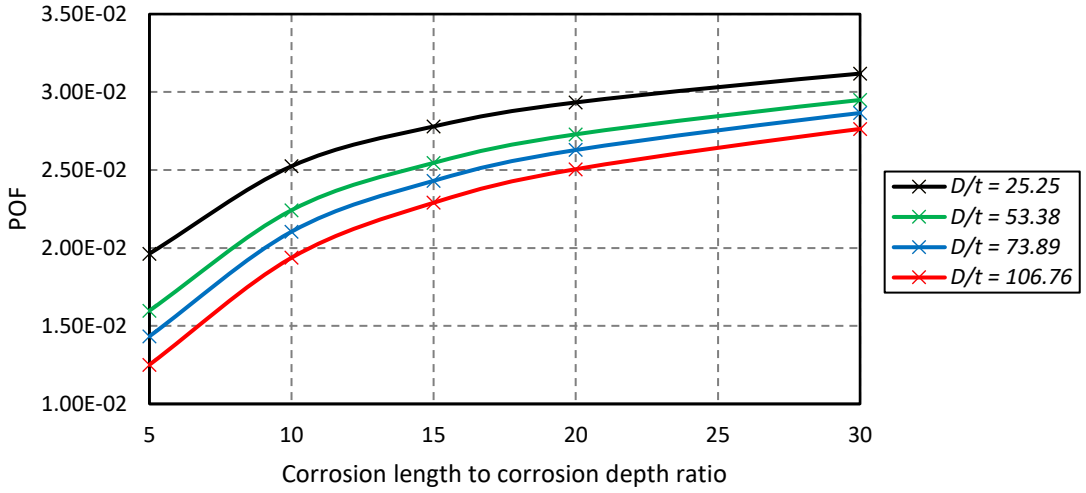

Figure 3.8. *POFs associated with SF = 1.25 for pipes with short deep corrosion defects considering different* $\overline{\boldsymbol{L/d}}$ *and different* $\overline{\boldsymbol{D/t}}$ *including* $\boldsymbol{ME}$*: X80 steel grade.*

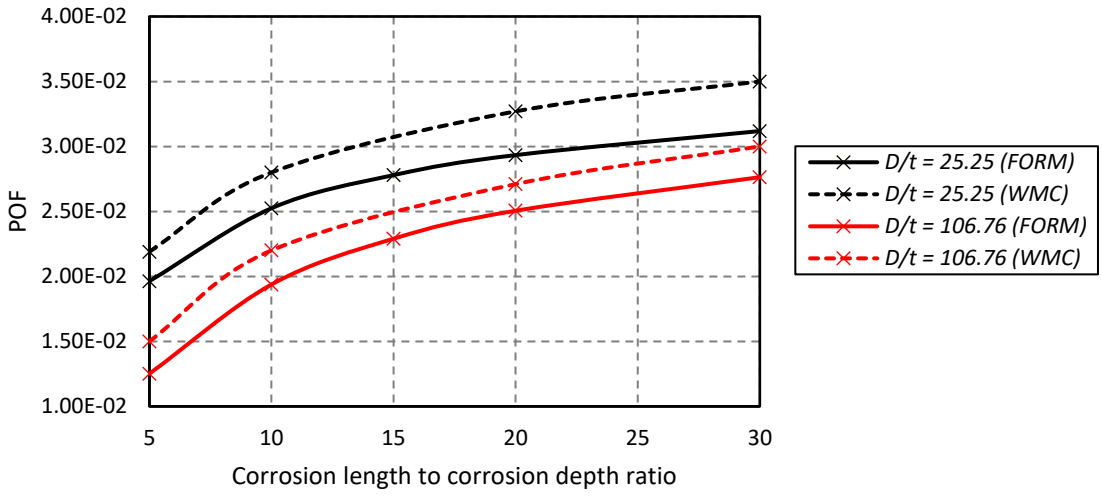

Figure 3.9. *Comparison of the predicted POFs associated with SF = 1.25 using FORM and WMC for pipes with short deep corrosion defects considering* $\boldsymbol{ME}$*.*

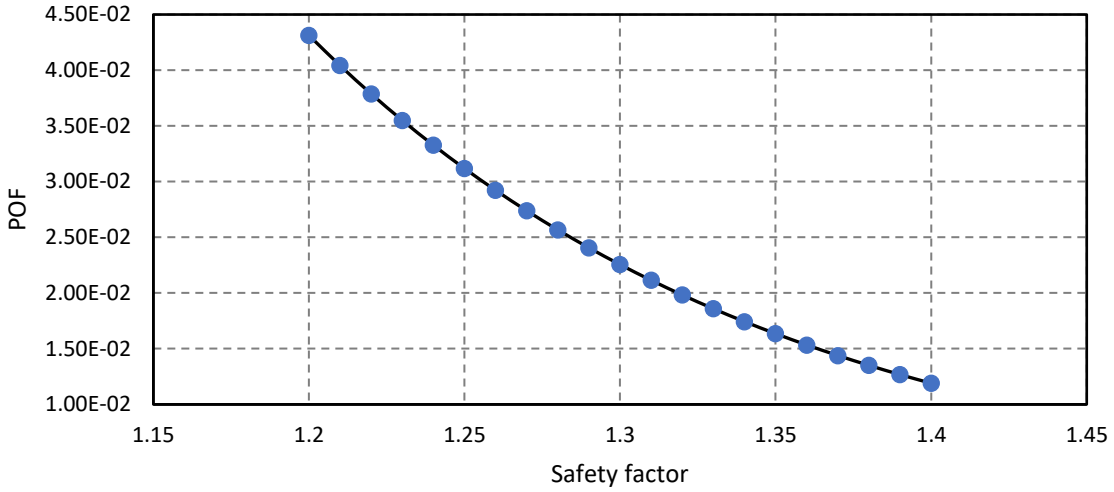

Figure 3.10. *POF associated with different SFs for pipes with short deep corrosion defects considering* $\boldsymbol{ME}$.

Calculated POFs for long shallow corrosion defects including ME

Figure 3.11 and Figure 3.12 illustrate the relationship between POF and $\overline{L/d}$ ratio for different steel grades, and different $\overline{D/t}$ ratios, respectively, for a SF of 1.25 for long corrosion defects. Figure 3.13 shows that the results of FORM and WMC are of the same order and following the same trend. It can be concluded that the maximum POF associated with the 1.25 SF for long corrosion defects is approximately $3.9*10^{-5}$. In Figure 3.14 the maximum POFs associated with the SFs for the extreme conditions mentioned above are calculated and plotted.

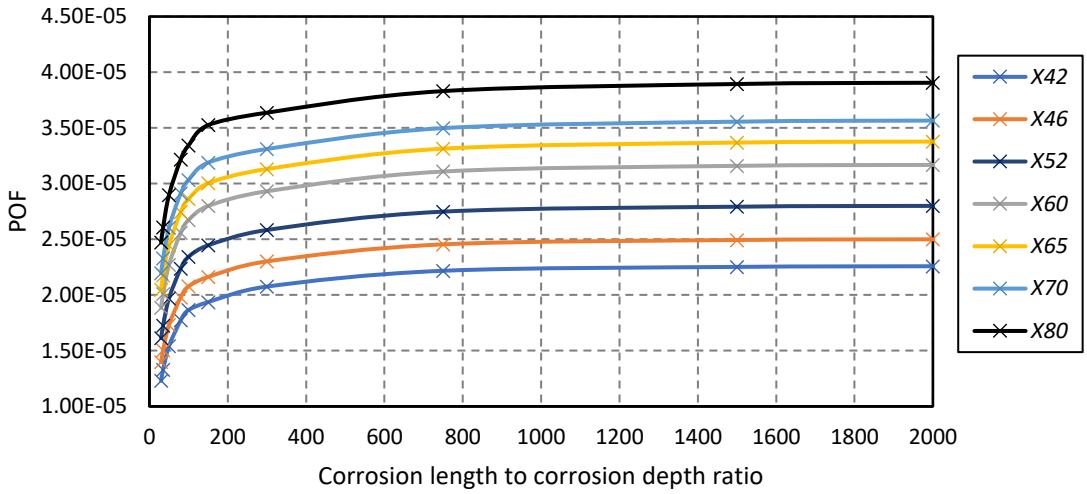

Figure 3.11. *POFs associated with SF = 1.25 for pipes with long shallow corrosion defects considering different* $\overline{\boldsymbol{L/d}}$ *and different steel grades including* $\boldsymbol{ME}$*:* $\overline{\boldsymbol{D/t}}$*=25.25.*

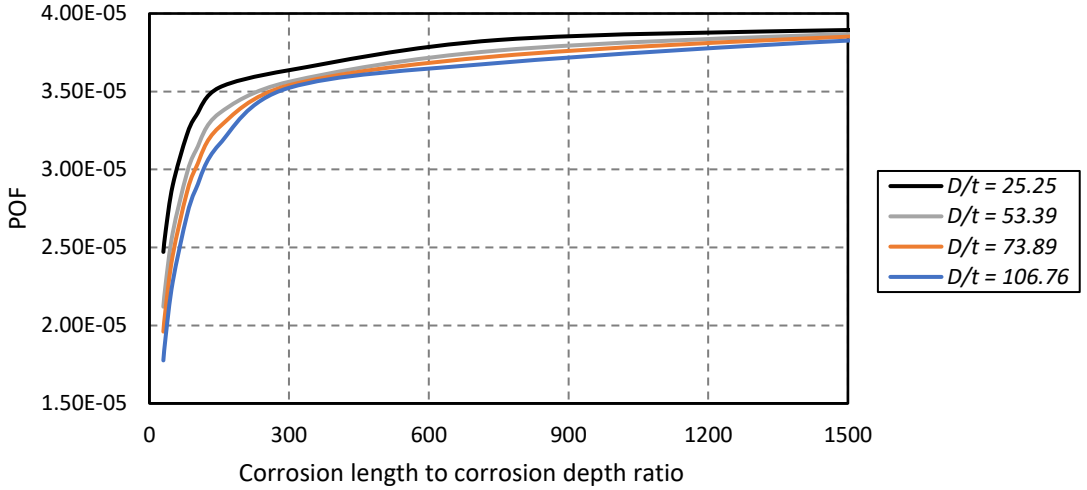

Figure 3.12. *POFs for long shallow corrosion defects considering different* $\overline{\boldsymbol{L/d}}$*, different* $\overline{\boldsymbol{D/t}}$*, and* $\boldsymbol{ME}$ *at SF=1.25: X80 steel grade.*

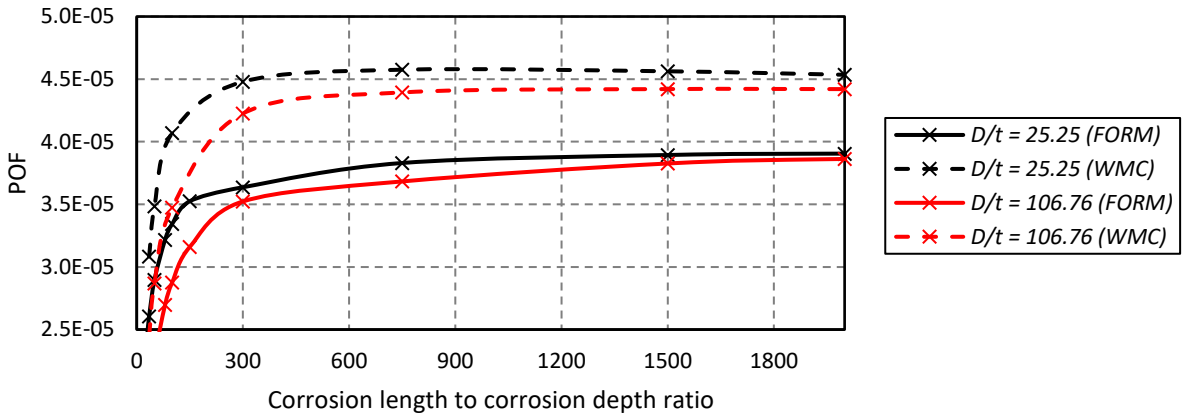

Figure 3.13. *Comparison between FORM and WMC for long shallow corrosion defects considering* $\boldsymbol{ME}$ *at SF=1.25.*

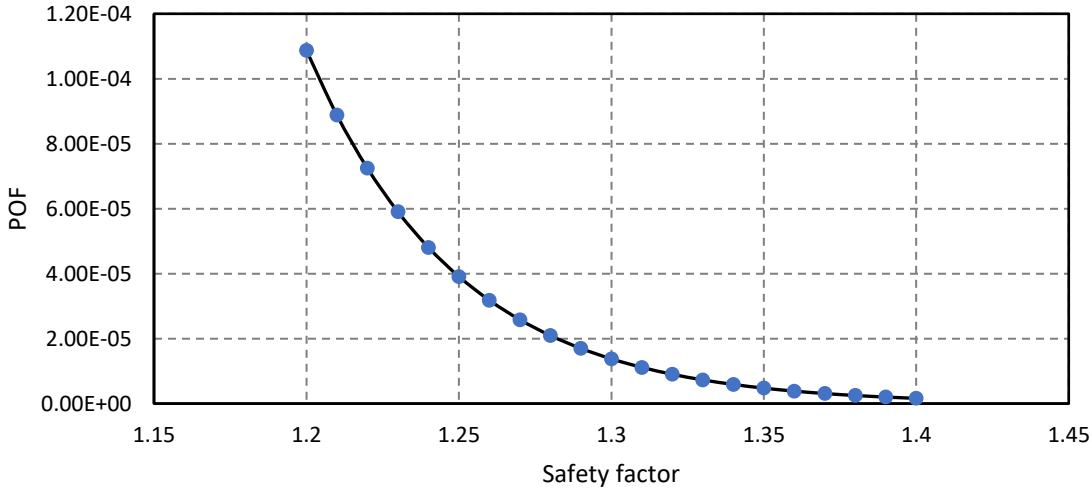

Figure 3.14. *POF associated with SFs for long shallow corrosion defects considering* $\boldsymbol{ME}$.

3.5.3. Interpretation of POF results for pipes with corrosion defects

It can be noticed that, after considering RSTRENG model error through ME, the POF dramatically increases, especially for pipes with short corrosion defects (Figure 3.7 and Figure 3.8). Specifically, for pipes with short corrosion defects, the RSTRENG model overpredicts the mean failure pressure P_f with relatively large uncertainty. As such, the true failure pressure is lower on average and more scattered as indicated by the COV (13.3%) for ME. This significant effect of ME is demonstrated in Figure 3.15(a): shifting the failure pressure distribution closer to the *MOP* distribution and inflating the distribution due to the large COV. Consequently, POF increases significantly after including ME. On the contrary, for pipes with long corrosion defects, the RSTRENG model underpredicts the mean failure pressure P_f, thus the true failure pressure is higher on average. However, the probability distribution of the failure pressure is inflated similarly due to the large COV (13.3%) for ME. Similar to the case of pipes with short corrosion defects, P_f increases but less (Figure 3.4 and Figure 3.5). The interpretation of this point is that the POF in the two cases highly depends on the shape of the tails of the P_f distributions. After incorporating the ME in the P_f, the distribution has a heavier left tail, i.e., the values of the distribution at the left tail are higher than the values of the P_f distribution without ME, as shown in Figure 3.15(b). This consequently increases the POF. The comparison between the pipes with short and long corrosion defects shows that the pipes with short defects have a larger POF and needs more care. The comparison between the POFs estimated considering ME shows that there is urgent need to improve the RSTRENG model or develop more accurate failure pressure prediction models.

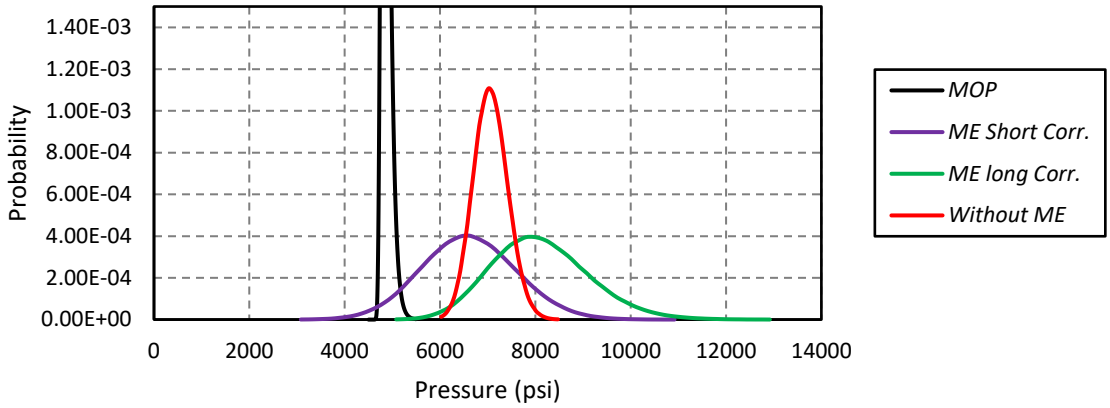

(a) P_f and MOP statistical distributions

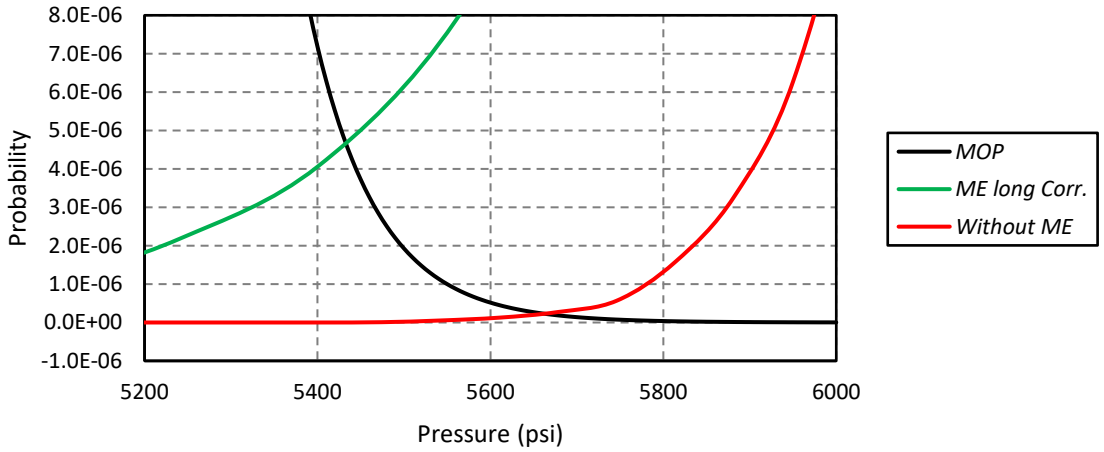

(b) Zoom in on the interaction of P_f distributions with the MOP distribution

Figure 3.15. *Change of failure pressure distribution with respect to MOP distribution after including model error/uncertainty (**ME**): $\bar{D}$=30, $\bar{t}$=1.188, SMYS=80500, $\overline{L/d}$=750.*

Further examination of all the curves describing the change of POF with the $\overline{L/d}$ shows a steep slope at low $\overline{L/d}$ values and they flatten as $\overline{L/d}$ increases. This can be interpreted by the rate of change of the corrosion defect length and depth values calculated for the different $\overline{L/d}$. At low $\overline{L/d}$ the value of the depth decreases precipitously and the

length increases linearly. Consequently, the value of the normalized depth decreases in Eq. (3.5), and the mean of the failure pressure decreases as shown in Figure 3.16, hence the POF increases (due to the decrease of the relative distance between the two curves in Figure 3.16). After a certain ratio of $\overline{L/d}$ (between 50 and 300) the change in depth become negligible and the change in the P_f distribution shape and position become very small, and the length continues to increase linearly with the increase of $\overline{L/d}$. However, the effect of the normalized depth and length increase (through the Folias factor) on the failure pressure become much lower than before, so the POF is still increasing but at a much slower rate.

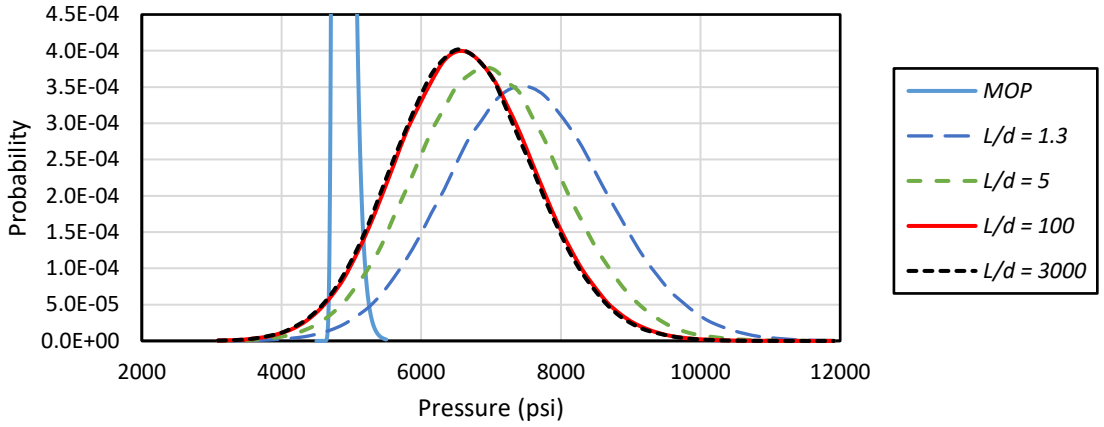

(a) Effect of changing $\overline{L/d}$ ratio on the P_f distribution

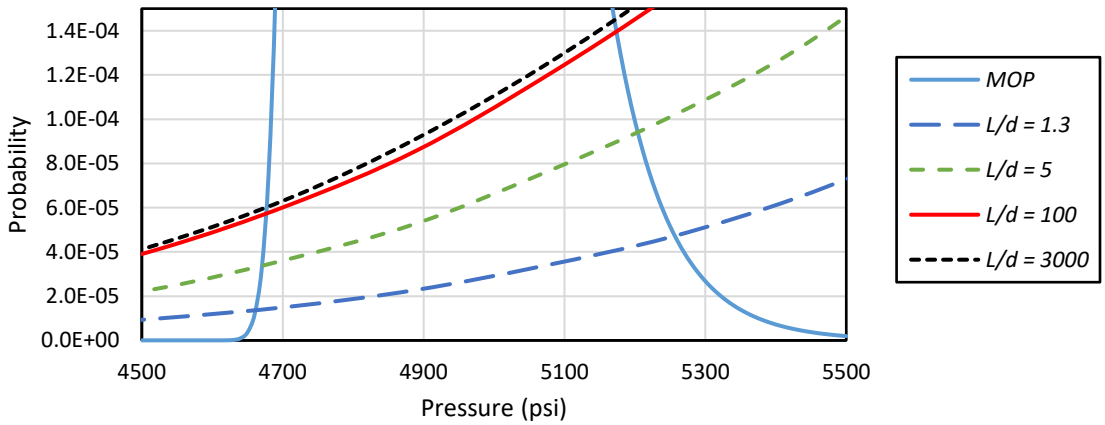

(b) Zoom in on the intersection of the P_f distributions with the MOP distribution

Figure 3.16. *Change of failure pressure distribution with respect to MOP distribution for different $\overline{L/d}$.*

It can be noticed (e.g., from Figure 3.4, Figure 3.7, and Figure 3.11) that the POF increases with the increase of *SMYS* (i.e., steel grade); the reason behind this is that the relative distance between the *MOP* and the P_f is based on the fixed value of the chosen SF, while with the increase of *SMYS* the standard deviations of the *MOP* and the P_f distribution increase, hence the overlap between the two distributions increase and the

POF increases. This shows a need to use different SFs for different pipe steel grades to achieve consistent reliability levels in the design and maintenance of pipelines.

It must be mentioned that the change of the POF curves due to the change of $\overline{D/t}$ is only due to the statistical properties of the corrosion length and depth, and in case these variables are substituted in the LSF as deterministic values there won't be a variation of POF curves due to the change of $\overline{D/t}$ or $\overline{L/d}$ as shown in Figure 3.17 and Figure 3.18.

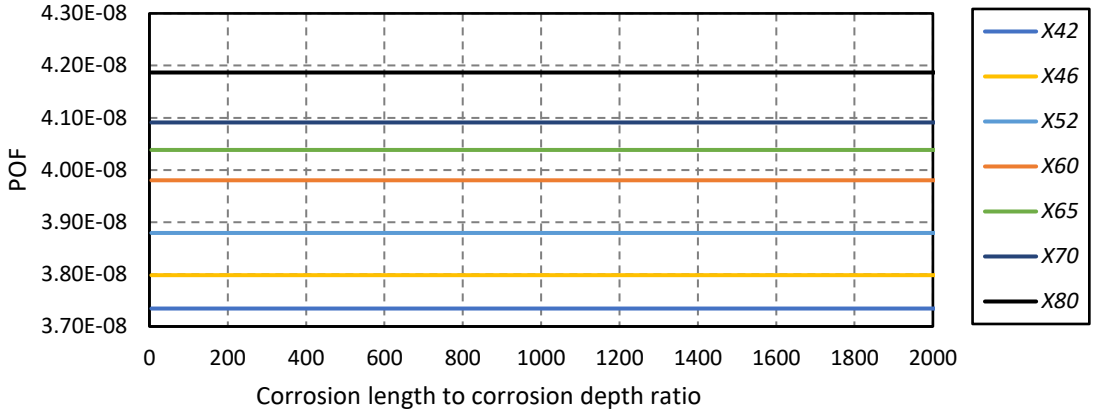

Figure 3.17. *POF for different* $\overline{\boldsymbol{L/d}}$ *and different steel grades with deterministic* $\overline{\boldsymbol{L}}$ *and* $\overline{\boldsymbol{d}}$ *values and without* $\boldsymbol{ME}$ *at SF=1.25.*

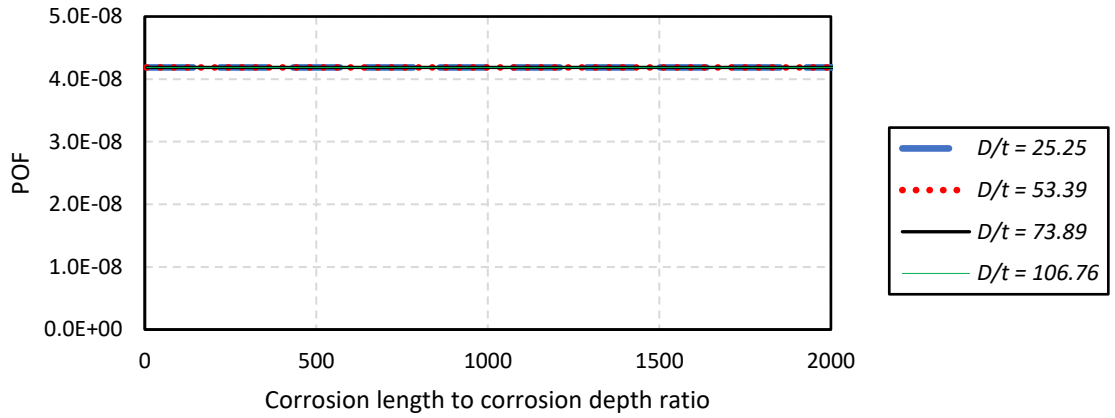

Figure 3.18. *POF for different* $\overline{\boldsymbol{L/d}}$ *and different* $\overline{\boldsymbol{D/t}}$ *with deterministic* $\overline{\boldsymbol{L}}$ *and* $\overline{\boldsymbol{d}}$ *values and without* $\boldsymbol{ME}$ *at SF=1.25.*

3.5.4. Comparison with target POFs

The target safety levels are dependent on many variables such as: the consequence of failure, location and contents of pipelines, relevant rules, access to inspection and repair. However, [96] proposed simpler classification that included three safety classes, i.e., low, normal, and high classes, depending on the failure consequence in terms of human injuries or environmental and economic damages. According to [96], the target POF ranges for low, normal, high safety classes against the ultimate limit state are $10^{-2} - 10^{-3}$, $10^{-3} - 10^{-4}$, and $10^{-4} - 10^{-5}$, respectively. The yield of defect-free and the burst of corroded pipes due to internal pressure considered in this paper are ultimate limit states. Therefore, the DF of 0.8 (which is the highest DF corresponding to highest POF) for yielding of intact pipes leads to very safe design, since POF = $5.3*10^{-8}$ is lower than the lower bound (10^{-5}) of the high safety class. The SF of 1.25 for pipes with long corrosion defects is $3.9*10^{-5}$, which is the close to the lower bound (10^{-5}) of the high safety class. However, for the pipes with short corrosion defects the POF associated with the SF of 1.25 is $3.12*10^{-2}$, which leads the pipes to be in a very low safety class.

3.6. Conclusion

In this paper reliability analyses were performed to determine the POFs associated with the design and safety factors, which are used in the design of intact steel pipes against yielding, and the integrity assessment of corroded steel pipes against burst failure. Different design cases of pipes with various corrosion defects were considered, as representative cases in engineering practice. Two different reliability methods, i.e., FORM and the WMC, were used for cross-checking. The POF associated with the design factor of 0.72 for yielding of intact pipes is found to be in a very high safety class with the maximum POF of $5.3*10^{-8}$. The maximum POF associated with the safety factor of 1.25 for corroded steel pipe failure is found to be approximately $2*10^{-9}$ when using the RSTRENG modified area method without considering the model error (uncertainty). However, the model error (uncertainty) ME affects the POF significantly. The comparison between the POFs estimated considering ME shows that there is urgent need to improve the RSTRENG model or develop more accurate failure pressure prediction models. The maximum POF is found to be approximately $3.9*10^{-5}$ and $3.12*10^{-2}$, respectively, for pipes with long and short corrosion defects. This implies that the safety factor of 1.25 makes pipes with long and short corrosion defects fall in a high safety class and a low safety class, respectively. The inconsistence in the reliability levels (or POFs) shows a need to use different safety factors to achieve consistent reliability levels in the design and maintenance of pipelines under different scenarios (e.g., different pipe steel grades, long or short defects).

4. Strain-Based Reliability Analysis of Dented Pipelines Using a Response Surface Method

4.1. Introduction

Transmission of oil and gas from their sources to consumers is crucial for the oil and gas industry. Pipelines are considered one of the best and safest methods [77] used by many oil and gas transporting companies in transporting oil and gas for long distances. One of the critical challenges of these companies is to maintain their pipelines and ensure their safety against any harm to humans or the environment, as unchecked pipelines defects can lead to oil and gas leakage or even pipeline burst. Therefore, these companies pay much attention to accessing the pipelines to check if there is a need to repair or change parts of their pipelines.

Several defect types can reduce the safety levels of pipelines. One type of defect is the over-straining of the pipe material beyond its yield capacity [97] from over-pressuring the pipe or from pipe dents, which will be the defect to be studied in this paper. Dent defects cause the development of high stress and strain regions in the pipe material, which can be a weak point for the development of cracks leading to the failure of the pipe after several internal pressure loading cycles. The assessment of the dent defects and the evaluation of their integrity and suitability for operation is performed by fatigue or strain-based analysis. Equations for the evaluation of strains within a plain dent defect are presented in the American code for liquid and slurries pipelines, ASME B31.4 [14]. Also, Kainat et al. [42] used the equivalent plastic strain as a measure for the severity of the dent defect in pipes. In this paper, a strain-based exceedance criterion is adopted for accessing the safety of the pipe.

The safety of the pipe defects is checked and evaluated by calculating their probability of failure (POF) by a reliability analysis technique. The POF is then compared to the reliability target of the defect to determine its safety level. Several reliability techniques

like the Monte Carlo Simulation (MCS) method [56], the first-order reliability method (FORM) [58], the second-order reliability method (SORM) [59], and the response surface method (RSM) [61–63,65,66,74,98] exist for the calculation of the POF. In this paper, an RSM will be used together with the FORM to perform the strain-based reliability analysis of dented pipes.

Several factors, or parameters, can control the value of the POF of the dented defects. This paper investigated the effect of indenter size, the dent depth (DD), the pipe outside diameter (OD), the pipe wall thickness (WT), and the pipe length on the POF of the dent defect. The POF of dented pipe defects is calculated using a strain-based RSM reliability analysis to determine the main factors controlling the POF. To be specific, the second section presents an overview of the dent defects in a pipeline and the pipe configurations used in this study. The third section describes the finite element (FE) model developed for this study to obtain the strain results and presents a description of the load case considered for analysis. Section 4 presents the limit state function (LSF) and the random variables (RVs) considered for the reliability analysis. Section 5 explains the RSM technique used for the calculation of the POF. In Section 6, the method of the RSM used in this paper is verified using two simple analytical examples before applying it to defected pipes. Finally, in Section 7, the reliability results of the defected pipes are presented to discuss the main factors affecting the POF of dent defects.

4.2. Dent defects and pipe configurations

Dent defects can reduce the life span of a pipeline [10], and they have to be constantly monitored and checked to ensure the safety and integrity of pipelines. Many reasons can cause dent defects in pipelines. A widespread reason is the impact of the construction equipment on the pipes, and dents are usually found on the top part of the pipes. Another reason is the constant pressure of rocks surrounding a buried pipeline, which can usually be found at the bottom of the pipe. In the case of a dent defect resulting from equipment impact, the dent defect is considered an

unconstrained dent defect, as the indenter is usually removed after causing the defect and before the pipe operation. In the other case of pipe indentation from rocks surrounding the pipeline, the dent defect is considered a constrained dent defect, as the indenter is restricting the rebound of the pipe during the pipe operation. The constrained and unconstrained dent defects produce different results for the stresses and the strains in the pipe; that is why they should be treated differently.

Dent defects can also be categorized by the shape of the dent, as mentioned by [10]. For example, there are smooth dents where the change in the dent profile is smooth, and there is no sudden change in the pipe curvature. Another type is the kinked dents, where the change in the dent profile is sudden. There is also a difference between plain dents and gauges. To explain, in plain dents, the WT of the pipe remains intact with no material loss, while in a gauge, part of the pipe material is lost, causing a metal-loss defect in the pipe. In this study, only unconstrained dent defects are considered, and no metal loss is deemed to happen in the pipe.

In this paper, a strain-based damage criterion is considered for the reliability analysis. To elaborate, the pipe is assumed to be damaged when the maximum equivalent plastic strain (MEPS) occurring the dented area reaches the strain capacity (SC) of the pipe material. The SC of the pipe material is obtained by performing standard uniaxial tensile test on the pipe material used in this study. The MEPS is chosen as a representative of the strain demand in the reliability problem for two main reasons. Firstly, the MEPS is a measure of the history of the plastic deformation of the pipe material, and it corresponds to the plastic strain value on the uniaxial stress-strain curve in case of a uniaxial loading of the material. The value of the equivalent plastic strain at any point in the pipe material represents the maximum strain level that this point has witnessed during its loading history. As previously mentioned, the main reason for dent failures is the exceedance of the material strain capacity at some points due to the mechanical stress from the indenter on the pipe, which create micro cracks that can develop to eventually cause the pipe failure. Therefore, the equivalent plastic strains are considered to have a strong indication of the material damage in the dent area, and

will be used in this study to assess the severity of the dent defects. Secondly, because in a 3D problem, the plastic strain tensor is a six-dimensional tensor, which is not practical to be used to describe failure in reliability analysis. Therefore, the equivalent plastic strain (EPS) value will be used to represent the state of the plastic strain tensor and the severity of the dent defect on the pipe material.

This study is to calculate the POF of unrestricted dent defects. The dent is going to be simulated by indenting a FE model of the pipe with a spherical rigid indenter of different sizes and with different DDs to investigate the parameters controlling the POF of the dent defect. Regarding the DD limits, CSA Z662:19 [13] states that pipes with DDs of more than 6% of the pipe's OD have to be mitigated, which sets the ceiling for the maximum DD that can be developed in a pipe. Also, in this study, two different pipe configurations, presented in Table 4.1, will be considered to test the effect of changing the pipe geometry on the results. Only one steel grade will be considered in this study, which is X52 vintage steel that has a specified minimum yield strength (SMYS) of 360 MPa [47].

Table 4.1. *Pipe configuration used in this study.*

Pipe designation	Outside Diameter (OD) (mm)	Wall Thickness (WT) (mm)	OD/WT ratio	Steel grade
NPS 30	762	7.14	106.7	X52 Vintage
NPS 12	323.85	6.35	51	X52 Vintage

4.3. Finite element model and loading scenario

This study is focused on strain-based reliability analysis of the pipes. Therefore, having a detailed and reliable FE model is essential to accurately calculate the internal strains in a pipeline generated from the dent defects. The reliability technique used in this study demands the analysis of many FE models per defect to calculate the POF of the defect. This calls for an FE model that produces accurate results for the strains while at the same does not take much time to calculate the maximum strains.

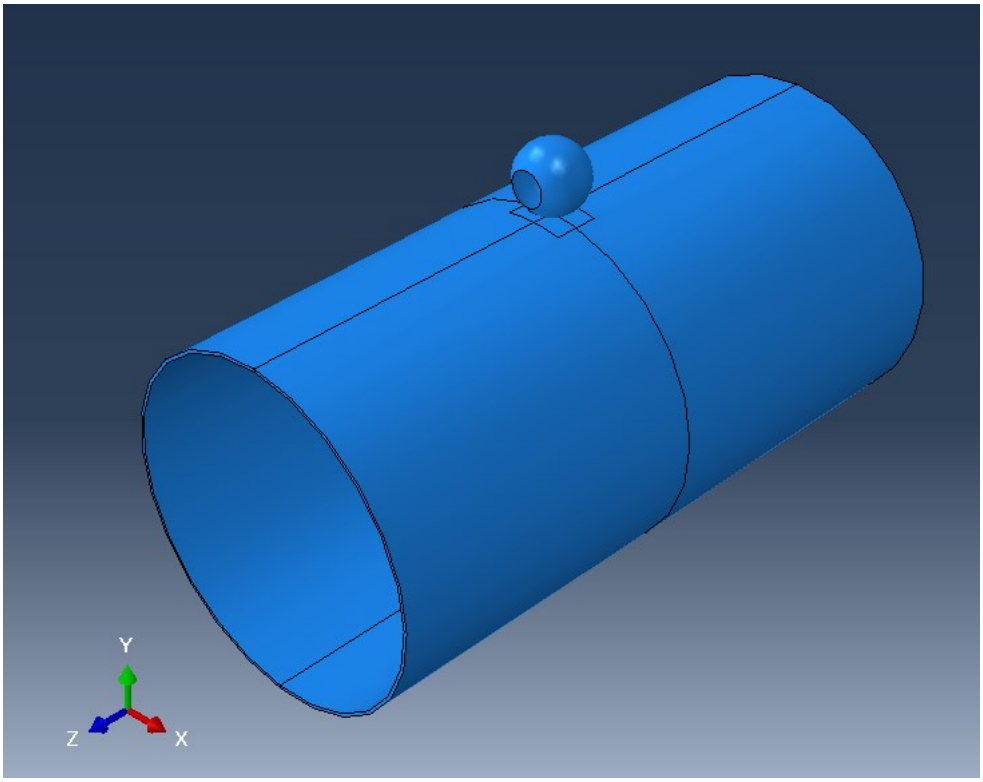

Figure 4.1. *Full pipe showing the global coordinate system and the indenter.*

Finite element analysis (FEA) software package, ABAQUS (version 2017) [99], was used to create and analyze the dent defects in this study. To create a computationally efficient model, the symmetry of the problem was taken into account. Figure 4.1 shows the full pipe to be analyzed, and it can be seen that this problem is symmetric about the XY and the YZ plane at the middle of the full pipe. This means that with considering the appropriate boundary conditions, only a quarter of the pipe can be used to accurately get the strains generated in the pipe.

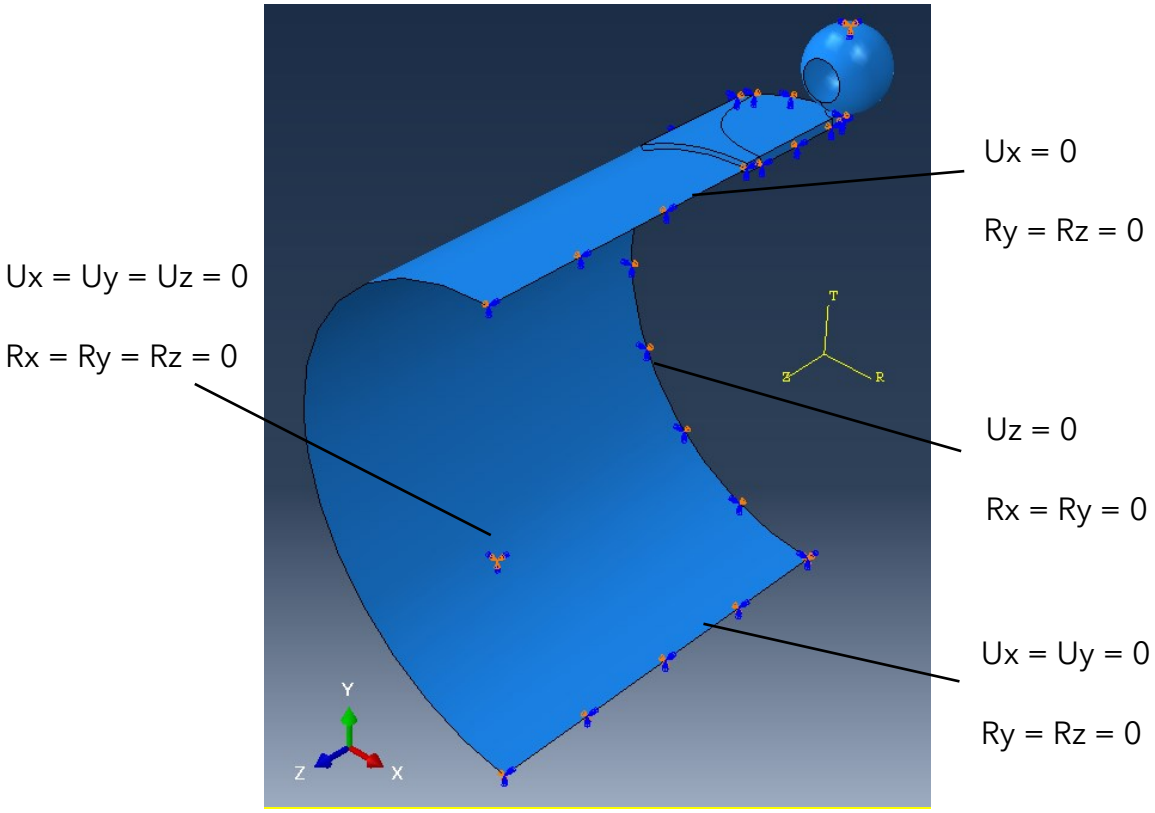

Figure 4.2. *FE model of the quarter of the pipe showing the boundary conditions.*

Figure 4.2 shows the quarter of the FE model for the pipe considered for analysis with the appropriate boundary conditions. The pipe is symmetric about the YZ plane that contains the axis of the pipe, so the quarter pipe is prevented from the translation in the X direction and from the rotation about the Y and Z axes at the YZ plane of symmetry of the full pipe. Also, the full pipe is symmetric in the longitudinal direction on both sides of the XY plane at the middle of the pipe, so the quarter pipe is prevented from translation in the Z-axis direction and from rotation about the X and Y axes at the XY plane of symmetry. The pipe will be resting on the ground, so the bottom of the pipe will be prevented from translation in the vertical direction (Y-axis direction), as shown in Figure 4.2. Regarding the end conditions of the pipe, all the displacements and rotations, except the displacement in the radial direction, of the far edge of the pipe is coupled with a reference point located at the center of the pipe at the same plane of

the far edge of the pipe. This point will be fixed from any translation or rotation. The reason behind fixing this point is that for long pipe segments, only part of the pipe from the middle of the segment is considered for the study. This part is attached (and partially restricted from movement) to the rest of the pipe segment from its two ends, which makes it more similar to a plane strain problem. Therefore, the ends of the pipe part considered for analysis is restricted from movement, except for the movement in the radial direction. The deformation in the radial direction is allowed as, in reality, the remaining pipe segment (attached to the ends of the pipe part under study) and pipe part considered for the study are expanding in the radial direction from the internal pressure with approximately the same amount.

Regarding the choice of elements of quarter pipe mesh, in case of only shooting for accurate results, the full quadratic integration solid element "C3D20" in ABAQUS can be chosen for the pipe. However, the problem's size and analysis time will be prohibitive for reliability analyses. On the other hand, if the pipe elements are chosen to shell elements S3 and S4 in ABAQUS, the models will be computationally efficient. However, the accuracy of the results will be compromised. Different pipe model has been found in the literature [36,100] contained mixed element types that are used for the structural assessment of pipes and pipe connections. Therefore, a new hybrid model using S3 and S4 shell elements and C3D20, C3D20R, and C3D8 solid elements were created to get the strains for the reliability analyses.

S3 and S4 shell elements are used for meshing the main body of the pipe to make the model computationally efficient. However, at the location of the indentation, several types of ABAQUS solid elements are used to obtain the strains accurately, as the changes in the strains at this location are significant. The solid and shell parts are connected with the ABAQUS "Shell-to-solid coupling" constraint to make sure of the continuity of the stresses and the strains.

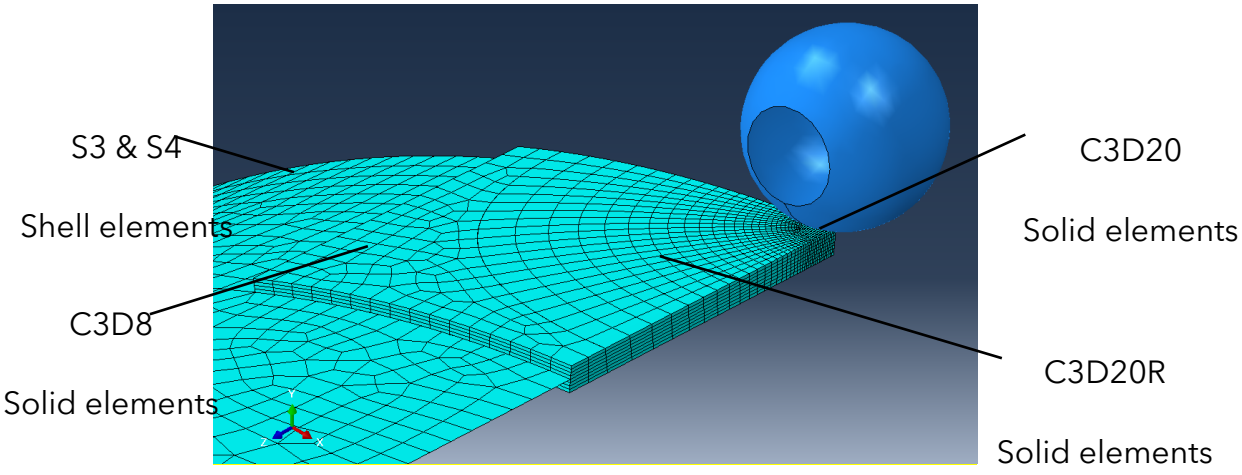

Figure 4.3. *Different types of FEs used in the FE model.*

The solid part consists of three parts, as shown in Figure 4.3, connected by tie constraints. A full-integration quadrilateral quadratic solid FE (C3D20) is used in the first part, as this region is in direct contact with the indenter to accurately capture the dramatic change in the strain values under the indenter. In the second part, a coarser mesh of the reduced integration version (C3D20R) of the same element was used as the variation of the strains along the thickness in this region is not very significant. The third part was meshed using full-integration quadrilateral linear solid FE (C3D8), and it only exists to connect the second part with the shell part without any irregularities in the geometric representation of the pipe.

Note that Figure 4.1, Figure 4.2, and Figure 4.3 are not to scale as they are only presented to explain the FE model and meshing. Also, in Figure 4.3, the shell element is shown as a surface. However, once the shell thickness is rendered, the thickness of the shell element will be matching the thickness of the solid part, namely the pipe thickness.

The pipe material stress-strain curve is modeled by the Ramberg-Osgood constitutive relation given in Eq. (4.1). The used steel is having a young's modulus of 210000 MPa and a yield strength of 386.6 MPa, and its stress-strain curve is plotted in Figure 4.4.

$$\frac{\varepsilon}{\varepsilon_y} = \frac{\sigma}{\sigma_y} + \alpha \left(\frac{\sigma}{\sigma_y}\right)^n \tag{4.1}$$

Where σ and ε are the stress and the strain, respectively. σ_y and ε_y are the yield stress and strain, respectively, of the pipe material. α is taken equal to 1.72 and n is taken equal to 12 in this study.

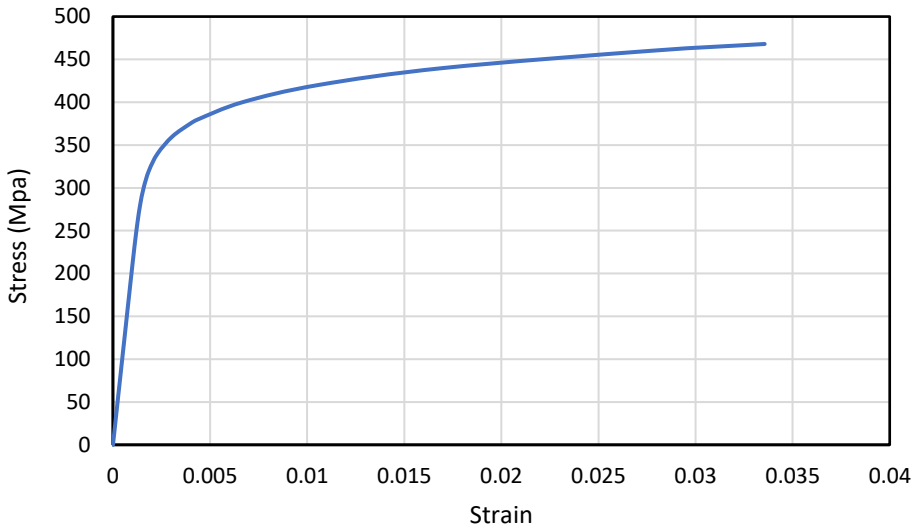

Figure 4.4. *Stress-strain curve modelled by the Ramberg-Osgood model.*

The pipe is indented by placing the spherical indenter on the pipe outer surface and moving it towards the center of the pipe by the specified DD value. In the ABAQUS model a "surface to surface" discretization method is chosen for the contact problem with a finite sliding formulation and a 0.5 friction coefficient for the tangential behaviour. The spherical indenter is defined as the master surface and the pipe outer surface as the slave surface, and the indenter is allowed to be separated from the pipe after the indentation to model the removal of the indenter. Indentation can be applied to the pipe in different ways. The difference between them is when the indentation is applied with respect to the internal pressure in the pipe. In this study, one load scenario will be used. In this load scenario, the pipe is indented at zero internal pressure, and then the indenter is removed away from the pipe. Afterwards, the internal pressure (*P)*

inside the pipe is elevated up to the allowable maximum operating pressure (MOP) in the pipe, which is calculated by Barlow's equation [2] using a design factor (*DF*) of 0.8, as shown in Eq. (4.2).

$$P = \frac{2 * DF * SMYS * WT}{OD} \tag{4.2}$$

After that, the pressure is dropped to zero. Then, the pressure is finally increased again to the in-line pressure, which will be set at 37.5% of the MOP.

The model presented in this work is verified with the model given by Shuai et al. in [39]. In [39] an experimental and a numerical of pipe model subjected to a dent defect was tested. The results of the developed model in this study is verified by the numerical model created in [39]. The experimental model results are not used in the comparison as the strain information at the end of the indentation process are not provided before the end of the indentation precess. The pipe is having an OD of 720 mm and a wall thickness of 8.1 mm. The pipe material is having a yield strength of 375 MPa and a modulus of elasticity of 208 GPa. The indenter is spherical with a 50 mm radius, and the indentation depth is equal to 67 mm. The design factor is taken 0.72, not 0.8 as in this study, and the pipe length is equal to 7466 mm. The vertical deflection results after the removal of the indenter and the MEPSs, at the end of indentation, after the removal of the indenter, and after the application of the MOP, at the dent apex are presented in Table 4.2.

Table 4.2. *Comparison of the vertical deflection and equivalent plastic strains for the FE model verification.*

Model	Vertical Deformation (mm)	Equivalent Plastic Strain		
	After indenter removal	At the end of indentation	After indenter removal	After applying MOP
Reference [39]	-48.68	0.123	0.122	0.124
Developed Model	-46.71	0.149	0.149	0.151

It can be seen from the comparison of the two models that the relative difference in vertical deformation between the two models is approximately 4.05%, and the maximum relative difference in the MEPS at the dent apex is 22.13%. Noticing that the values of the MEPSs at dent apex in the developed model are higher than the MEPSs in the reference model. Also, the strain values reported in the of the physical model in reference [39] were higher than the strain values from the numerical model developed in the reference by up to 50% as the pressure increases. This indicates that the developed model is reliable and can be used for predicting the strains in this study.

4.4. Reliability problem formulation

In this study, strain-based reliability analyses are to be performed to calculate the POF of a pipe dent defect, namely to quantify the probability of the exceedance of the SC of the pipe steel material, which is X52 vintage steel. The MEPS are chosen as the strain demand in this study. The main parameters affecting the MEPS in the dent defect considered in this study are the pipe WT, the DD, and the yield strength (YS) of the pipe material. Therefore, the LSF of the reliability problem is presented in Eq. (4.3),

$$g(\overline{WT}, \overline{DD}, \overline{YS}) = \overline{SC} - MEPS(\overline{WT}, \overline{DD}, \overline{YS}) \quad (4.3)$$

Where $g(X)$ is the LSF of the problem RVs, X, that represents the surface of exceedance. The exceedance happens when the MEPSs exceed the SC, which will result in a

negative value for the LSF and indicate that the failure has happened in the reliability analysis.$\overline{SC}$ is the RV of the SC of the X52 vintage steel having a mean of 0.3 and a standard deviation (STD) of 0.018 [46], $MEPS$ is the function of the maximum equivalent plastic strain generated in the pipe, and it will be presented by the FE model developed and approximated by a quadratic function RS_{MEPS} as it is going to be explained in the next section in the RSM. RS_{MEPS} is a function of the problem variables WT, DD, and YS. The statistical data for the RVs are presented in Table 4.3. Please note that the nominal or characteristic values, which are deterministic, and their corresponding RV are differentiated by adding a bar over the RVs and that all RVs are assumed to be statistically independent in this study.

Table 4.3. *Statistical data for RVs.*

Random Variable	Unit	Mean	STD	Distribution	Reference
Wall thickness ($\overline{WT}$)	mm	Nominal Value	2.35% of the mean value	Normal	[78]
Yield strength ($\overline{YS}$)	MPa	386.55	21.63	Normal	[78]
Strain capacity ($\overline{SC}$)	-	0.3	0.018	Normal	[46]
Dent depth ($\overline{DD}$)	mm	See section 4.7*	1.25**	Normal	-

* The mean value of the $\overline{DD}$ will be calculated depending on the MEPS to be generated in the dent defect.

** The STD of 1.25 mm is obtained from the industry based on the accuracy of the in-line inspection tool used to measure the DD.

4.5. Reliability techniques and the RSM

The main goal of this study is to calculate the POF for the strain-based (MEPS) problem. In order to obtain accurate MEPS values, non-linear FE models have to be used. The FE

model usage is necessary as the analytical functions for the accurate calculation of the MEPSs in the dent defects do not exist.

Generally, the POF of LSFs can be calculated using several reliability methods. The MCS method [6] is considered one of the primary, simple, and most accurate methods for calculating the POF. However, to perform MCS for the MEPS problem, a large number of simulations have to be created. For each of these simulations, a nonlinear FE simulation has to be performed. Each FE simulation takes about 1 to 2 hours to obtain accurate and reliable results for the MEPS, making it impractical to run MCS because of the massive time required to solve the reliability problem.

This problem-solving time obstacle generated the need to use a method where much fewer number of FE models have to be analyzed to calculate the POF. Therefore, the RSM will be considered in this study to calculate the POF of the stain problem. As in the RSM, a much fewer and finite number of FE model runs can be used to construct a local RS with a specific local range, as it is going to be explained later in this section, to perform the reliability analysis on it. During the reliability analysis using the RSM, the FORM will be performed on the local RS to obtain the most probable point (MPP) and the POF. In case the MPP is within the range of this RS, the analysis will be considered correct. However, if the MPP is outside of the local RS range, a new local RS will be generated at the newly obtained MPP, and this process will go on until convergence is reached.

The reason for choosing the FORM over the MCS in calculating the MPP and the POF for the local RS is that the MCS will not be able to predict the MPP, making it impossible to check if the MPP of the problem is within the range of the generated RS and if there is a need to generate a new local RS and perform another iteration. The discussion at the beginning of the section about using the MCS to solve the whole strain (MEPS) problem is not to be confused with considering the MCS to calculate to POF of the locally generated RS, as the two tasks are totally different.

The RS [67] is a multivariable (depending on the number of RVs considered) fitting surface representing the desired response. In this study, a second-order RS will be used to represent the non-linearity that may exist in the MEPS as a function of the basic RVs considered. Moreover, interaction terms are included in the RS to investigate the effect of the interaction of an independent variable (factor or regressor) on the response.

The general equation of the second-order RS [60] that will be used is presented in Eq. (4.4).

$$Y(\chi_1, \chi_2, \dots, \chi_k) = \beta_0 + \sum_{i=1}^{k} \beta_i \chi_i + \sum_{i=1}^{k} \beta_{ii} \chi_i^2 + \sum \sum_{i<j=2}^{k} \beta_{ij} \chi_i \chi_j + \varepsilon \qquad (4.4)$$

where Y is the response (i.e., the RS_{MEPS}), β_i and β_{ij} are the RS regression coefficients to be calculated from the regressor values χ_i (in our case, the variables of the problem WT, DD, and YS) and the interaction terms, and ε is the random error component.

In this study, a three-level full factorial design of experiment (DOE) [56,67] is adopted for the determination of the number of models needed to calculate all the coefficients of the RS. According to the three-level factorial design, 3^n number of numerical experiments, or in our case FE models, will be analyzed to construct the RS, in which n is the number of variables in the RS. In our problem, only three variables, or factors, are considered, which means that 27 FE models will be analyzed to calculate the coefficients of one RS. Each variable will have three different values or levels (low, central, high). The central value of each variable will be set to a certain number, and the choice of these values will be explained later in this section. The upper and lower values are set to be ± 2 times the STD of the corresponding RV away from its central value. Using the MEPSs results of the 27 FE models and the response surface (RS) in Eq. (4.4), the least square method [60] is applied to calculate the coefficients of the RS equation to minimize the sum of squares of the residual between the predicted values by the RS equation and the presumably real values of the MEPS from the 27 FE models.

The steps to perform the analysis will be as follows:

1- Calculating the MEPS values for the 27 FE models, then constructing a second-order RS using these values. The initial central values for the variables to create the initial RS will be the mean value of their corresponding RVs. However, in case of any extra iteration, the central values of the variables are set to the MPP values.

2- Performing FORM reliability analysis on the LSF "g" to get the MPP.

3- Checking if the MPP is within the limits of the RS (central value $\pm$ 2×STD) constructed in the first step and used to perform the FORM analysis.

4- If the MPP is within the RS limits or the reliability index converged to a number (the difference is explained further in section 7), then the obtained POF is the final POF.

5- If the MPP is outside the range of the RS limits, then a new RS will be constructed with the RVs values of the MPP $\pm$ 2×STD. Furthermore, the whole process starting from 1 to 5 will be repeated until reaching convergence.

4.6. RSM Verification

In order to use the RSM explained in the previous section in the pipelines problem, a verification of the method has to be performed. Several problems can be found in the literature that has been used to verify different types of RSMs. Two different LSFs were used to test the performance of the RSM. The first LSF considered was given by [98], and it is presented as follows:

$$G(\overline{u_1}, \overline{u_2}) = 0.1(\overline{u_1} - \overline{u_2})^2 - \frac{\overline{u_1} + \overline{u_2}}{\sqrt{2}} + 2.5 \tag{4.5}$$

The second LSF considered is given by [66], and it is presented as follows:

$$G(\overline{u_1}, \overline{u_2}) = e^{(0.2\overline{u_1}+1.4)} - \overline{u_2} \tag{4.6}$$

The RVs $\overline{u_1}$ and $\overline{u_2}$ in the two LSFs have standard normal RVs with a mean of zero and unit STD. The first LSF is chosen to be a quadratic function, which will be the same degree as the RS equation representing the MEPS in the pipeline problem. However, the second LSF is chosen to be an exponential function to check the RSM's ability to predict the MPP and the POF of an LSF that is not quadratic.

The RSM used in this study is validated by the two LSFs given above. The final results of the used RSM are compared to the results from applying FORM analysis to the LSFs and the results presented in the reference papers [66,98] in Table 4.4 and Table 4.5. The converging criterion chosen here is whether the relative difference between the reliability index (Beta) from 2 consecutive iteration is less than 10^{-2}.

Table 4.4. *Verification of the used RSM on the LSF of Eq. 4.5.*

	Iteration number	**MPP**		**Reliability Results**		**If MPP is within RS range**
		$\overline{u_1}$	$\overline{u_2}$	**Beta**	**POF**	
FORM analysis	-	1.7677	1.7677	2.4999	0.006209	-
Exact solution [98]	-	1.7677	1.7677	2.5000	0.006209	-
RSM (RS with interaction terms)	1	1.7677	1.7677	2.4999	0.006209	Yes
	2	1.7677	1.7677	2.4999	0.006209	Yes

It can be seen from the results in Table 4.4 that the used RSM is successful and efficient in predicting the reliability index and the POF of the LSF.

Table 4.5. *Verification of the used RSM on the LSF of Eq. 4.6.*

	Iteration number	MPP		Reliability Results		If MPP is within RS range
		$\overline{u_1}$	$\overline{u_2}$	Beta	POF	
FORM original LSF	-	-1.67978	2.89806	3.3496	0.0004045	-
MCS Results [66]	-	-	-	3.382	0.000338	-
RSM (RS with interaction terms)	1	-1.64044	2.91015	3.3406	0.0004178	No
	2	-1.70735	2.88108	3.3489	0.0004055	Yes
	3	-1.70761	2.88198	3.3498	0.0004042	Yes

It can be seen from Table 4.5 that the used RSM is also successful in performing the reliability analysis. However, in the second LSF, the RSM took larger numbers of iterations to reach the solution. This can be interpreted by that both the LSF and the RS equation for the first LSF are quadratic functions, which made the RS equation perfectly represent the LSF and reach the solution within two iterations. However, in the second LSF, the type of the LSF and the RS functions are different, which increases the number of iterations required to reach the solution. It has to be noted also that the RSM reached a good convergence of the numbers, once the MPP was inside the range of the RS for a specific iteration. It can be concluded that the rate of convergence of the results depends on the form and the shape of the LSF.

The form of the RS of the MEPS problem is found to more linear and flatter than the problems tested above. Also, the time taken to construct a RS is high, as 27 FE models are required to be analyzed per RS. Therefore, in this study, the RSM iterations are stopped once the MPP obtained in an iteration is within the range of the RS constructed for that iteration.

4.7. Pipe Defect Reliability Analysis

4.7.1. Pipeline reliability results

From the LSF function presented in Eq. (4.3), it can be shown in the right-hand side (RHS) of the equation that the POF is dependent on the statistical distribution of the MEPS function, which is dependent on the statistical data of its RVs ($\overline{WT}$, $\overline{DD}$, and $\overline{YS}$). The statistical distribution of the remaining term of the $\overline{SC}$ in the RHS of the equation will be constant throughout all the results as it represents the steel properties, and only X52 vintage steel is used in this study.

It has to be mentioned that the MEPS values obtained from the FEM models are dependent on the length of the pipe considered for the analysis. To be realistic, a significantly long pipe has to be considered for analysis if an accurate MEPS is to be obtained. However, this will be computationally expensive in this study. Therefore, the ratio of the pipe length to the pipe OD is set to 3.3 to 3.4 in this study. Moreover, more defects of different pipe lengths are going to be analyzed to check the effect of the pipe length considered for the analysis on the reliability results.

We can deduct from the above that the POF of a defect is most likely highly dependent on the value of the MEPS generated in this defect. Therefore, in this study, several defects having mainly three different MEPS levels (nominal MEPS of 0.2, 0.26, and 0.28) were created, remarking that the SC of the used steel grade has a mean of 0.3 and an STD of 0.018. Two different pipe configurations were used to test the effect of the OD change, and two different indenter sizes were considered for testing their effect on the POF. Table 4.5 represents all the various defects created for this study.

Table 4.6. *Dent defects used in this study.*

Defect Designation	Pipe configuration		Pipe Length (mm)	Indenter Radius (mm)	Initial DD (mm)	Initial DD to OD %	MEPS at the end of indenta-tion	DD after spring back (mm)	MEPS after spring back	DD after rerou-ndin g (mm)	Final Nominal MEPS
	OD (mm)	WT (mm)									
D762-IND30-EPS20	762	7.14	2500	30	14	1.84%	19.2%	8.21	19.5%	5.51	20.00%
D762-IND15-EPS20	762	7.14	2500	15	9.6	1.26%	19.2%	4.95	19.7%	3.42	20.00%
D323-IND20-EPS20	323	6.35	1100	20	7.2	2.23%	19.1%	4.93	19.5%	4.07	20.00%
D323-IND10-EPS20	323	6.35	1100	10	4.9	1.52%	19.4%	3.02	19.8%	2.57	20.00%
D762-IND30-EPS26	762	7.14	2500	30	20.3	2.66%	25.6%	13.21	25.6%	8.97	26.00%
D762-IND15-EPS26	762	7.14	2500	15	12.9	1.69%	25.2%	7.51	25.6%	5.26	26.00%
D323-IND20-EPS26	323	6.35	1100	20	10.3	3.18%	25.2%	7.74	25.4%	6.33	26.00%
D323-IND10-EPS26	323	6.35	1100	10	6.8	2.11%	25.3%	4.73	25.7%	4.04	26.00%
D762-IND30-EPS28	762	7.14	2500	30	23	3.02%	27.8%	15.32	27.8%	10.43	28.00%
D762-IND15-EPS28	762	7.14	2500	15	14	1.84%	27.2%	8.43	27.5%	5.92	28.00%
D323-IND20-EPS28	323	6.35	1100	20	11.4	3.53%	27.3%	8.73	27.4%	7.16	28.00%
D323-IND10-EPS28	323	6.35	1100	10	7.5	2.32%	27.2%	5.34	27.5%	4.55	28.00%

It has to be noted that for each of these defects, the indentation depth is obtained by setting all the FE model parameters (pipe length, pipe OD and WT, indenter size) then the pipe is indented until reaching the desired MEPS for the defect. The initial DDs used to make the dent defect in the FE model are provided in Table 4.6. However, after removing the indenter, an elastic spring back of the pipe will occur. Also, after increasing the internal pressure,the pipe is expected to reround having a final lower DD compared to the initial DD value. To check the effect of the spring back and the rerounding, the values of the DDs after the spring back and the rerounding together with values of the MEPSs right after the indentation, after the spring back, and after the MOP application are also provided in Table 4.6. It can also be seen from Table 4.6 that with the decrease of the indenter radius, the DD decreases to produce the same amount of MEPS. It has to be also noted that some stress and strain peaking are generated in the FEs of the pipe due direct contact with the rigid indenter, but in reality, the indenter is not perfectly rigid and such peaks will not probably happen and they should not be considered in this study. That is why in this study only the MEPS measured at the inside surface of the pipe are considered. Reliability analyses using the RSM are performed on each of these defects to obtain their POF. The mean values of the $\overline{WT}$, and the $\overline{DD}$ for each defect are obtained from Table 4.6.

Table 4.7. *Reliability results of the dent defects.*

	RS with interaction terms	
Defect Designation	**Beta**	**POF**
D762-IND30-EPS20	2.964	1.52E-03
D762-IND15-EPS20	3.427	3.05E-04
D323-IND20-EPS20	3.307	4.72E-04
D323-IND10-EPS20	2.352	9.34E-03
D762-IND30-EPS26	2.017	2.19E-02
D762-IND15-EPS26	1.415	7.85E-02
D323-IND20-EPS26	1.365	8.61E-02
D323-IND10-EPS26	1.003	1.58E-01
D762-IND30-EPS28	1.010	1.56E-01
D762-IND15-EPS28	0.730	2.33E-01
D323-IND20-EPS28	0.662	2.54E-01
D323-IND10-EPS28	0.531	2.98E-01

The results in Table 4.7 are plotted in Figure 4.5 to show the relative change of POF between different pipe configurations and different indenter sizes.

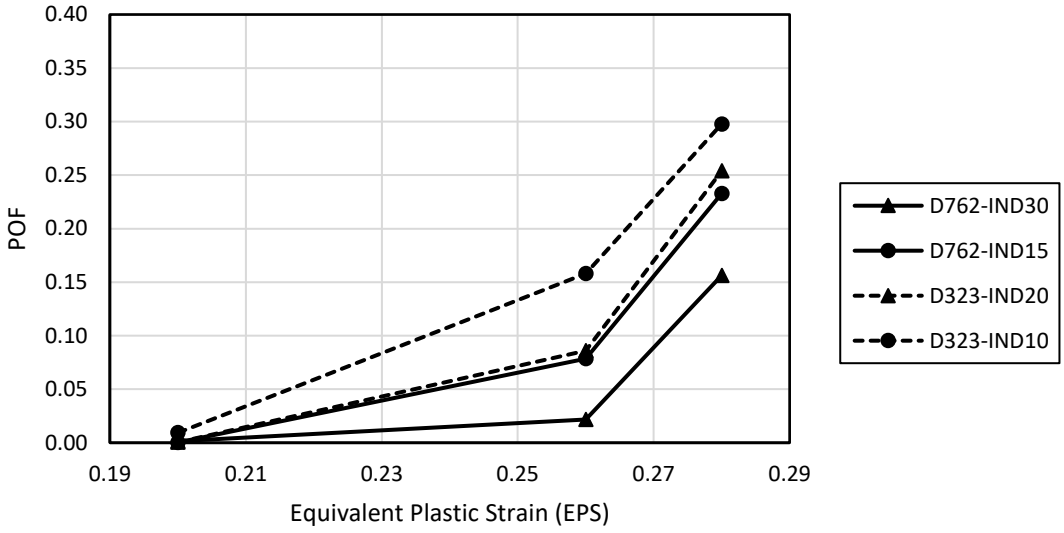

Figure 4.5. *POFs results of the dent defects.*

It can be seen from the results in Table 4.7 and Figure 4.5 that the POF is highly dependent on the value of the nominal MEPS generated in the defect. The difference between the results for the same nominal MEPS is interpreted in the following subsection.

It can be seen from Table 4.6 that the MEPS has reached almost 95% of its final nominal value at the end of the indentation process, before the removal of the indenter, and almost 97.5% of its final nominal value after the after the removal of the indenter. The values of the MEPSs after the application of the MOP were almost equal to the values of the final nominal MEPSs. This means that the POF at the end of the indentation process and after the removal of the indenter will be slightly less than the final POFs reported in Table 4.7. This indicates that, according to the strain exceedance criterion adopted in this study, most of pipe damage from dents is almost equal from the indentations, after the spring back and rerounding, and the application of the MOP to the pipe.

It has to be mentioned that these results are conservative as if longer pipes were used for the analysis with the same indenter size and DD used above, lower MEPS and hence

lower POFs will be obtained. However, different pipe lengths with different indenter sizes and different DDs but with the same nominal MEPS were analyzed to check the effect of pipe length on the results. The NPS 30 with 7.14 mm WT having different pipe lengths, indenter sizes, and DD (see Table 4.8) are considered for analysis.

Table 4.8. *Dent defects within pipes of different pipe lengths.*

Defect Designation	Pipe configuration		Pipe Length (mm)	Indenter Radius (mm)	DD (mm)	DD to OD %	MEPS at the end of indentation	DD after spring back (mm)	MEPS after spring back	DD after rerou-nding (mm)	Nominal MEPS
	OD (mm)	WT (mm)									
D762-IND25-L1250	762	7.14	1250	25	15.2	2.00%	25.5%	10.5	25.6%	7.4	26.00 %
D762-IND30-L2500	762	7.14	2500	30	20.3	2.66%	25.6%	13.2	25.6%	8.9	26.00 %
D762-IND40-L4000	762	7.14	4000	40	46	6.04%	26.3%	31.8	26.3%	17.5	26.33 %

The reliability results for these cases are presented in Table 4.9.

Table 4.9. *Reliability results of dent defects within pipes of different pipe lengths.*

	RS with interaction terms	
Defect Designation	Beta	POF
D762-IND25-L1250	1.879	3.01E-02
D762-IND30-L2500	2.017	2.19E-02
D762-IND40-L4000	1.939	2.62E-02

It can also be seen from Table 4.9 that despite the dramatic changes in the values of the length of the pipe, the indenter radius, or the DD, the POF did not change dramatically, and it stayed in the same order. This can lead to the conclusion that the value of the POF is highly related to the nominal MEPS of the defect.

According to the MEPS exceedance criterion adopted in this study and the obtained results, the POF is highly dependent on the nominal MEPS developed in the pipe. Without considering the effect of the pipe length, the same nominal MEPS can be produced from an indenter of a large radius with a large DD or from an indenter of a small radius with a small DD (like a case of a sharp indentation), which shows that the POF is not only dependent on the DD. This conclusion raises questions about the consistency and validity of the criteria specified by the CSA Z662:19 for the replacement and mitigation of the dent defects, i.e., the 6% OD DD limit. For example, a defect can have low DD (less than the 6% of OD) with high MEPS, hence high POF, that requires mitigation and replacement, but it will be considered a safe defect according to CSA Z662:19. On the contrary, a defect may have a large DD with low MEPS and POF that can be wrongly considered unsafe according to CSA Z662:19.

4.7.2. Interpretation of the reliability results

In this subsection, the interpretation of the results given in Table 4.7 and Figure 4.5 and in Table 4.9 are discussed.

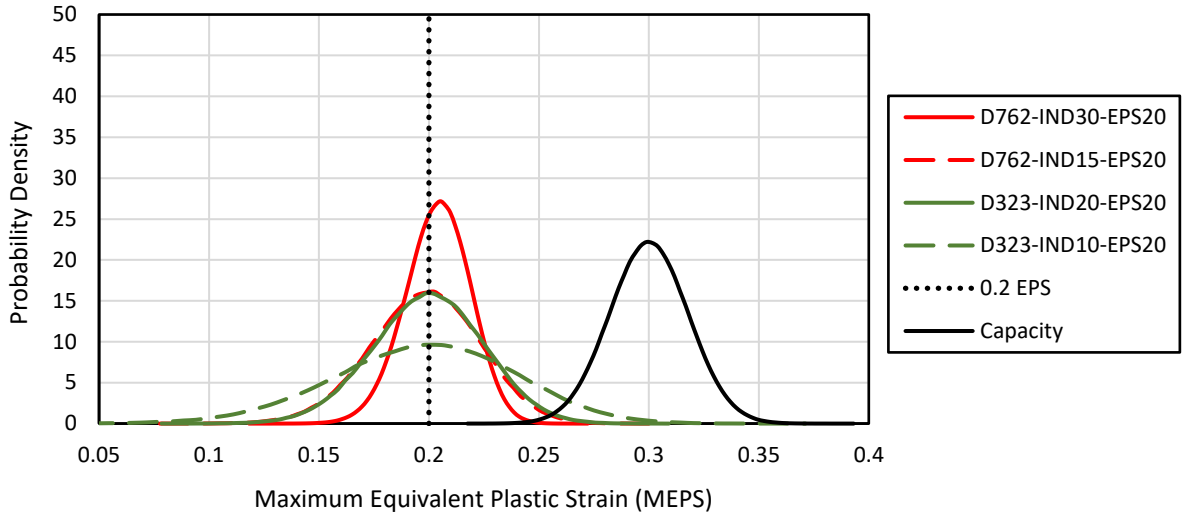

Figure 4.6. *Probability distributions of the MEPS demand and capacity for different pipe defects but with the same nominal MEPS = 20%.*

In Table 4.6 it can be noticed that for the same pipe configuration, the decrease in the indenter radius caused an increase in the POF value. To explain this, Figure 4.6, Figure 4.7, and Figure 4.8 are plotted. These three figures represent the statistical distribution of the $\overline{MEPS}$ of each of the defects with respect to the statistical distribution of the $\overline{SC}$ for the three different MEPS levels considered in this study.

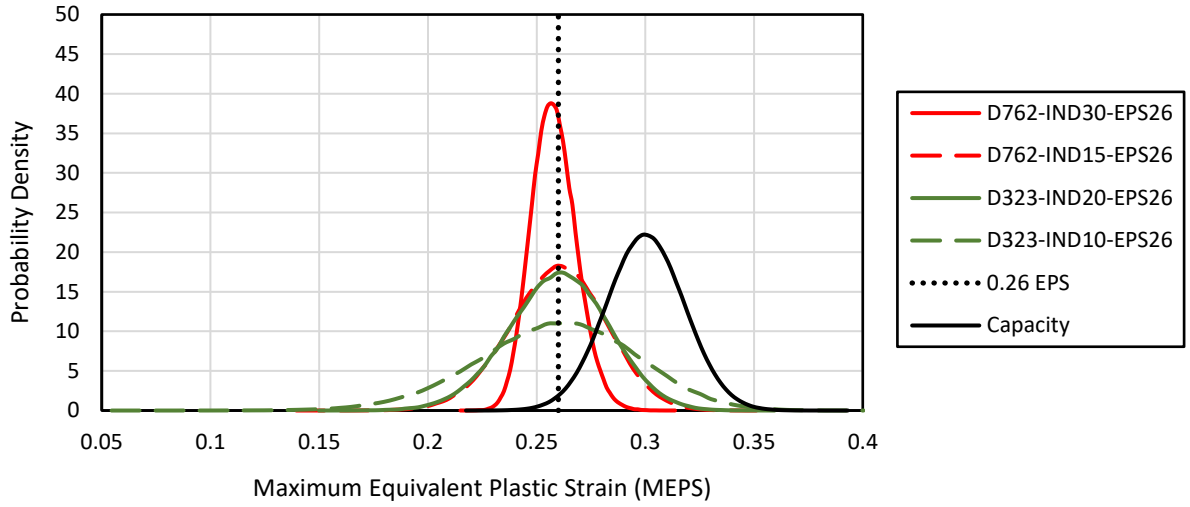

Figure 4.7. *Probability distributions of the MEPS demand and capacity for different pipe defects but with the same nominal MEPS = 26%.*

It can be seen from the figures that with the decrease of the indenter radius for any pipe configuration, the STD of $\overline{MEPS}$ distribution increased, which increased the overlap with the $\overline{SC}$ distribution and caused the increase of the POF. The increase of the STD can be interpreted by the following: for the same pipe configuration and the same nominal MEPS, the DD value decreases with the decrease of the indenter size; at the same time, the STD of the DD is set to a constant value of 1.25 mm, which is the accuracy of the in-line inspection tool; the decrease of the DD mean value with the same STD led to the increase of the increase of the STD of the DD compared to DD mean value as the DD mean value decreases; this resulted in an $\overline{MEPS}$ distribution of larger STD at decreased DD values.

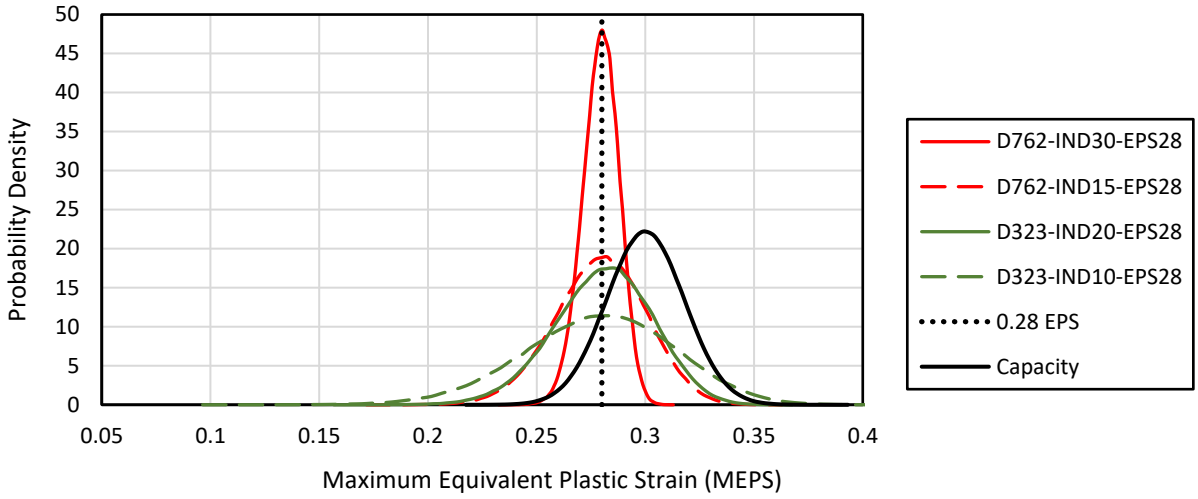

Figure 4.8. *Probability distributions of the MEPS demand and capacity for different pipe defects but with the same nominal MEPS = 28%.*

The effect of the pipe OD can also be concluded from the current results. It can be seen from Table 4.6, for two pipes having the same nominal MEPS and the same DD/OD ratio, the pipe with the lower OD has a higher POF. This can be interpreted as follows: pipes with a small OD will have a small DD compared to pipes with a larger OD as they have the same ratio of DD/OD; the STD for $\overline{DD}$ is the same for all $\overline{DD}$ mean values, which makes the statistical distribution of the $\overline{MEPS}$ flatter for the dents in pipes with a smaller OD. This can be observed in Figure 4.6, Figure 4.7, and Figure 4.8 that the distributions of the pipes with 323.85 mm OD (the green curves) are always flatter than those of the pipes with 762 mm OD (the red curves). This leads to the conclusion that pipes with smaller ODs will produce higher POFs than the pipes with larger ODs if they have the same DD/OD ratio and the same nominal MEPS.

4.8. Limitations

It has to be mentioned that the POF calculated in this chapter is a conditional one, as some other random variables of the problem are not included in the reliability analysis, such as the pipe outside diameter and the maximum operating pressure of the pipe.

4.9. Conclusions

In this paper, strain-based reliability analyses were performed on plain dent defects of pipelines using the RSM and the FORM as the reliability method. Different defected pipe parameters such as the pipe outside diameter (OD), the pipe wall thickness (WT), the pipe length, the indenter size, the dent depth (DD) are considered for the analyses to determine the main factors affecting the probability of failure (POF) and the safety of the dented pipelines. It has been found that the nominal value of the maximum equivalent plastic strain can be used as a measure of the severity of the dent defect generated in the defect and it is the primary factor affecting the POF of the defect. Moreover, smaller indenter sizes and pipes with smaller ODs are found to produce higher POFs for the same nominal MEPS levels generated in the defects. However, only using the DD/OD percentage to predict the severity of the dent defect does not always lead to consistent POF of the dent defect from the perspective of strain-based reliability analysis.

5. Reliability Analysis of Pipelines Containing Plain Dent Defects Using Different Strain Damage Criteria

5.1. Introduction

Pipelines are widely acknowledged as one of the most efficient ways of transporting oil and gas from refineries to consumers. However, pipelines are susceptible to various defects, including corrosion, cracking, and denting, caused by external factors such as equipment impact, external pressure from smooth and kinked rocks. These defects can compromise pipeline safety, increasing the risk of content leakage into the environment or potential explosions. Gas and oil pipeline companies pay close attention to monitoring the safety of their pipelines to avoid pipe failures that can have dire environmental consequence in addition to the concomitant financial cost.

One of the most common types of pipeline defects is pipe dents. These dents can occur during or after the construction stage, whether the pipes are buried underground or suspended over the ground surface. To ensure the safety of pipelines with dent defects, different oil and gas design standards specify the allowable dimensions of the dent defect and the allowable strain levels in the dent area. Design standards, including the Canadian oil and gas design standard CSA Z662:19 [13] and the US oil and gas design standards ASME B31.4-19 [14] and ASME B31.8-2018 [15], state that the depth of the dent defect should not exceed 6% of the outside diameter (OD) of the pipe. In CSA Z662:19 and ASME B31.8-2018, If this threshold is exceeded, the curvature-strain level in the pipe should not exceed 6%. Otherwise, the dent is classified as a defect that requires repair, unless it is proven to be acceptable by engineering assessment. The limit of the dent depth (DD) not exceeding 6% of the pipe OD was set to allow the passage of inline inspection (ILI) tools inside the pipe to inspect it, so it should not be an indication of the severity of the dent defect [13]. Abdelmoety et *al*. [101] showed, using strain-based reliability analyses, that dents with different DDs can have similar

probabilities of failure (PoFs). They also showed that dents with small DDs can be very severe and have high PoFs, depending on the indenter size. These findings suggest that considering the DD as a measure of the dent defect severity is problematic.

The other limit of not exceeding a 6% strain level recommended by the standards is considered very conservative by several researchers. Adeeb and Horsley [28] used a 20% maximum principal strain as the failure criterion for pipelines with internal pressure subjected to puncture from falling rocks. Arumugam et *al*. [49] showed in an actual case study, using ILI data, manual grid data, and LaserScan data, that the measured maximum equivalent plastic strain for a dent combined with a severe metal loss at failure was between 16% and 22%, which is significantly higher than the 6% limit provided by the design standards. To avoid determining a threshold value for the limiting strain, Zhao and Cheng [48] suggested a different strain assessment criterion based on the strain damage models. These models take into consideration the stress tri-axiality to determine the strains that will lead to the cracking of the pipe material and the accumulation of the strain damage at each point of the pipe material.

Several studies have been conducted on the use of different damage criterion for the prediction of pipelines cracking and damage. Arumugam et *al*. [49] quantified the plastic strain limit of dent defects using the Strain Limit Damage (SLD) and Ductile Failure Damage Indicator (DFDI) damage models. The minimum elongation limit criterion for dented pipes showed that the experimental information highly favours the DFDI and SLD models as effective means to assess the severity of dent defects. Li and Dang [51] used the DFDI to examine the ductile damage of the pipes subjected to constrained and unconstrained dents. Their analysis showed that the plastic damage is higher on the inside walls of the pipe compared to the outside walls. Furthermore, they observed that the dent depth and the pipe internal pressure has significant effect on the constrained dent damage. Gao et *al*. [52] used the DFDI criterion and finite element modeling to predict dent defect cracking, demonstrating that the DFDI with the inline inspection based on magnetic flux leakage can effectively identify the potential risk of dent with cracking. Wu et *al*. [53,102] used Oyane's damage criterion with finite

element modeling to assess pipelines [53,102] instead of using the dent depth-based failure criterion that does not account for several other parameters such as the internal pressure, the loading sequence, and the pipe geometry. Moreover, as described in [55], Wu et *al*. performed damage analysis by applying an ellipsoidal indenter to create indentations on the pipe in both longitudinal and circumferential directions. Their findings revealed that the longitudinal dent resulted in more damage to the pipe material and the amount of damage positively correlated with the indentation depth and negatively correlated with the indenter size. Note that all the previous studies used the damage criterion to assess dent defects deterministically.

Compared to the deterministic approach, the probabilistic approach allows explicit consideration of pertinent uncertainties involved for pipeline defect assessment. The advantage of using the probabilistic approach is providing more information about, or quantifying, the safety level used in the assessment methods. Most of the design and assessment methods and equations provided in the oil and gas standards are deterministic, using safety or design factors to consider the uncertainty indirectly. To perform probabilistic assessment, different methods exist in the literature. One of the most accurate reliability methods is Monte Carlo Simulation [56], which, however, is impractical for the calculation of extremely low PoFs due to the large number of samples required. This is particularly true when computational expensive models are involved in the limit-state function evaluation process. Other approximate analytical methods exist such as the First Order Reliability Method (FORM) [58] that is suitable for calculating extremely low PoFs. However, the FORM requires the gradient information (e.g., first-order) for the limit-state function, which is troublesome for reliability problems with implicit limit-state functions. To address this challenge, Response Surface Method (RSM) [60–66], which took advantage of the concept of experimental design and the Response Surface (RS) to approximate the limit-state function in an explicit form. It is widely acknowledged as a practical method for engineering reliability problems with implicit limit-state functions.

Damage criteria present an alternative strain-based failure criteria to assess dent defects, compared to using material strain threshold for the pipe dent defect failure. Also, damage criterion such as the DFDI is shown by different studies to be accurate at predicting the cracking and the damage of pipes containing dent defects. However, according to the authors' knowledge, the probability of failure associated with using the damage criteria at assessing dent defects in pipelines is not provided in the literature. Therefore, this paper is considered one of the first studies to present a strain-based reliability analysis of pipelines with dent defects based on the SLD and DFDI damage models. Different dent defects provided in [101] are considered. The reliability analysis results based on the damage criteria models are compared with to reliability results when the maximum equivalent plastic strain (MEPS) was used in [4]. The remainder of this paper is organized as follows. Section 5.2 presents the background and the equations of the SLD and DFDI damage strain models. Section 5.3 provides a summary about the response surface method used to perform reliability analysis in this study. Section 5.4 presents the finite element model used to calculate the stresses and the strains generated in the dented area, that are required for the limit-state function evaluations in reliability analysis. Section 5.5 presents the case study data [4] used in this study. Section 5.6 provides the validation of the finite element model for damage prediction, and the reliability analysis results based on the damage models with comparison to the results based on MEPS [4].

5.2. Damage models

Ductile failure occurs in an elastoplastic material because of void formation caused by debonding or fracture of metal, which subsequently grows to a macrocrack. Several studies, such as [103] by McClintock and [104] by Rice and Tracey, have been conducted to relate the growth of voids in ductile materials to the stresses and the strains in a tri-axial state of stress in the late 1960s. In 1972, Oyani [105] focused on improving the prediction of fracture strain in porous materials using experimental data.

Later in 1976, Hancock and McKenzie [106] proposed a reference failure or a strain limit ε_f, given in Eq. (5.1), for ductile failure.

$$\varepsilon_f = 1.65\varepsilon_o e^{-\frac{3\sigma_m}{2\sigma_{eq}}} \tag{5.1}$$

Where σ_m is the average of the principal stresses (also referred to as the hydrostatic stress) in a tri-axial stress field, σ_{eq} is the equivalent von Mises stress, and ε_o is the critical strain of the ductile material at the start of crack initiation, which can be determined by uniaxial tensile testing.

Eq. (5.1) is also used in the API 1183-2020 [35] standard for the assessment and management of pipeline dents for damage analysis. Another equation used by the ASME boiler and pressure vessels code (ASME BPVC.VIII.3-2021) [50] for the calculation of the failure strain is given in Eq. (5.2).

$$\varepsilon_f = \varepsilon_o e^{\frac{-m_5}{1+m_2}\left(\frac{\sigma_m}{\sigma_{eq}}-\frac{1}{3}\right)} \tag{5.2}$$

Where m_2 is a factor depending on the yield and the ultimate strengths of the ductile material, m_5 is a factor determined based on the type of metal used and is taken equal to 2.2 for ferritic steel.

ε_o is determined according to ASME BPVC.VIII.3-2021 by the maximum of the three formulas given in Eq. (5.3) for ferritic steel.

$$\varepsilon_o = maximum \begin{cases} m_2 = 0.6 * (1 - \dfrac{S_y}{S_u}) \\ m_3 = 2\ln[1 + (El/100)] \\ m_4 = \ln[100/(100 - RA)] \end{cases} \tag{5.3}$$

Where S_y and S_u are the yield strength and the ultimate strength of the pipe steel material at analysis temperature, respectively. El is the minimum specified elongation,

and RA is the minimum specified reduction of area as a percentage. m_4 formula provides the critical true strain of the steel specimen in uniaxial tensile test based on the reduction of the specimen area during the test. Arumugam et *al*. [107] used the area reduction formula to calculate the critical true strain for the X52 steel based on experimental measurement of area reduction during the uniaxial tensile test and they provided a lower bound for the critical true strain equal to 50.7%. In [49], Arumugam et *al*. used a critical true strain of 51.2% for the X52 steel for dent assessment using the SLD and the DFDI equations. For the vintage X52 steel used in this study,the value of m_4, obtained from [49],governs the value of ε_o. [6]

From the previous strain limit equations, it can be noticed that the strain limit is a function of the principal stresses, the von Mises stress at the damage calculation point, which is not constant and changes with the change of the load and stresses at the calculation point. What is meant by the calculation point, is the pipe material point at which the damage is to be calculated. The amount of damage ΔD_i at the calculation point i at the current loading step is calculated by Eq. (5.4) [108].

$$\Delta D_i = \frac{\Delta \varepsilon_{eq}}{\varepsilon_f} \tag{5.4}$$

While the total amount of damage at the calculation point i will be equal to the summation of all the damage at the point through all the n loading steps given in Eq. (5.5).

$$D_i = \sum_{i=1}^{n} \Delta D_i \tag{5.5}$$

Depending on the strain limit equation used in the damage calculation, two terms are commonly used in the literature for the calculation of the damage D_i at a certain point. When the ASME BPVC.VIII.3-2021 stain limit equation, Eq. (5.2), is used in the calculation of the damage, the damage model is referred to as the SLD; when Eq. (5.1)

is used the damage model is referred to as the DFDI. Some researchers [48,55] used Oyani's criterion and the DFDI in their damage analysis, and Zhao and Cheng [48] demonstrated that the DFDI is more conservative than Oyani's criterion in the prediction of damage accumulation. Therefore, the DFDI will be used beside the SLD in this study instead of Oyani's criterion.

5.3. Reliability analysis

5.3.1. Limit state function (LSF)

Reliability analysis is performed to calculate the PoF of pipelines containing dent defects assuming that the failure is described as the damage measure exceeding unity and the damage measure is determined using either the SLD or DFDI damage model. Consequently, a LSF, which can be mathematically employed to signify failure when it is below zero, is presented in Eq. (5.6),

$$g_{DM}(DD, WT, YS) = 1 - DM(DD, WT, YS) \tag{5.6}$$

where DM represents the maximum damage in the pipe material within the dented area and is a function of the DD, wall thickness (WT), and yield strength (YS). The damage capacity in the LSF is set to 1 [49]. The underlying assumption is that when the damage in the pipe material reaches 1, the initiation of cracks within the pipe material will commence. This occurrence is regarded as failure (i.e., limit state exceedance) herein in the reliability analysis.

5.3.2. Response surface (RS)

Due to the lack of an analytical expression for the maximum damage within a dent defect, as a function of the dent dimensions, the pipe geometry, and steel properties, a response surface [60] will be generated and used to predict the maximum damage of the dent defect.

The response surface model used in this study is a quadratic RS containing constant, linear, and quadratic terms of random variables as shown in Eq. (5.7).

$$Y(X_1, X_2, \dots, X_k) = \beta_0 + \sum_{i=1}^{k} \beta_i X_i + \sum_{i=1}^{k} \beta_{ii} X_i^2 + \sum \sum_{i<j=2}^{k} \beta_{ij} X_i X_j + \varepsilon \qquad (5.7)$$

Where $Y(X_1, X_2, \dots, X_k)$ is the response quantity, which will be in our study the maximum damage in the dent defect. $X_1, X_2, \dots, X_k$ are the problem parameters or the basic random variables (RV) in the reliability problem considered in the study. β_i and β_{ij} are the RS regression coefficients to be calculated from the regressor X_i and the response Y values of several data points. ε is the random error component representing the difference between the predicted response value and the real response value for different parameters values. The random error is unknown and not carried over in the RS equation during reliability analysis. The RS shown in Eq. (5.7) contains also terms considering the interactions between the problem parameters. At the performance of the reliability analysis, the RS is used including and excluding the interaction terms. The interaction terms are included in the RS to check the effect of the interaction between the problem random variables at different values on the response and hence on the reliability analysis.

In this study, the random variables selected for the dent defect reliability analysis are the X_1 =DD, X_2 = WT, X_3 = YS. The statistical data for the three RVs considered in this study including the mean, the STD, and the statistical distribution are provided in Table 5.1.

Table 5.1. *Statistical data for RVs.*

Random Variable	Unit	Mean	STD	Distribution	Reference
Wall thickness (WT)	mm	Nominal Value	2.35% of the mean value	Normal	[78]
Yield strength (YS)	MPa	386.55	21.63	Normal	[78]

Dent depth (DD)	mm	See section 5.5	1.25*	Normal	-

$*$ The DD is obtained from the industry based on the accuracy of the used in-line inspection tool.

5.3.3. Design of experiment (DoE)

To construct the RS, it is necessary to generate multiple discrete data points or (numerical) experiments, the quantity of which must be equal to or greater than the number of unknown coefficients or terms within the RS. Then, the coefficients of the RS are determined from the data points or experiments using the least square method. Each of these points or experiments is comprised of a value for each of DD, WT, and YS and a dependent value which is the maximum damage (DM) generated in the dent. To get the maximum damage value of an experiment, a finite element (FE) model will be built and run for the corresponding point or experiment, then FE model results will be processed to perform the damage analysis, determining the maximum damage location and value within the dented region.

The full-factorial DoE is used in this study. In order to account for the nonlinearity in the RS depicting the maximum damage concerning the problem parameters, the construction of the RS involves incorporating three levels or values for each parameter. According to [67] a three-level full-factorial DoE for three parameters requires $3^3 = 27$ experiments to consider all the combinations of the three levels of the three parameters.

The selection of the three levels depends on the specific values of the three independent parameters for which the maximum damage needs to be calculated in the reliability analysis. The RS locally represents the maximum damage behaviour around a middle value for each of the three parameters (DD, WT, YS). For each parameter, once its middle value is determined, a value preceding and a value following the middle value are calculated. This is achieved by ensuring that the interval

is equal to β times the standard deviation (STD) of the random variable associated with this parameter. The value of β can be around 2 or 3 according to [64], and in this study, it is set to 2.

5.3.4. Response surface method

Considering the fact that the limit state function evaluation requires the analysis of an FE model to calculate the maximum damage, RSM is used to solve the reliability problems, because it warrants sufficient accuracy with a relatively smaller number of limit state function evaluations or FE model runs. In RSM, after constructing a local RS based on DOE, the FORM is used based on the developed RS to estimate the PoF, as well as the design point or the most probable point (MPP). The convergence is considered to be achieved when the estimated MPP is within the range of the constructed local RS. If the estimated MPP is outside the range of the RS parameters, a new local RS is constructed around the last calculated MPP and the FORM is redone. This process is repeated until convergence is achieved.

5.4. Finite element model

As noted earlier, the reliability analysis in this research requires analyzing numerous FE models for each defect to determine the PoF associated with the defect. This requirement underscores the need for an FE model capable of generating accurate stress and strain results, while also being computationally efficient.

The finite element (FE) model used in this study is the same model used and validated in [101]. Without repeating the details to preserve space and avoid duplication, it is briefly discussed in this section to facilitate the readability of this presented work. However, this study focuses on damage calculation, which are based on triaxial stress and strain states. Therefore, an FE model, developed on the commercial software ABAQUS, is used to calculate the principal stresses (and hence the von Mises stress) and the equivalent plastic strains (EPS) inside the dented area.

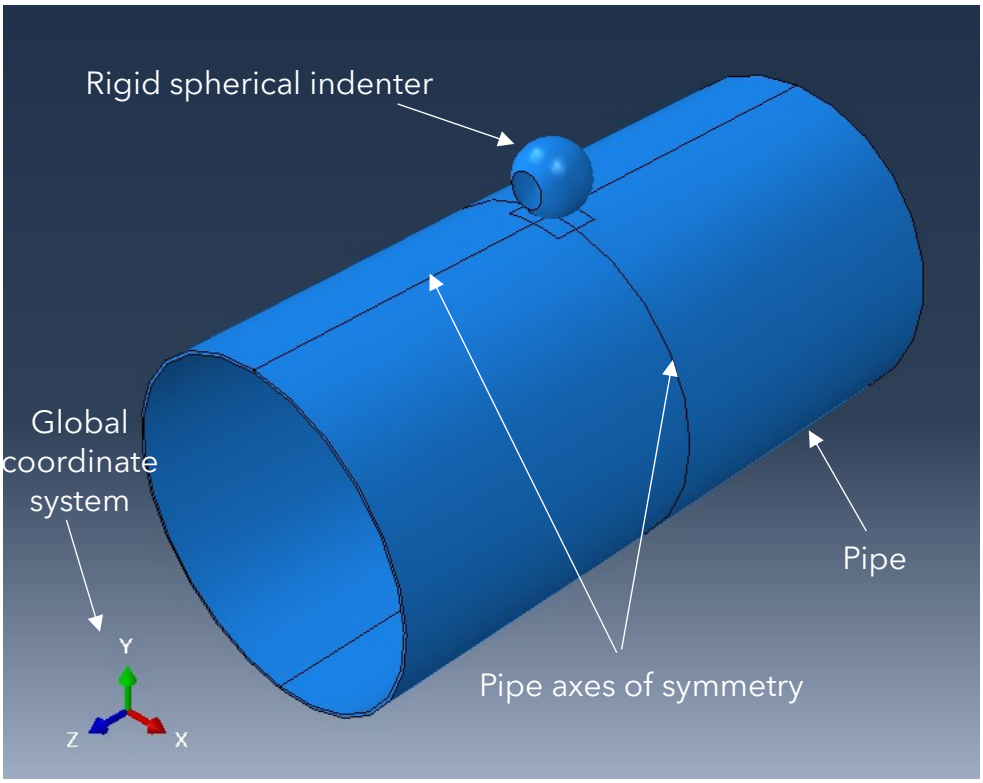

Figure 5.1. *Full pipe showing the global coordinate system, the indenter, and the symmetry of the problem.*

The pipe, shown in Fig. 5.1, is indented by a spherical indenter while restraining the bottom of the pipe from vertical motion in the y-axis direction. To reduce the computational work, the symmetry of the problem shown in Fig. 5.2 is used, therefore only a quarter of the pipe for analysis while considering the proper boundary conditions. Regarding the end conditions of the pipe, all the displacements and rotations, except the displacement in the radial direction, of the far edge of the pipe is coupled with a reference point located at the center of the pipe at the same plane of the far edge of the pipe. The three-dimensional translations and rotations of this point are fixed at zero.

In order to reduce the computational effort without sacrificing the simulation accuracy, the major part of the pipe is modelled by ABAQUS S3 and S4 shell elements. However, the pipe part in close contact with the spherical indenter is modelled by various solid

elements, as shown in Fig. 5.3, such as ABAQUS C3D8, C3D20R, and C3D20, to be able to capture the significant change in the strains at the indentation area. An appropriate connection between the solid and shell elements is achieved by using the ABAQUS "Shell-to-solid coupling" constraint to ensure the compatibility of the stresses and the strains.

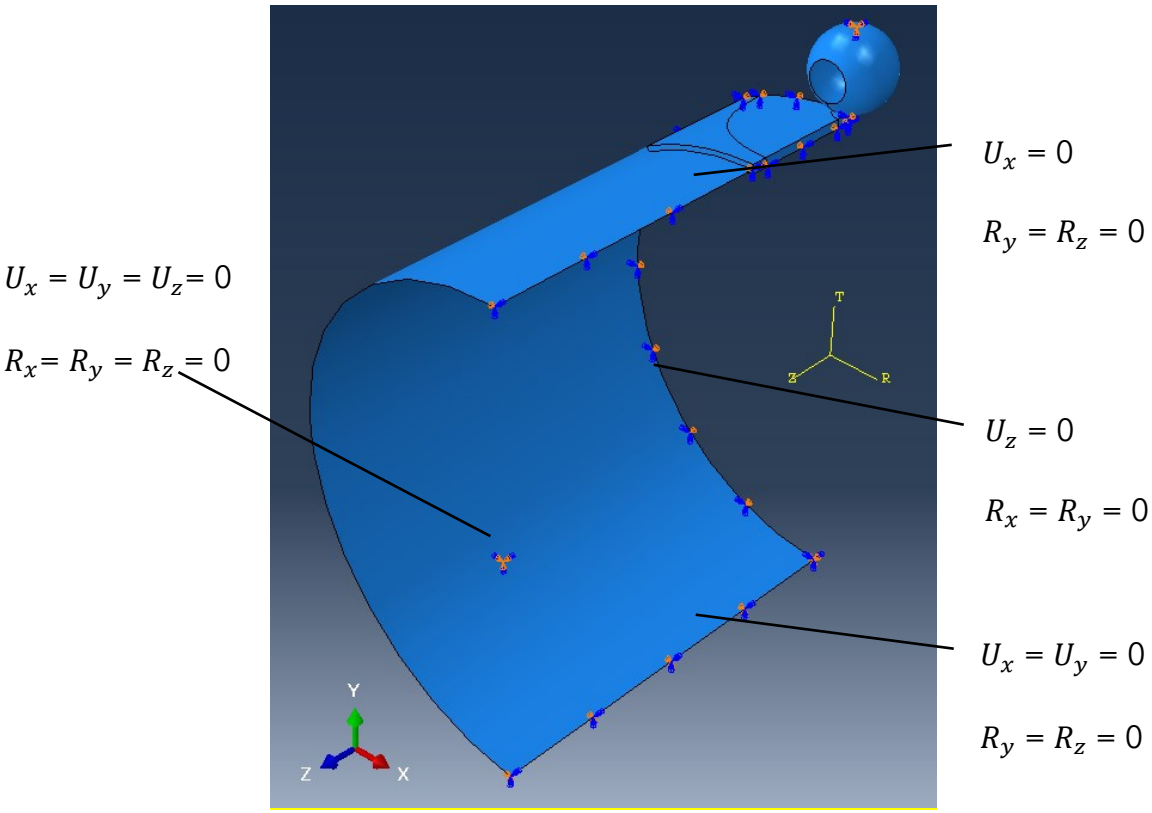

Figure 5.2. *FE model of the quarter of the pipe showing the boundary conditions***.**

Note that Figs. 5.2 and 5.3 are not to scale as they are only presented to explain the FE model and meshing. Also, in Fig. 5.3, the shell element is shown as a surface. However, once the shell thickness is rendered, the thickness of the shell element will be matching the thickness of the solid part, namely the pipe thickness.

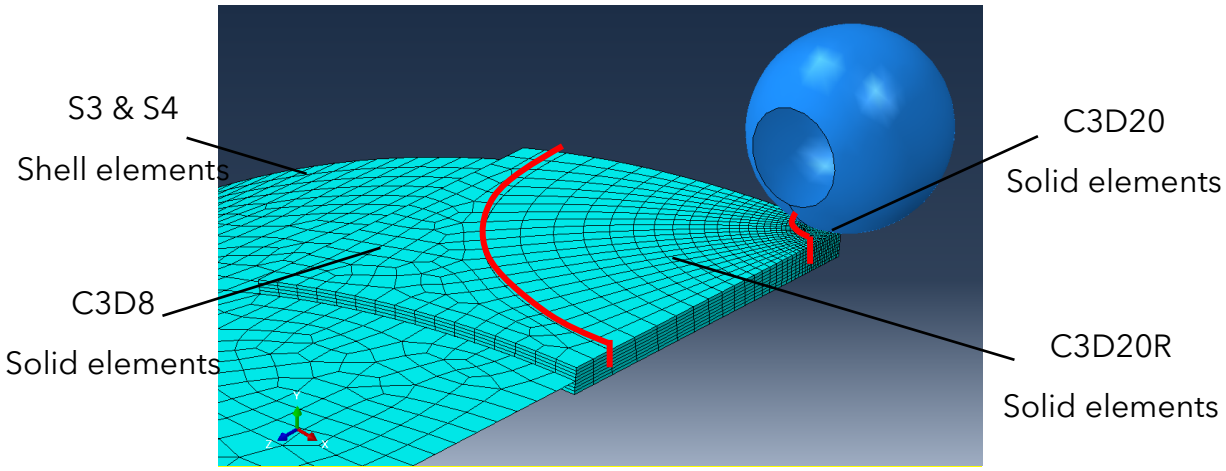

Figure 5.3. *Different types of FEs used in the FE model.*

The pipe steel material used in this study is X52 vintage steel. The Ramberg-Osgood nonlinear stress-strain model given in Eq. (5.8), as shown in Fig. 5.4, is used for modelling the pipe steel material.

$$\frac{\varepsilon}{\varepsilon_y} = \frac{\sigma}{\sigma_y} + \alpha\left(\frac{\sigma}{\sigma_y}\right)^n \tag{5.8}$$

Where σ_y and ε_y are the yield stress and the yield strain of the pipe steel material, respectively. α and n are taken equal to 1.72 and 12, respectively in this study to model the X52 vintage steel [101].

To create an indentation on the pipe, a spherical indenter is positioned on the outer surface of the pipe and gradually moved towards the pipe's center by a designated DD. In the ABAQUS model, a "surface to surface" discretization method is utilized for the contact problem, employing a finite sliding formulation and a tangential behaviour with a friction coefficient of 0.5 [101]. The spherical indenter is considered the master surface, while the outer surface of the pipe is regarded as the slave surface. After the indentation, the indenter is allowed to separate from the pipe, simulating the removal of the indenter.

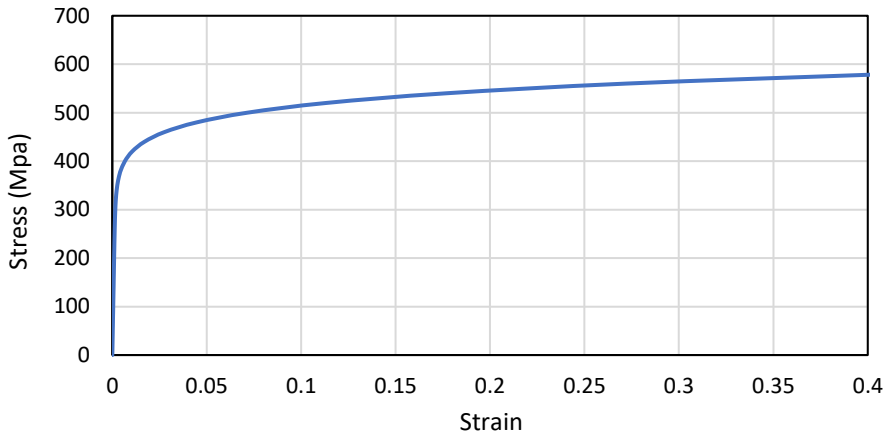

Figure 5.4. *Ramberg-Osgood non-linear model of the stress-strain relation for X52 vintage steel.*

Loading is applied following the sequence below:

1. Indenting the pipe.
2. Removing the indenter.
3. Pressurizing the pipe to the maximum allowed operating pressure (MAOP).
4. Reducing the pressure to zero.
5. Pressurizing the pipe with the inline pressure.

The above sequence is adopted to model a highly probable loading scenario of pipelines, where the pipe is indented due to any of several external effects (such as, construction equipment impact or the external pressure of gravels surrounding buried pipes). Then, after the indentation at some point of pipe operation, the pressure inside the pipe can increase to the MAOP and later decrease to the normal operating pressure.

The internal pressure (P) inside the pipe is set to be equal to MAOP which is calculated by Barlow's equation [2] using a design factor (DF) of 0.8, as shown in Eq. (9), and the inline pressure is set to 37.5% of the MAOP.

$$P = \frac{2 * DF * SMYS * WT}{OD} \tag{5.9}$$

SMYS in Eq. (5.9) is the specified minimum yield strength of the pipe steel material.

5.5. Study cases

In this study, the study cases are taken from [101] to compare the MEPS based reliability analysis with the reliability analyses based on SLD and DFDI damage models. Two pipes are considered for the damage analysis. The first one is NPS 30 with 7.14 mm WT having an OD/WT ratio of 106.7. The pipe is indented using two different spherical indenters of 15 and 30 mm radius, and each indenter is used to indent the pipe with three different dent depths, given in Table 5.2, to produce MEPS in the pipe dent defect of 20%, 26%, and 28%. The pipe designation in the first column in Table 5.2 and Table 5.3 is determined so that the pipe OD is written in millimeters after the "D", the indenter radius in millimeters after "IND", then the MEPS generated in the pipe is written as a percentage after "EPS".

Table 5.2. *Geometry and indentation data for the NPS 30 pipe.*

Defect Designation	Pipe configuration		Pipe Length (mm)	Indenter Radius (mm)	Dent Depth (mm)	DD to OD percentage	MEPS
	OD (mm)	WT (mm)					
D762-IND15-EPS20	762	7.14	2500	15	9.6	1.26%	20.00%
D762-IND15-EPS26	762	7.14	2500	15	12.9	1.69%	26.00%
D762-IND15-EPS28	762	7.14	2500	15	14	1.84%	28.00%
D762-IND30-EPS20	762	7.14	2500	30	14	1.84%	20.00%
D762-IND30-EPS26	762	7.14	2500	30	20.3	2.66%	26.00%
D762-IND30-EPS28	762	7.14	2500	30	23	3.02%	28.00%

The second pipe is NPS 12 with a WT of 6.35 mm and an OD/WT ratio of 51. The same indentation scheme is applied to the second pipe, such as two spherical indenter radii of 10 and 20 mm are used. Also, three different dent depths, given in Table 5.3, for each

indenter are applied to the pipe to produce MEPS of 20%, 26%, and 28% in the dent defect.

Table 5.3. *Geometry and indentation data for the NPS 12 pipe.*

Defect Designation	Pipe configuration		Pipe Length (mm)	Indenter Radius (mm)	Dent Depth (mm)	DD to OD percentage	MEPS
	OD (mm)	WT (mm)					
D323-IND10-EPS20	323.85	6.35	1100	10	4.9	1.52%	20.00%
D323-IND10-EPS26	323.85	6.35	1100	10	6.8	2.11%	26.00%
D323-IND10-EPS28	323.85	6.35	1100	10	7.5	2.32%	28.00%
D323-IND20-EPS20	323.85	6.35	1100	20	7.2	2.23%	20.00%
D323-IND20-EPS26	323.85	6.35	1100	20	10.3	3.18%	26.00%
D323-IND20-EPS28	323.85	6.35	1100	20	11.4	3.53%	28.00%

The DD in Tables 5.2 and 3 is determined by fixing all the geometric parameters of the problem in the FE model and increasing the DD until the required MEPS in the dented area is achieved. It has to be also mentioned that the MEPS are measured in the inside diameter material of the pipe. The dent depths provided in Tables 5.2 and Table 5.3 are the initial dent depths. After the removal of the indenter and the application of the internal pressure, the pipe springs back and rerounds making the permanent DD almost half the initial DD.

5.6. Results and discussion

5.6.1. Damage analysis and calculations

The damage calculations for the SLD or the DFDI damage criteria are similar. The only difference is the equation used to calculate the critical cracking strain at the calculation point using Eq. (5.1) for the DFDI and Eq. (5.2) for the SLD. During the different stages of loading, whether it is pipe indentation or pressure application, the load is increased incrementally during the simulation in ABAQUS. At each increment, all the stresses and the strains are calculated in the FE mesh nodes within the dented area under the indenter on the inner surface of the pipe. The damage using DFDI and SLD criteria

provided in section 5.2 is calculated at all the selected FE mesh nodes, and the damage at the node that has the maximum damage value is used as the maximum damage generated in the pipe from the dent defect. The point at which the MEPS occurs is not necessarily the same point at which the maximum damage occurs. As an example, the locations of the MEPS and maximum damage occurrence for the defect D762-IND30-EPS26 provided in Table 5.2 is shown in Fig. 5.5. This same defect is used to show in detail how the damage is developed at the maximum damaged node in the dented area.

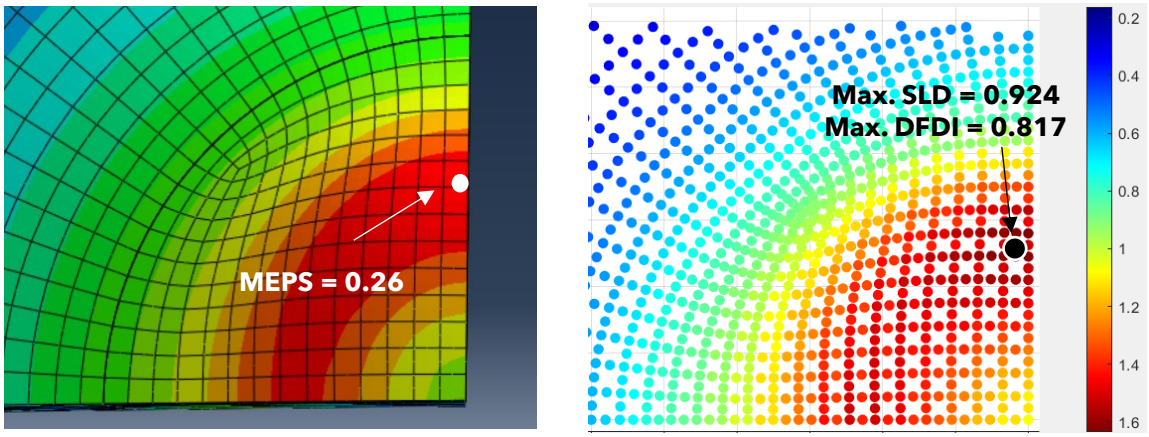

(a) EPS in dent region (b) Damage in dent region

Figure 5.5. *Different locations for (a) MEPS and (b) Max. damage in the same dent defect.*

The loading steps are shown in Fig. 5.6, where Fig. 5.6(a) and Fig. 5.6(b) show the indentation process (Step 1). Fig. 5.6(b) to Fig. 5.6(d) show step 2 (removal of the indenter). Fig. 5.6(b) shows the end of the indentation process and the beginning of the indenter removal, while Fig. 5.6(b) to Fig. 5.6(c) display the gradual process of moving the indenter away from the pipe. While Fig. 5.6(d) to (g) look similar, the difference between them in the vertical displacement of the dent profile accompanied with the change of pressure in the pipe and a very slight increase in the EPS during pipe pressurization. Figs. 5.6(e), 5.6(f), and 5.6(g) show the pipe after pressurization

with the MAOP (load step 3), depressurization (load step 4), and repressurization with the inline pressure (load step 5) respectively.

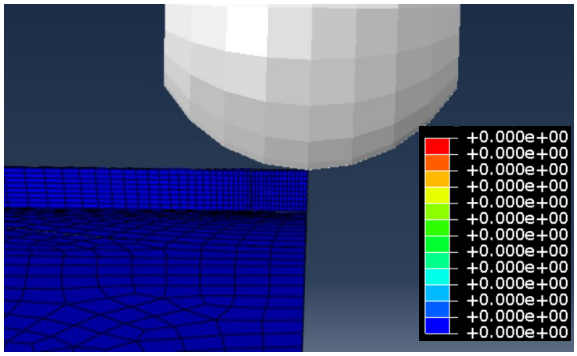

(a) beginning of indentation process (stage 1)

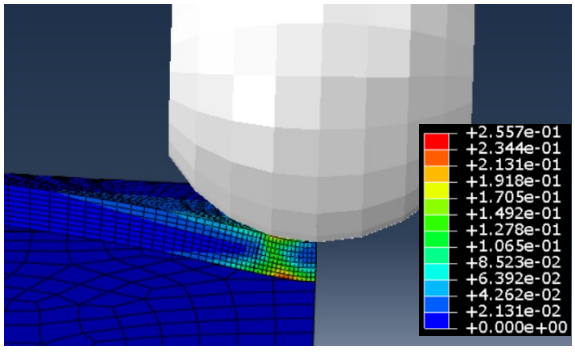

(b) end of indentation process

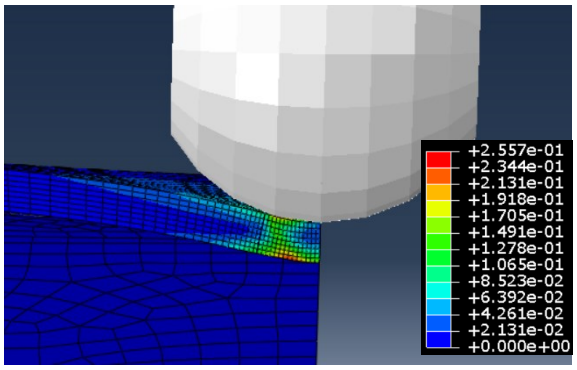

(c) last contact of the indenter with the pipe in stage 2

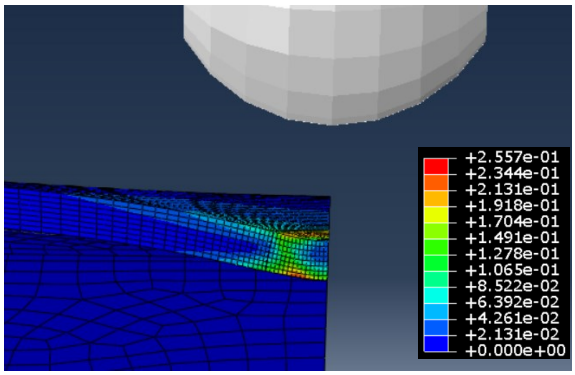

(d) Indenter removal and end of stage 2

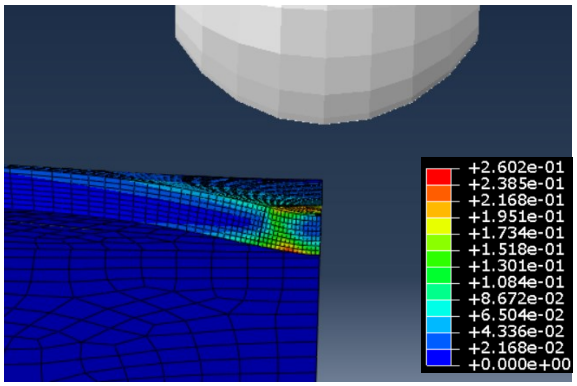

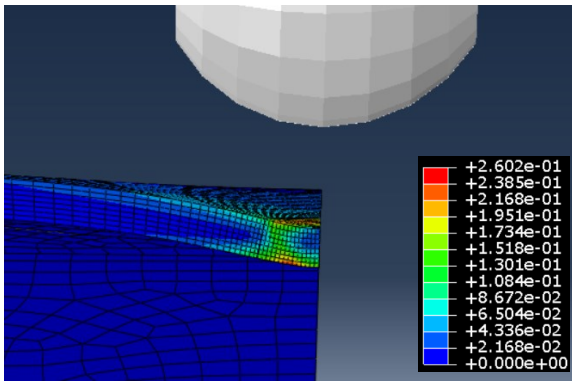

(e) after the application of MAOP (end of stage 3)

(f) after depressurizing the pipe (end of stage 4)

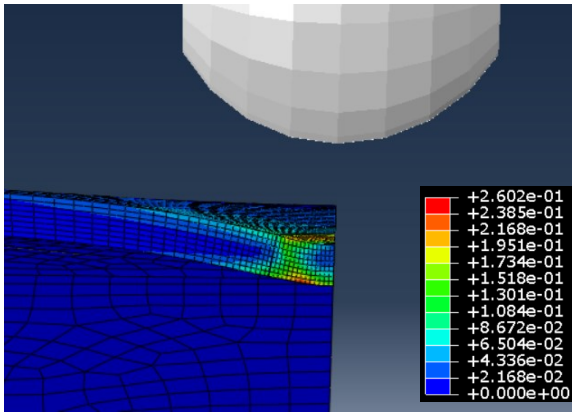

(g) after the application of the inline pressure (end of step 5)

Figure 5.6. *Dent profile showing the EPS distribution throughout different loading stages.*

Damage, as described by damage equations provided in section 5.2, is dependent on the hydrostatic stress, von Mises stress and the EPS generated at the calculation node. The hydrostatic stress and von Mises stress are based on the six components of stress at the node. From the obtained results of all the loading stages, the contribution of the shear stresses components in von Mises stress did not exceed 7%. I.e., the von Mises stress is mainly influenced by the normal stress components at the node exhibiting maximum damage. That node is usually located near the apex of the dent. S_{11}, S_{22}, and S_{33} designate the circumferential stress, the through thickness stress, and the longitudinal stress, respectively.

Fig. 5.7 shows the development of these stresses at the node with maximum damage throughout the different stages of loading. The through-thickness stress (S_{22}) is negligible compared to the longitudinal (S_{33}) and circumferential stresses (S_{11}) (Fig. 5.7) rendering S_{33} and S_{11} the major contributors to the hydrostatic and von Mises stresses values. In the following, the development and progression of the normal stresses (S_{11},

S_{22}, and S_{33}), the hydrostatic and von Mises stresses, the EPS through the loading stages are presented to show how they affect the damage at the target node.

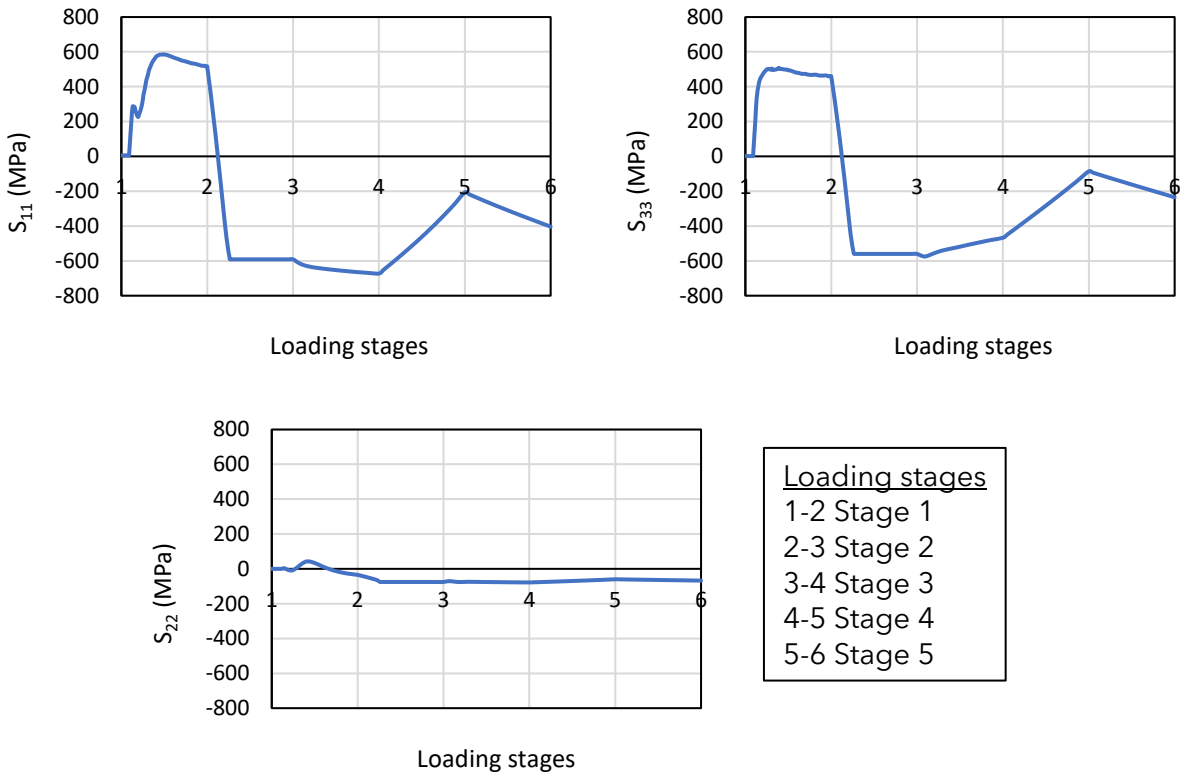

Figure 5.7. *S_{11}, S_{22}, and S_{33} at the maximum damage node throughout the loading stages.*

At the beginning of the indentation process, stage 1 in Fig. 5.7, the tensile stresses in the longitudinal and circumferential directions increase to reach their respective maximum values which then drop for the rest of the indentation process. The increase and slight drop of the tensile stresses during the indentation process is due to the change of the contact point or region of the indenter with the pipe at the different steps of the indentation process. Through the indentation process, the contact of the indenter with the pipe moves away from the center of the indenter, making the maximum damage node at a certain point of the indentation process under the contact area with the indenter. Later, the contact region moves farther from the dent apex and the maximum damage point causing a slight drop in the tensile stresses. The same

behaviour is reflected on the hydrostatic stress given in Fig. 5.8. However, the von Mises stress on the other hand continues to increase during the indentation process.

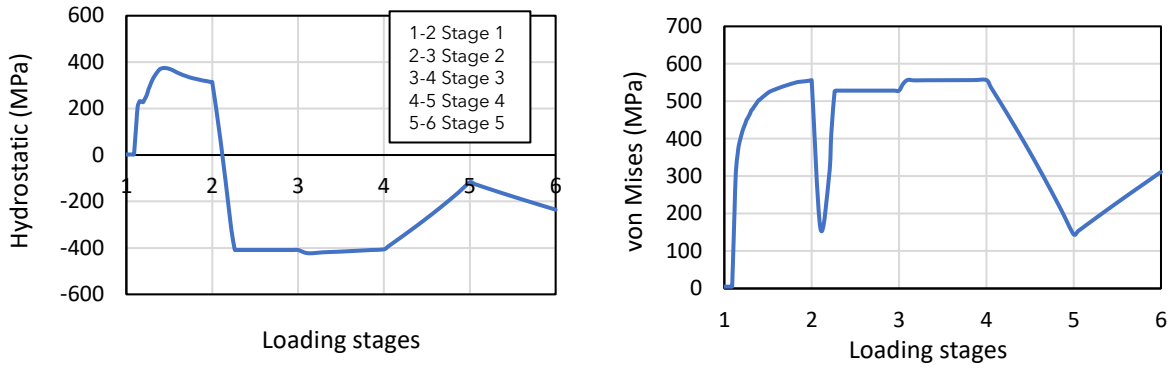

Figure 5.8. *Hydrostatic and von Mises stresses at the maximum damage node throughout the loading stages.*

The ratio between the hydrostatic pressure to the von Mises stress, which is the main variable in Eq. (5.1) for DFDI and Eq. (5.2) for SLD. This ratio changes between 0.45 and 0.75 throughout the indentation process making the cracking strain between 0.28 and 0.42 for DFDI and between 0.24 and 0.4 for SLD as shown in Fig. 5.9. The calculated SLD cracking strain is always less than the DFDI one at any loading step during the first stage. The slight decrease in the cracking strain values for the SLD over the DFDI leads to the SLD predicting higher damage strain than DFDI as shown in Fig. 5.10.

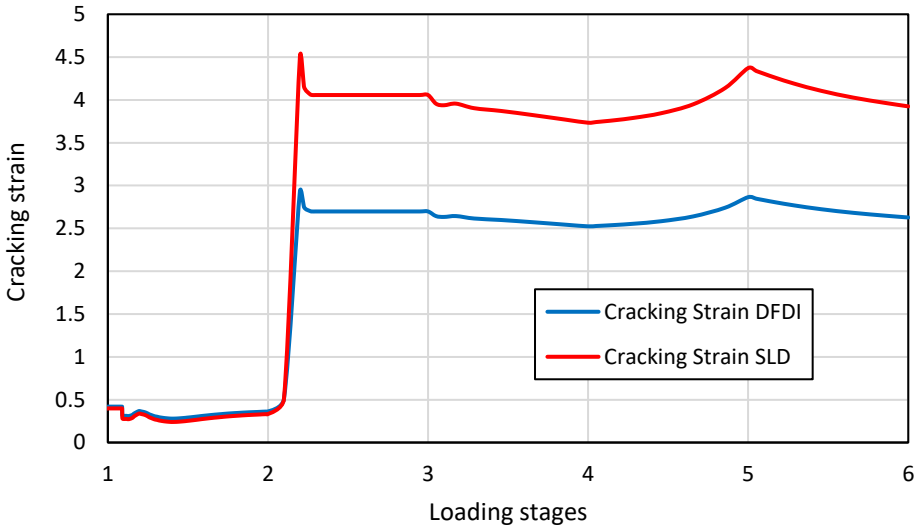

Figure 5.9. *Cracking strain at the maximum damage node through loading stages.*

During the second stage, stage 2 in Fig. 5.7, the indenter is moved away from the pipe with a controlled displacement. At the beginning, the indenter is in contact with the pipe while the indenter is being removed and the stresses at the target node changes, then the indenter lose contact with the pipe for the remaining of the loading stage and the stresses remains constant.

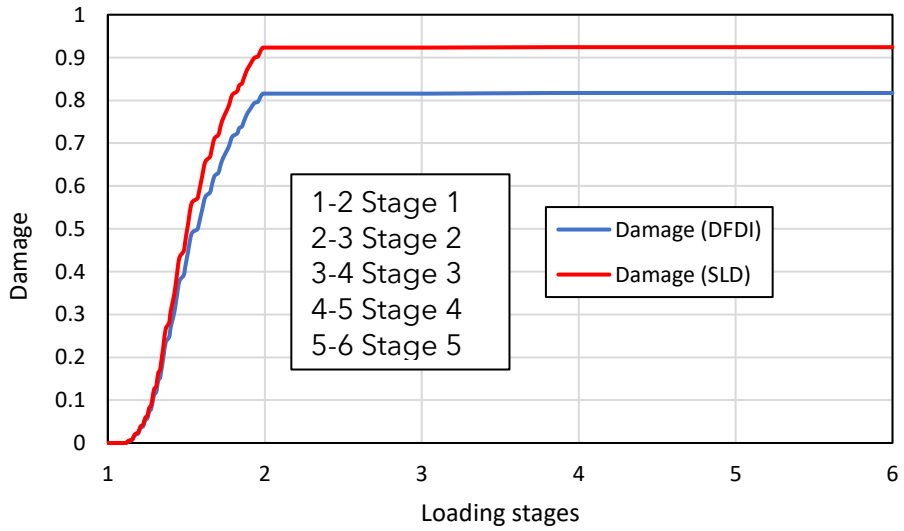

Figure 5.10. *Damage at the maximum damage node through loading stages using the DFDI and SLD damage criteria.*

As the pipe rerounds, the stresses S_{11} and S_{33} switch from tension to compression passing by zero. The hydrostatic stress follows the same trend. The von Mises stress, on the other hands, drops when S_{11} and S_{22} reach zero and increases again to almost its previous value when the normal stresses switch from tension to compression. At this instance, the DFDI and SLD equations show a discrepancy in the cracking strain values with the SLD predicting higher cracking strain than the DFDI. The reason behind that is the difference between the DFDI and the SLD equations at predicting the cracking strain for negative values of the hydrostatic to the von Mises stress ratio, as shown in Fig. 5.11, as the hydrostatic stress switch from positive to negative while the von Mises stress remains always positive. However, this significant increase in the cracking does not affect the SLD and the DFDI damage results as there is no increase in the EPS at the indenter removal stage, as shown in Fig. 5.12.

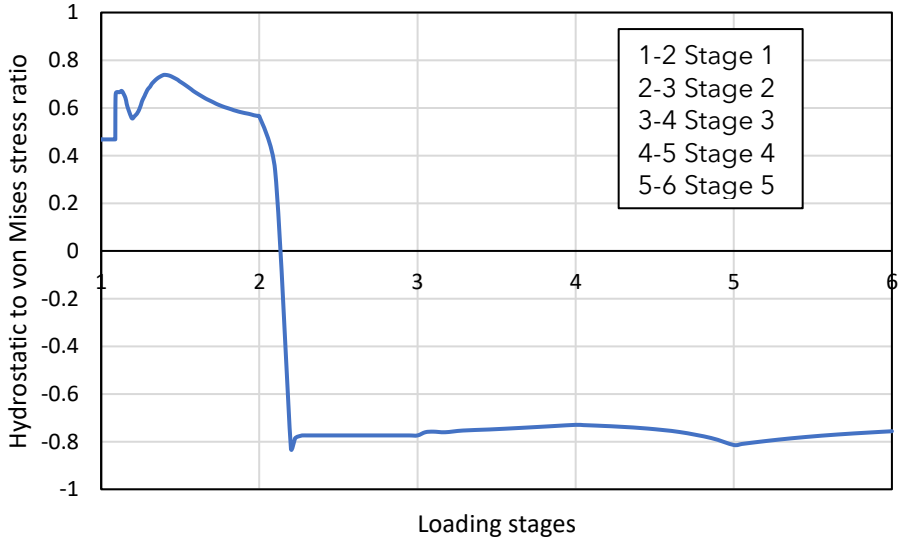

Figure 5.11. *Hydrostatic stress at the maximum damage node through loading stages.*

In stage 3, the application of the MAOP does not significantly affect the damage. The cracking strain slightly decreases in magnitude, as shown in Fig. 5.9, due to a slight decrease of the hydrostatic to von Mises stress ratio magnitude, as shown in Fig. 5.11. With a small increase in the EPS due to the application of the MAOP and the cracking strain slightly changing in value, the damage using both criteria slowly increases.

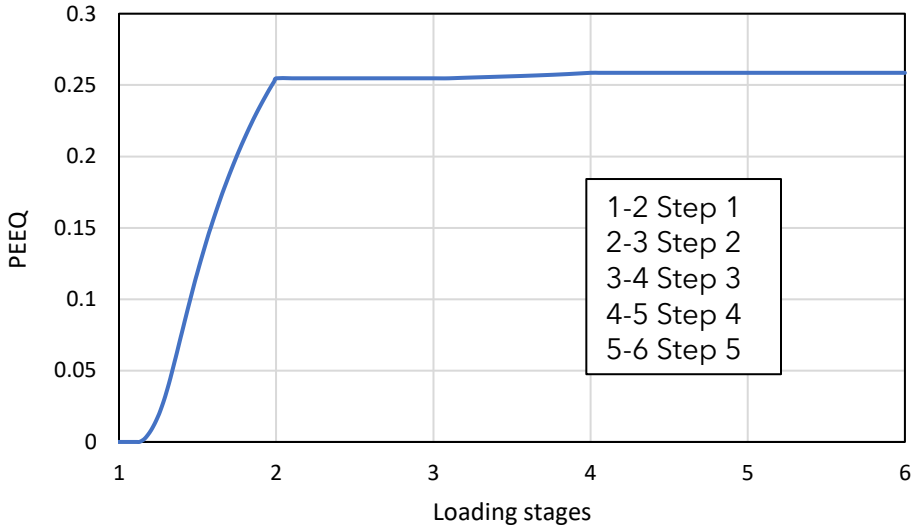

Figure 5.12. *EPS at the maximum damage node through loading stages.*

The validity of using the DFDI and SLD cracking strain equations had to be investigated when using negative triaxiality value (hydrostatic to von Mises stress ratio) occurring after stage 1. Referring to ASME BPVC.VIII.3-2021 for the SLD equation and to API 1183-2020 for the DFDI equations, the standards do not provide a limit on the principal stresses' values used in the cracking strain equations, meaning that the equations should be valid for negative triaxiality values. In Hancock and McKenzie [106], only tensile tests were used to calibrate the DFDI equations, however, it was shown from tensile test results that the with the decrease of the positive the value of the cracking strain increases exponentially. Bao et *al.* [109], Brunig et *al.* [110], and Khan and Liu [111] provided studies for the ductile damage focusing on negative triaxialities for different metals. Bao et *al.* showed that for the 1045 steel and Al 2024-T351 aluminum

the cut-off value for the triaxiality below which fracture does not occur is equal to -1/3. Bao et *al.* also showed, based on numerical analysis and the experimental test done by Kao et *al.* [112], that the fracture strain is increasing exponentially with the increase of the negative triaxiality magnitude, as shown in Fig. 5.13, which matches the behaviour of the DFDI and the SLD equations at the increase of the negative triaxiality in magnitude, as shown in Fig. 5.13. Later, Khan and Liu showed that the cut-off value for negative triaxiality is not constant and is dependent on the stress state. Brunig et *al.* provided a cut-off equation with a minimum negative triaxiality cut-off of -0.6. While the cut-off may be different for the X52 steel used in this study, the above discussion shows that with the increase of the negative triaxiality magnitude, the failure is less likely to occur.

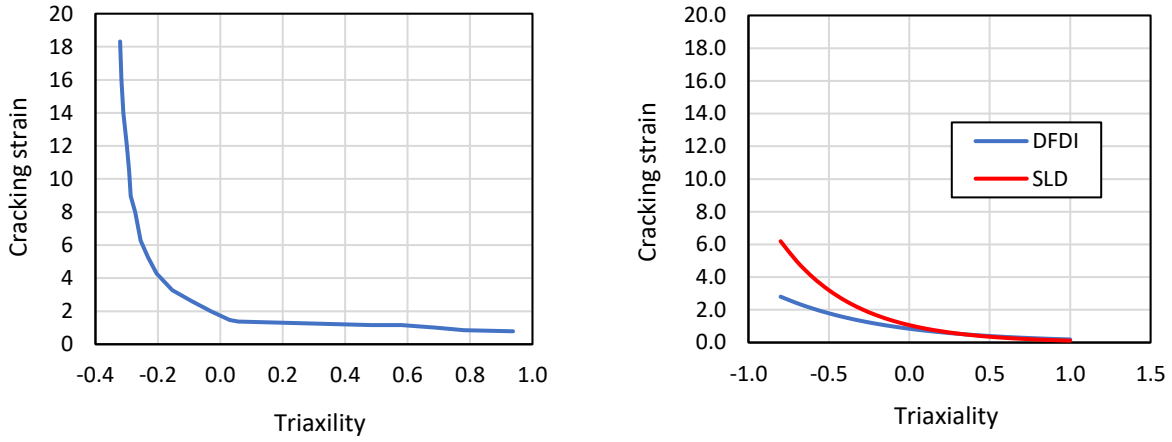

(a) cracking strain vs. triaxiality for 1045 steel

(b) cracking strain predicted by the DFDI and SLD equations

Figure 5.13. *Cracking strain vs. triaxiality for the (a) 1045 steel presented by Bao et al.* [109] *and predicted by (b) the DFDI and SLD equations.*

The cracking strain values predicted by the DFDI and SLD equations for the negative triaxiality ratio is less than the values provided in [109], showing that the DFDI and SLD equations are conservative at predicting the fracture or cracking strain for negative

triaxiality. There is probably a need for more studies on the accuracy of the DFDI and SLD equations at predicting the cracking strain at negative triaxiality values and the value of the negative hydrostatic stress cut-off for steel grades. However, for this study, the DFDI and SLD equations are used with the negative hydrostatic pressure, knowing that the predicted value of the damage predicted by these equations is highly probable to be on the conservative side. Additionally, it has to be mentioned that the effect of loading stages where the triaxiality is negative on the final damage value is miniscule as explained in the remaining of this section.

In stage 4 and stage 5 the internal pressure is decreased to zero then increased to the inline pressure, which is less than the MAOP. Therefore, the EPS at the target node will not increase in these two steps keeping the damage constant for both damage criteria.

The main observation on the damage analysis is that the main portion of the damage occurs during the indentation process with higher damage predicted by the SLD over the DFDI criterion due to the slightly higher (less than 1) prediction of the cracking strain by the DFDI damage equations. The damage also slightly increases during the application of the MAOP load stage, however, the other loading stages do not affect or increase the damage.

The damage curves provided in Fig. 5.10 match with the results of the study conducted by Li and Dang in [113]. Li and Dang developed an ANSYS FE model to analyze the indentation of the unconstrained pipe with a semi elliptical indenter, and they used the DFDI damage criterion to calculate the damage in the pipe. They reached a conclusion that the main part of the damage occurs during the indentation process and that a slight damage is done when applying the MAOP, which is matching the damage results shown in Fig. 5.10.

5.6.2. Verification of the FE model damage results

To verify the FE-predicted damage results, the experimental damage results provided by Arumugam et *al.* in [107] are used. The 2500 mm long pipe tested in [107] is an NPS 34 (863.6 mm OD) with a WT of 9.6 mm and made of X52 steel grade. The pipe is

indented with an indentation depth of 12% of OD (103.32 mm) using a high-strength steel spherical indenter of 63.5 mm radius.

In [107], the pipe is tested experimentally by denting the pipe until cracks start to appear. Then, the dent profile is scanned using a laser scanner, and the MEPS at the final stage of loading was calculated from the dent profile using a curvature-based strain method. Arumugam et *al.* calculated the upper limit of the DFDI using simplified DFDI equations by using the MEPS they calculated at the final stage of loading.

A pipe with the same geometry as the pipe provided by Arumugam et *al.* in [107] is modelled using the FE model developed for this study. The comparison between the results of the developed FE model in this study and the results provided in [107] are provided in Table 5.4.

Table 5.4. *MEPS and DFDI results comparison for the developed model validation.*

Model	**MEPS (%)**	**DFDI**	**SLD**	**DFDI upper bound**
Developed model	29.5	0.881	0.9797	-
Model from [107]	30.1	-	-	0.98

Comparing the MEPS results from Table 5.4, the absolute relative error is 1.99% which shows a good agreement between the developed model and the reference model. Also, the DFDI result of the developed FE model in this study is around 90% of the DFDI upper bound provided for the cracked pipe in the reference results.

5.6.3. Reliability analysis results

In this section, the results of the damage reliability analysis using the SLD and the DFDI are presented. The reliability results, i.e. the reliability index "beta" and the PoF, are also compared to the MEPS-based reliability results obtained from [101] to show the

difference between using different strain-based reliability assessment methods. Table 5.5 and 5.6 presents the reliability results of the NPS 30 and NPS 12 pipes respectively. The reliability analysis is performed including and excluding the interaction terms from the RS equations.

The strain-based reliability results, for the three strain-based criteria, including and excluding the interaction terms in the response surface are in good agreement, which indicates acceptable stability and convergence in the achieved results. It also shows that the inclusion of the interaction terms did not have a significant effect on the reliability analysis results.

For some cases (SLD results for D762-IND15-EPS26, and D762-IND15-EPS28, and SLD and DFDI results of D323-IND10-EPS26, and D323-IND10-EPS28) the PoF is higher than 0.5. Therefore, the reliability index has a negative sign. It has to be mentioned that the PoFs for these cases were also calculated by the Monte Carlo Simulation to check the validity of the results obtained from FORM analysis.

Comparing the results obtained using the SLD and DFDI damage models, the same trend is observed: the PoF increases with the increase of the DD in all the cases as expected. However, the PoF calculated using the SLD damage models are higher and thus more conservative than the DFDI damage model in all cases, which is consistent with the literature. Arumugam et *al*. [49] calculated the DFDI and SLD values for an actual study case of a dented pipe based on the FE models accurately. Additionally, they calculated the maximum strain developed in the actual pipe from the dent profile obtained by laser scanning the internal wall of the pipe, which was substituted into simplified DFDI and SLD equations to calculate the upper and lower bounds of the damage values to verify the accuracy of the FE-predictions. For the pipe that had already developed cracks, the DFDI value calculated for the dent was equal to 1.1. This indicated a realistic prediction of the crack initiation by the DFDI criterion. However, the accurate SLD value for the same dent defect is equal to 1.52, showing a more conservative prediction of the cracking for the SLD equation. According to [6], the DFDI

is more realistic at predicting failure and predicting lower values for the damage, which is also reflected from the reliability analysis results.

For each of the dent defect case having the same pipe geometry and the same indenter size, the nominal MEPS values (20%, 26%, and 28%) are increased by the increase of the DD of the indenter, as shown in Table 5.2 and Table 5.3. Therefore, the MEPS reliability results, provided in Table 5.5 and Table 5.6, show an increase of the PoF with the increase of the DD for all the cases studied. The same trend is showed by the results using the SLD and DFDI damage models. However, the increase rate of the PoFs estimated using the damage models are higher than the increase rate of the PoF when using the MEPS criterion. An example is the DFDI damage for NPS 30 with the 15 mm indenter, the PoF at the lowest MEPS of 20% has the same order (of 10^{-4}) as the MEPS criterion PoF results. However, with the increase of the DD, the PoF associated with the DFDI criterion increases at higher rate compared to that associated with the MEPS. This indicates that the two damage criteria are more sensitive to the increase of DD than the MEPS criterion.

The PoFs associated with the SLD criterion are higher than those associated with the DFDI. The PoF results associated with DFDI are relatively closer to those associated with the MEPS when using the smaller indenter radius for both NPS 30 and NPS 12 pipes. However, when using the bigger indenter radius for both pipes the PoF using the DFDI reduces drastically compared to those when using the MEPS, which shows that the DFDI criterion is more sensitive to the change in the indenter size.

The reliability results are also supported by another study in the literature, Wu et *al*. [114], which developed an FE model using C3D8R in ABAQUS to test the effect of different parameters on the damage of dent defects. Wu et *al*. used an ellipsoidal indenter to indent the pipe and used the Oyane's damage criterion to calculate the damage in the dent defect. They concluded that for the same pipe size and the same DD, the smaller the indenter size the more the pipe is damaged. The 762 mm OD pipes, D762-IND15-EPS28 and of D762-IND30-EPS20 have the same pipe size and DD,

presented in Table 5.2, but different indenter radii: 15 mm in D762-IND15-EPS28 and 30 mm in D762-IND30-EPS20. Table 5.5 shows PoFs for D762-IND15-EPS28 are higher compared to D762-IND30-EPS20, which is consistent with the findings provided by Wu et *al*. The same observation applies to the 323.85 mm OD pipe: the D323-IND10-EPS28 and D323-IND20-EPS20. They have very close DDs, as provided in Table 5.3, and their PoFs associated with the DFDI and the SLD are higher for the smaller indenter size. Also, Wu et *al*. reached the same conclusion that the internal MAOP pressure had a negligible effect on the damage of the dent defect.

It is important to note that the DFDI- and SLD-based reliability analyses using the LSF given in Eq. (5.6), with a deterministic damage limit of 1. Conversely, the reliability analyses based on MEPS arise from the LSF defined in Eq. (5.10) [101], where the limit is the strain capacity (SC) of the pipe material treated as a random variable. This makes the explanation of the difference between the MEPS-based and the DFDI- or SLD-based reliability results difficult to explain.

$$g_{MEPS}(DD, WT, YS) = SC - RS_{MEPS}(DD, WT, YS) \tag{5.10}$$

Additionally, the SLD and DFDI damage criteria are functions of the whole stress and strain history of the point where the maximum damage occurs, while the MEPS criterion only depends on the MEPS reached at the end of loading at the point where the MEPS occurs.

Table 5.5. *Strain based reliability analysis results for the NPS 30 (762 mm OD) pipe with 7.14 mm WT.*

	MEPS				DFDI				SLD			
	Interaction		No Interaction		Interaction		No Interaction		Interaction		No Interaction	
Defect	Beta	PoF	Beta	PoF	Beta	PoF	Beta	PoF	Beta	PoF	Beta	PoF
D762-IND15-EPS20	3.427	3.05E-4	3.452	2.78E-4	3.681	1.16E-04	3.602	1.58E-04	1.736	0.0413	1.600	0.0548
D762-IND15-EPS26	1.415	0.0785	1.489	0.0682	0.993	0.1604	0.836	0.2017	-1.173	0.8797	-1.273	0.8984
D762-IND15-EPS28	0.730	0.2328	0.769	0.2210	0.129	0.4485	0.066	0.4736	-2.082	0.9813	-2.158	0.9845
D762-IND30-EPS20	2.964	0.0015	2.977	0.0015	8.397	1.95E-16	8.366	2.53E-16	4.230	1.17E-5	3.893	4.96E-5
D762-IND30-EPS26	2.017	0.0219	1.848	0.0323	6.333	1.20E-10	6.268	1.82E-10	2.841	0.0022	2.659	0.0039
D762-IND30-EPS28	1.010	0.1563	0.956	0.1695	4.592	2.20E-06	4.743	1.05E-06	0.147	0.4414	0.041	0.4835

Table 5.6. *Strain based reliability analysis results for the NPS 12 (323.85 mm OD) pipe with 6.35 mm WT.*

	MEPS				DFDI				SLD			
	Interaction		No Interaction		Interaction		No Interaction		Interaction		No Interaction	
Defect	Beta	PoF	Beta	PoF	Beta	PoF	Beta	PoF	Beta	PoF	Beta	PoF
D323-IND10-EPS20	2.352	9.34E-3	2.42	7.82E-3	1.442	0.0746	1.358	0.0872	0.041	0.4837	0.026	0.4898
D323-IND10-EPS26	1.003	0.1579	1.077	0.1408	-0.219	0.5866	-0.42	0.6616	-1.699	0.9553	-1.777	0.9622
D323-IND10-EPS28	0.531	0.2978	0.569	0.2846	-0.669	0.7481	-0.86	0.8061	-2.309	0.9895	-2.433	0.9925
D323-IND20-EPS20	3.307	4.72E-4	3.355	3.96E-4	8.076	3.35E-16	8.054	4.01E-16	6.383	8.69E-11	6.030	8.21E-10
D323-IND20-EPS26	1.365	0.0862	1.415	0.0785	6.546	2.96E-11	6.365	9.75E-11	3.998	3.19E-05	3.560	1.86E-04
D323-IND20-EPS28	0.662	0.2539	0.628	0.2651	4.059	2.46E-05	4.041	2.66E-05	2.505	6.12E-03	2.374	8.81E-03

5.6.4. Interpretation of reliability results

The interpretation of some reliability results provided in Tables 5.5 and 5.6 are presented in this subsection. The reliability results using the RS including the interaction terms will be used to compare between the different damage models and the MEPS reliability results. The reliability results for pipes of NPS 30 with dent defects created by 15 mm indenter radius are used to demonstrate the interpretation of results for more insights.

To compare the reliability results associated with SLD and DFDI, the statistical distributions of damage measure (i.e., DFDI, SLD) for pipes of NPS 30 with dent defects created by 15 mm indenter radius are plotted in Fig. 5.14. The statistical distributions are obtained by running a Monte Carlo simulation using the RSs constructed in the last iteration from the full-factorial design of experiment. The reliability analyses are based on the LSF given in Eq. (5.6), in which the maximum limit allowed for the damage is equal to 1 assuming that any damage greater than one will initiate cracks in the dent defect and lead to failure. In Fig. 5.14, the area under the probability density curve for damage when greater than the limit of 1 is representing the PoF.

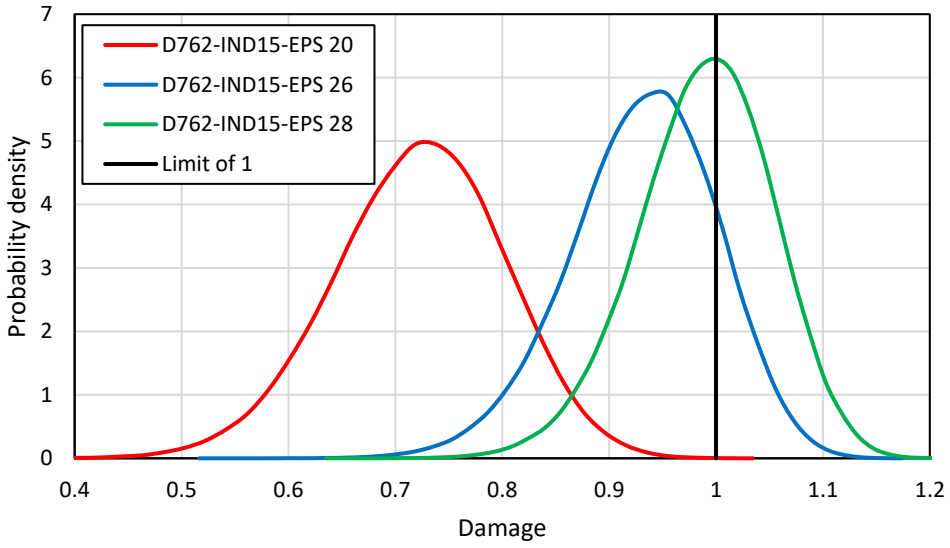

(a) probability density curves for DFDI.

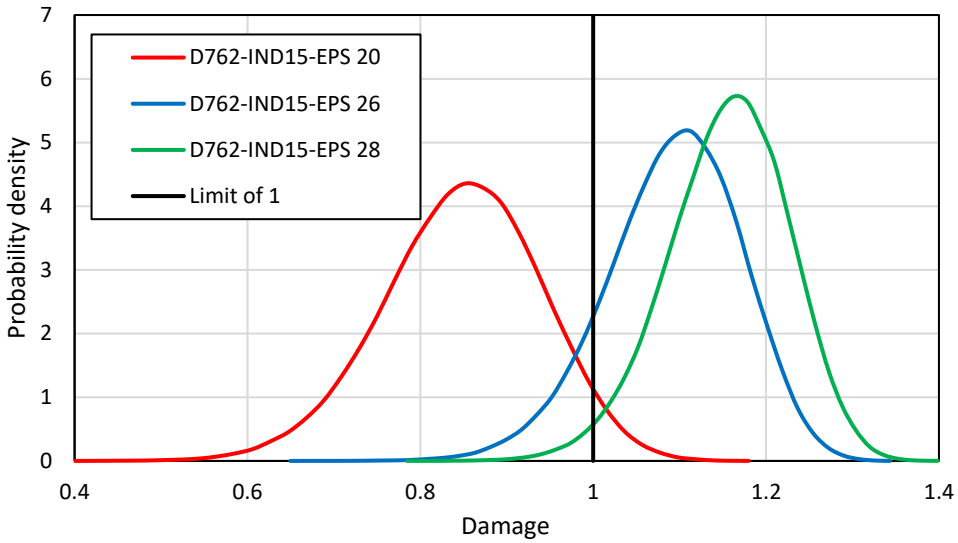

(b) probability density curves for SLD.

Figure 5.14. *Damage probability density curves for the pipe using (a) the DFDI damage criterion and (b) the SLD damage criterion for the pipe having 762 mm OD with dent defects created by 15 mm indenter radius.*

It can be seen from the distributions in Fig. 5.14 that with the increase of the strain generated in the pipe, the damage distribution in the SLD and the DFDI criteria shifts to the right with higher mean value while the standard deviation of the distribution decreases. The mean value of the distribution increases due to the expected increase of the damage in the dent defect associated with the higher MEPS generated in the pipe as the indenter is pushed further into the pipe to generate higher strains. The standard deviation, however, is decreased with the increase of the damage level or with the increase of the MEPS because the precision of the in-line inspection tool has a fixed value (with a standard deviation of 1.25 mm) independent of the value of the DD. However, the steel grade is constant for all the cases making the YS statistical data constant, and the WT standard deviation is a percentage of the WT mean value. With the increase of the DD while keeping its standard deviation constant, the resultant statistical distribution of the damage has a relatively smaller standard deviation.

The significant increase of the PoF for the dent defects on the NPS 30 using the 15 mm from 20% (D762-IND15-EPS20) MEPS to the 26% (D762-IND15-EPS20) and 28% (D762-IND15-EPS28) MEPS can be explained by Fig. 5.14(a) for the DFDI results and Fig. 5.14(b) for the SLD results. As for both damage criteria, the 20% MEPS damage distribution shifts to the left making only a small part of the distribution tail exceed the damage limit, while for the 26% and 28% MEPS a significant part (for the SLD the mean of the distributions is exceeding the damage limit of 1) of the distribution exceeds the damage limit.

It can be also seen from Fig. 5.14 that the SLD damage distributions have higher mean values than their corresponding DFDI distributions. This is because the SLD damage values for the same defect are higher than their corresponding DFDI values as shown in the damage results of the 762 mm OD pipe with indenter radius of 15 mm and MEPS of 26% given in Fig. 5.15. The mean value of all the RVs considered in this problem is used to produce the damage results of the defect in Fig. 5.15.

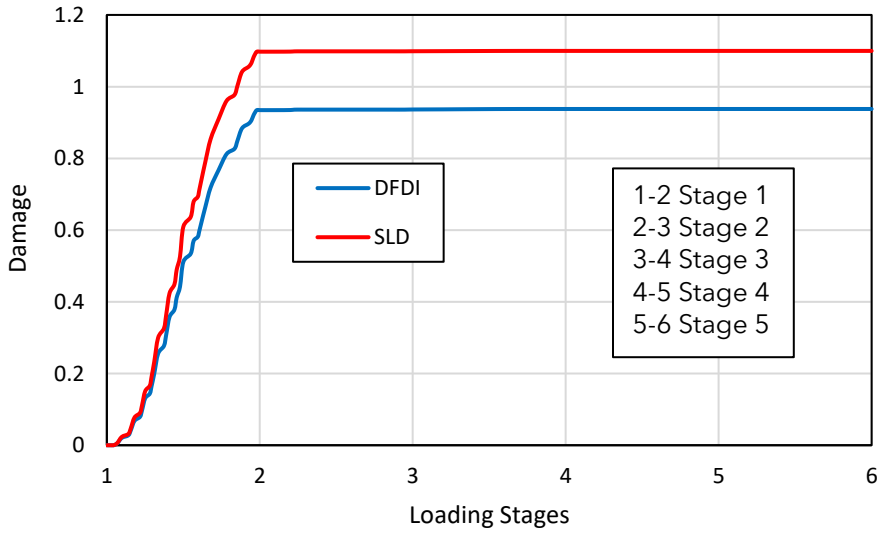

Figure 5.15. *Damage at a point in the dented during loading stages using the DFDI and SLD damage criteria.*

Comparing the reliability results of the SLD and the DFDI, the probability distributions of the DFDI and the SLD are plotted together for the D762-IND15-EPS20, D762-IND15-EPS26, and D762-IND15-EPS28 defects in Fig. 5.16. Note that the distributions plotted in Fig. 5.16 are the same distributions as plotted in Fig. 5.14, but they are grouped differently in the plots so that the distributions of the SLD and DFDI are plotted on the same plot for the different defects to compare the reliability results of the two damage criteria.

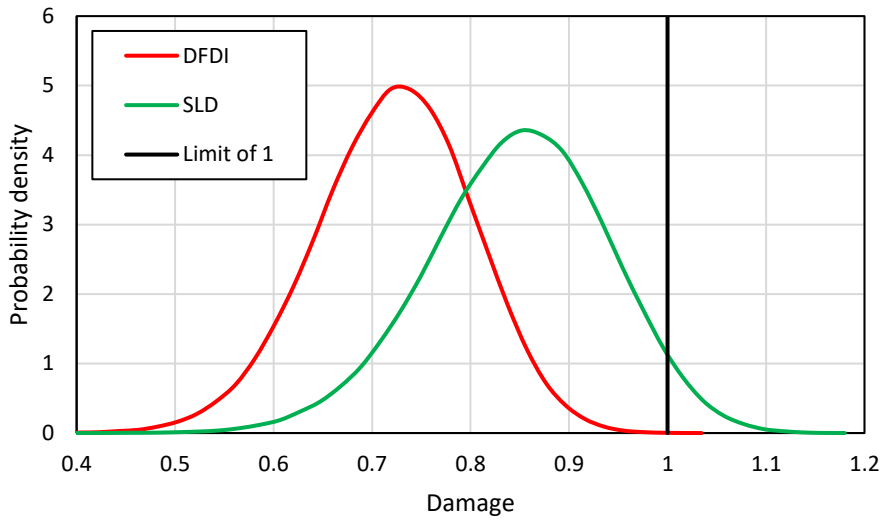

(a) D762-IND15-EPS20

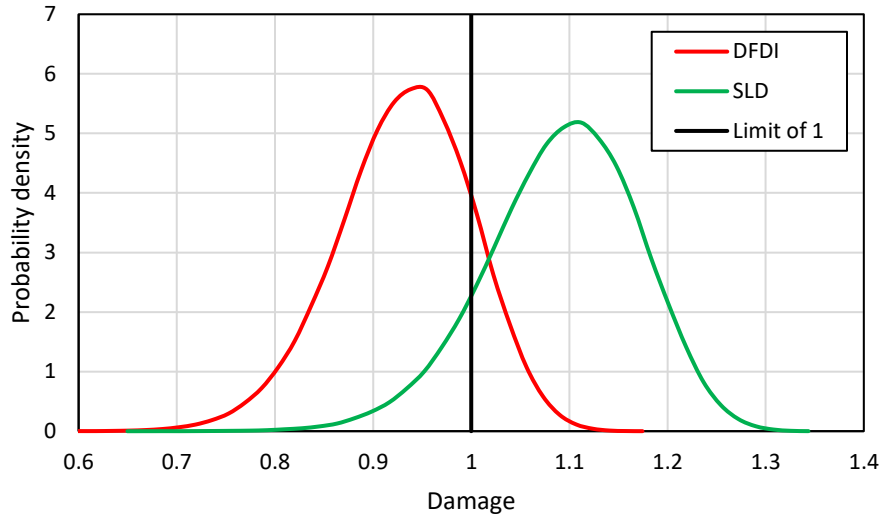

(b) D762-IND15-EPS26

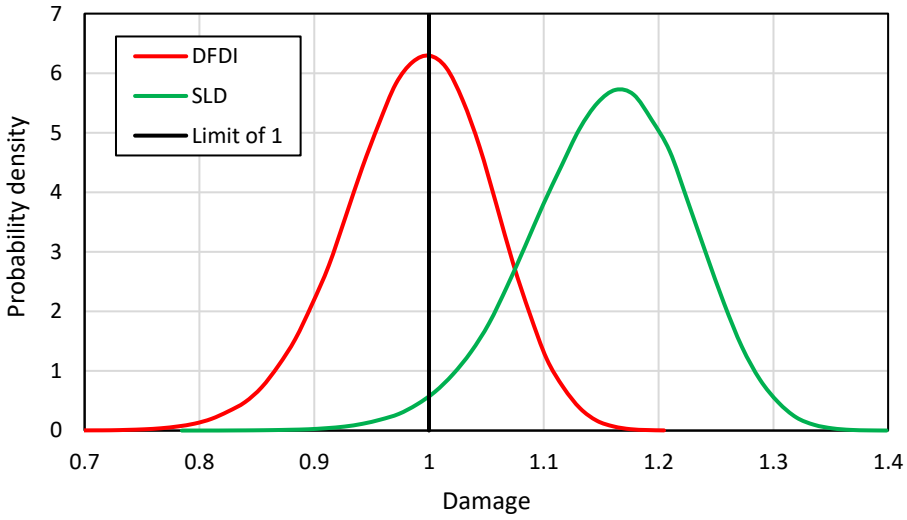

(c) D762-IND15-EPS28

Figure 5.16. *Damage statistical distribution for DFDI and SLD criteria for (a) D762-IND15-EPS20, (b) D762-IND15-EPS26, and (c) D762-IND15-EPS28.*

From the distributions in Fig. 5.16, the ratio of the mean value of the SLD distribution over the mean value of the DFDI distribution is around 1.17, which is reflected in the

SLD distributions producing higher PoFs. The shift of the SLD distribution to the right leads to higher PoF. For example, the PoF for D762-IND15-EPS20 based on the DFDI is of the order of 10^{-5} as only the tail of the distribution is above the limit of 1 in Fig. 16(a), but the right shift of the SLD distribution results in a PoF of the order of 10^{-2}.

5.7. Limitations

It has to be mentioned that the POF calculated in this chapter is a conditional one, as some other random variables of the problem are not included in the reliability analysis, such as the pipe outside diameter and the maximum operating pressure of the pipe.

5.8. Conclusion

This paper successfully presented reliability analysis of pipe containing dent defects using damage models. Damage-based reliability analysis using strain limit damage (SLD) and the ductile failure damage indicator (DFDI) is conducted on two different pipes with 51 and 106.7 outside diameter to wall thickness ratio subjected to plain dent defect. A finite element model was developed and verified to calculate the stresses and the strains developed in the pipes from the indentation and pressurization process. For each pipe, two spherical indenters with different indenter radii were used to indent the pipe with different indenter depths. The response surface method with the first-order reliability analysis was used to perform the reliability analyses. Two different response surfaces (RSs) including and excluding the interaction terms were used for the reliability analysis per defect. The following points was concluded:

- A sample dent case was presented to show the development of the maximum damage throughout the loading steps. The major amount of damage in the unconstraint dent was shown to occur during the indentation process of the pipe and an insignificant damage is caused by pressurizing the pipe to the maximum allowed operating pressure, however, all the other loading steps did not affect the pipe damage.

- The difference in the reliability results from using the RSs including and excluding the interaction terms are insignificant, showing the insignificance of the interaction between the problem parameters at different values on the reliability results.
- The reliability analysis results based on two damage criteria were compared to reliability analysis results based on the maximum equivalent plastic strain (MEPS). It can be concluded that using the damage models for the reliability analysis, the probability of failure (PoF) of the SLD is higher and more conservative than the DFDI. However, the DFDI results are expected to be more realistic based on experimental and numerical results provided in the literature. It can be concluded also that, the PoF increases with the increase of the indentation depth and that the PoF significantly increases with the decrease of the indenter size. The SLD and DFDI damage criteria are more sensitive to the change of the indenter size and the increase of the dent depth than the MEPS criterion.

6. Strain-Based Reliability Analysis of Pipelines Containing Dent Combined With Corrosion Defects Using Response Surface Method

6.1. Introduction

Pipeline is a major component of the oil and gas industry as it is used by many companies for transporting hydrocarbon fluids for long distances. Maintaining pipelines and ensuring their safety against any harm to humans or the environment is a crucial challenge faced by oil and gas transmission companies. If pipeline defects go unchecked, it can lead to oil and gas leakage or even pipeline bursts, which can have dire environmental consequences with a concomitant financial cost. That's why these companies focus heavily on accessing the pipelines to decide if any repairs or part replacements are necessary.

Pipelines can be subjected to many defects, which can affect their life span and cause their failure. One of these defects is the corrosion defect that can cause the burst of pipes [2], as the metal loss from the pipe's inner or outer layers reduce the amount of metal resisting the internal pressure stresses causing the reduction of its burst pressure. Failure of the pipe subjected to corrosion is highly probable to occur if the burst pressure of the pipe is lower than the maximum allowable operating pressure (MAOP) of the pipe. Typically, design factors incorporated into pipe design provide a safety margin that enables pipelines to withstand corrosion defects up to a certain limit without failure [1]. Nevertheless, corrosion defects must be regularly monitored and evaluated to guarantee that they are not compromising the pipeline's integrity. Several analytical, empirical, and numerical-models-based criteria [3–9] have been provided in the literature and in the pipeline assessment standards to calculate and evaluate the remaining strength or the failure pressure of the pipes subjected to corrosion defects. The manual for determining the strength of corroded pipelines, ASME B31G-2012 [17]

provides several methods for assessing corrosion defects. Among those methods, the most accurate, based on experimental results [3,21], is the RSTRENG model.

Another type of defect that can cause pipeline failure and affect its life span is the dent defect. The presence of dents creates areas of high stress and strain in the pipe material, which may become vulnerable points for the formation of cracks. These cracks can gradually worsen over several cycles of internal pressure loading, eventually leading to the pipe's failure. Plain dents can be divided into either smooth or kinked dents depending on the radius of curvature of the sharpest part in the dented part of the profile. Kinked dents are those dents whose radius of curvature of the sharpest part is less than five times the wall thickness of the pipe [10]. This study focuses on smooth dents, therefore the spherical indenters used in the study will have a radius larger than five times the wall thickness of the pipe. The acceptance criteria for plain dents in the Canadian and American design standards, CSA Z662-19 [13], ASME B31.4-2019 [14], ASME B31.8-2018 [15], for oil and gas pipelines are based on the dent depth (which should not exceed 6% of pipe OD) and the strain level in the dent (which should not exceed 6% in CSA Z662:19 and ASME B31.8-2018). Zhao and Cheng [115], however, reported that the 6% limit is excessively conservative. Different studies used strain levels of more than 6% for dented pipelines. Adeeb and Horsley [28] used a 20% principal strain limit instead of the 6% in their study investigating the effect of internal pressure on the possibility of rupturing high-pressure gas pipes due to the punctures resulting from the impact of falling rocks. Abdelmoety et *al*. [101] performed a reliability analysis on plain dents in which they used the strain capacity in the dented area as high as 28%. Also, Arumugam et *al*. [49] showed in an actual case study, using ILI data, manual grid data, and LaserScan data, that the measured maximum equivalent plastic strain for a dent combined with a severe metal loss at failure was between 16% and 22%, which is significantly higher than the 6% limit provided by the design standards.

The strain-based assessment is considered an important method for evaluating dent defects. Rosenfeld *et al*. [25] suggested that the severity of a dent defect should be

determined by its strain level. The ASME B31.8-2018 provided equations for estimating the strains at the dent location in its Appendix R. However, Okoloekwe *et al.* [26] reported the inaccuracy of those equations in predicting the maximum strains generated at the dent location and provided a new method based on the dent profile for predicting the maximum strains generated at the dent location. Zhao *et al*. [115] also reported the inaccuracy of those equations and provided a new technique based on the Finite Element (FE) method to accurately predict the maximum dent strains. Additionally, Kainat et *al*. [42] utilized equivalent plastic strain as a gauge of the dent defect's severity in pipes.

In contrast to plain dents, dents can also occur together with other types of pipe defects, like internal and external corrosion, gouges, grooves, arc burn, and cracks, which can occur at a mill or weld location. Many research papers studied dents combined with gouges [29–31] or dents combined with cracks [32–34] defects, but to the best of the author's knowledge, only few recent studies focused on the assessment of dents combined with corrosion defects (DCCD) [116–120] without considering the pertinent uncertainties of the problem. As pointed out by the API assessment and management of pipeline dents standard, the API 1183-2020 [35], a generalized dent-corrosion feature interaction has not been developed yet. There is an obvious lack of research investigating DCCDs, as most of the design and assessment standards treat it as a plain dent or a plain corrosion defect without considering their interactions. The DCCD is treated similarly to plain dent or plain corrosion defects or considered unsafe and needs replacement. Therefore, in this study, dent combined with corrosion defects is studied considering their interactions.

In order to perform pipeline defect assessment, operators can use a deterministic or a probabilistic approach. While the deterministic approach is direct and easier to perform, the probabilistic approach provides more transparency about the degree of safety because it accounts for the uncertainty of the problem parameters explicitly, which makes it more realistic and indicative of the defect safety levels. The probabilistic approach via reliability analysis will provide probability that the demand will exceed

the capacity, namely the probability of failure (PoF). By comparing this PoF with a target probability of failure, the pipeline can be assessed. Several reliability analysis techniques are available for calculating, such as, stochastic sampling methods like the Monte Carlo Simulation (MCS) [56], approximate analytical methods like the First order reliability method (FORM) [58], and other methods based on surrogate models such as the Response surface method (RSM) [61–63,65,66,98], which can take advantage of sampling methods or approximate analytical methods. The method used for reliability analysis depends on its suitability to assess the PoF of the problem. In this study, the RSM together with the FORM is used for reliability analysis as will be explained in detail later.

In this paper, reliability strain-based analysis will be performed on DCCD to provide quantitative data on the effect of the corrosion defect on the dent defect. To consider the complex interaction between dents and corrosion defects, FE models will be developed in this study to obtain the strain results as detailed in Section 6.2, which also presents a description of the load scenario considered. Section 6.3 introduces the limit state function (LSF), the RSM and the random variables (RVs) considered for the reliability analysis. Section 6.4 presents the different study cases used in this study to investigate the effect of the corrosion defect on the dent. Finally, in Section 6.5, the sensitivity analyses and the verification of the developed FE model are presented beside the reliability results of the plain dents and DCCD to investigate the effect of the corrosion metal loss on the dent defect.

6.2. Finite element analysis

To accurately calculate the maximum equivalent plastic strains (MEPS)s generated in the pipe due to indentation and corrosion a finite element (FE) model of the pipe subjected to the applied defects and the internal pressure is created using the commercial multiphysics platform software ABAQUS. The basic components in the FE model are the pipe and the indenter as shown in Fig. 6.1.

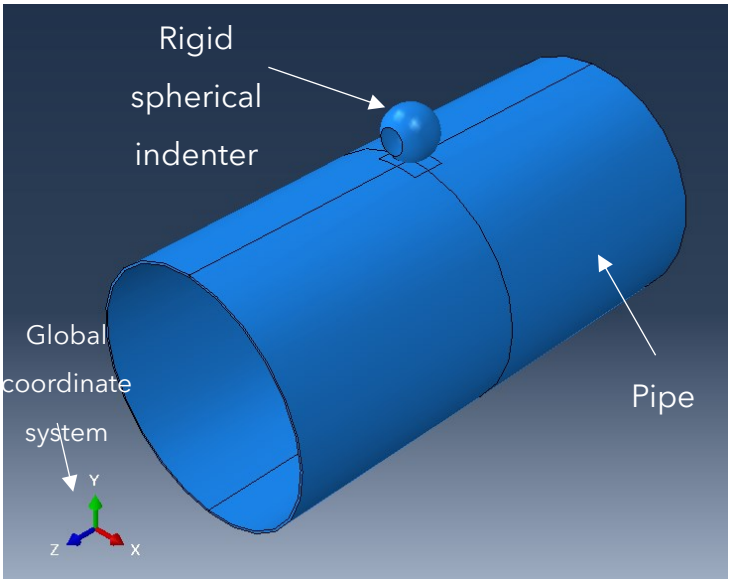

Figure 6.1. *The FE model used to calculate the MEPS in the pipe shows the main pipe body and the indenter.*

The FE model must be computationally efficient as it will be running numerous times in the reliability analyses. To this goal, the major part of the pipe is represented by shell elements (e.g., S3 and S4), and solid elements (e.g., C3D8) are used at the indentation and corrosion metal removal areas to obtain an accurate stain solution. ABAQUS C3D8 solid elements are used at and around the indentation location where the strain gradients are expected to have relatively higher amplitudes. Meanwhile, the S3 and S4 ABAQUS shell elements will be used to model the remainder of the pipe, as shown in Fig. 6.2.

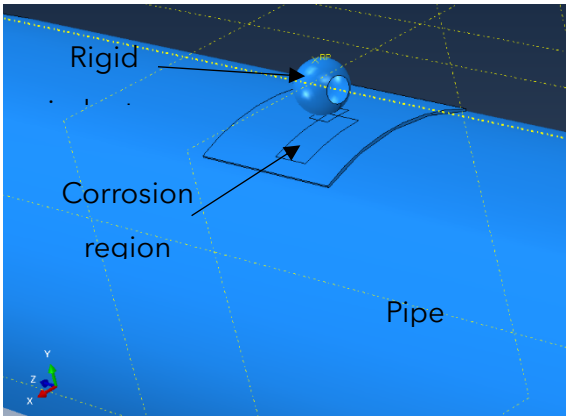

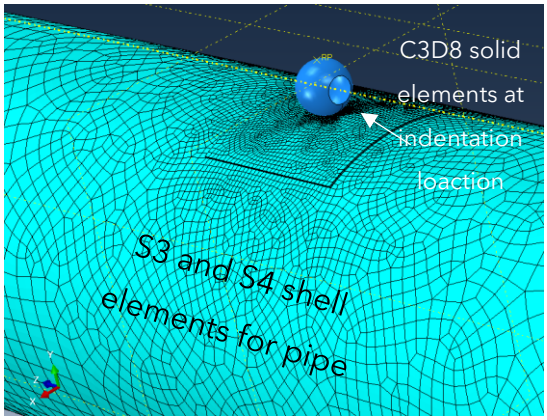

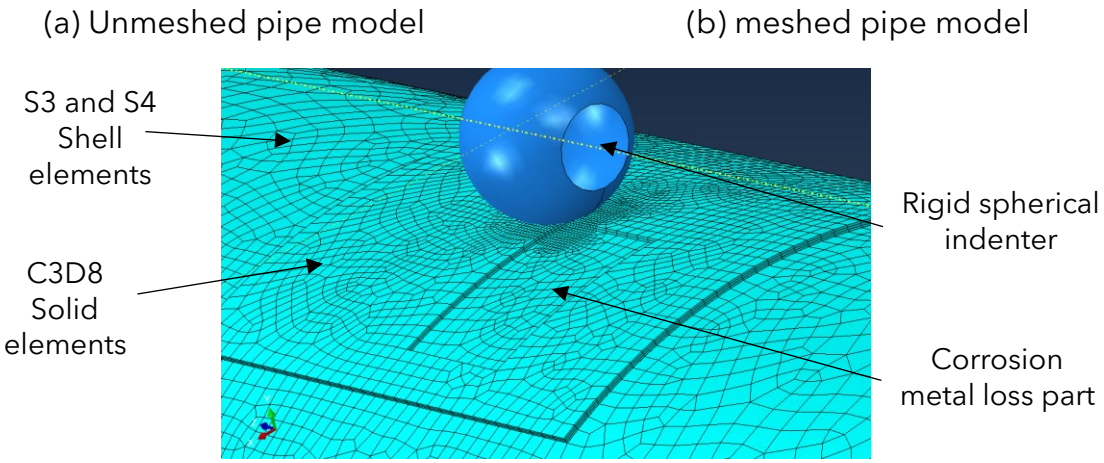

Figure 6.2. *The FE model used to calculate the MEPS in the pipe.*

The whole pipe is modelled without using any symmetry because the problem studied in this paper is not assumed to be symmetric. The pipe considered is situated on the ground, which means that its bottom is prevented translation in the Y-axis direction. As for the end conditions of the pipe, any movements or rotations, except for radial displacement, of the far edge will be coupled with a reference point positioned at the center of the pipe on the same plane as the far edge. This reference point will be fixed, with all rotational and translational degree of freedom restrained. The reason behind fixing this point is that for long pipe segments, only part of the pipe from the middle of the segment is considered for the study. This part is attached (and partially restricted from movement) to the rest of the pipe segment from its two ends, which makes it more similar to a plane strain problem. Therefore, the ends of the pipe part considered for analysis is restricted from movement, except for the movement in the radial direction. The deformation in the radial direction is allowed as, in reality, the remaining pipe segment (attached to the ends of the pipe part under study) and pipe part considered for the study are expanding in the radial direction from the internal pressure with approximately the same amount.

To create the indentation on the outer surface of the pipe, the spherical rigid indenter is placed on the surface and moved towards the center of the pipe by the specified

initial dent depth (DD) value. For the contact problem in the ABAQUS model, a "surface to surface" discretization method is used with a finite sliding formulation and a tangential friction coefficient of 0.5. The spherical indenter is considered the master surface, while the pipe's outer surface is the slave surface. Once the indentation is complete, the indenter is allowed to move away from the pipe to simulate its removal.

$$\frac{\varepsilon}{\varepsilon_y} = \frac{\sigma}{\sigma_y} + \alpha \left(\frac{\sigma}{\sigma_y}\right)^n \tag{6.1}$$

The steel grade used in this study is X52 vintage steel with 360 MPa specified minimum yield strength (SMYS). The nonlinearity in the stress-strain relation of the pipe steel material is considered and modelled in the FE model using the Ramberg-Osgood [121] nonlinear model given in Eq. (6.1) and shown in Fig. 6.3. In Eq. (6.1) σ and ε are the yield stress and strain, respectively, of the pipe material. α is taken equal to 1.72 and n is taken equal to 12 in this study to produce a reasonable matching to a generic X52 stress strain curve [101].

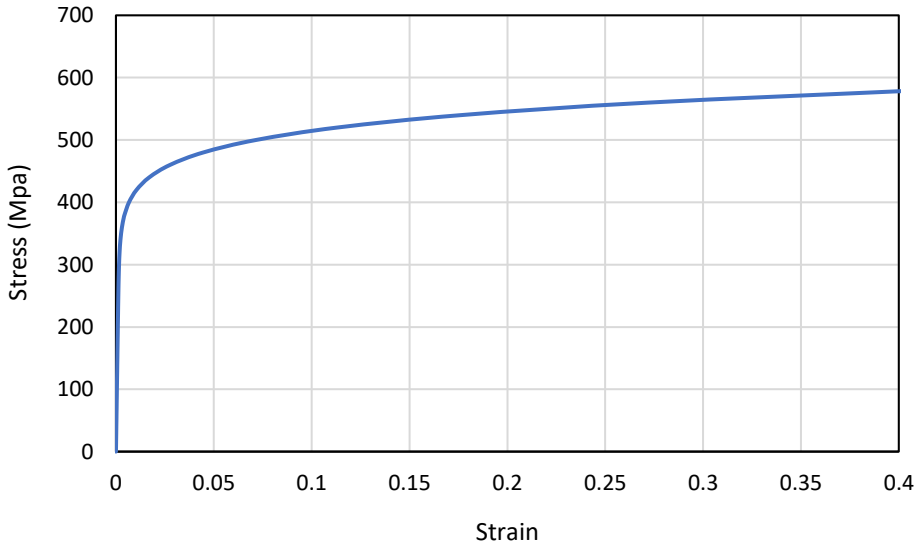

Figure 6.3. *Ramberg-Osgood non-linear model of the stress-strain relation for X52 vintage steel.*

A highly probable loading scenario for the pipe containing dent defects is indentation of the pipe by an external indenter, which will damage the external coating of the pipe at the indentation location making this area more susceptible to develop a corrosion defect. Later, the pressure inside the pipe can increase to reach the MAOP, which will further strain the pipe material in the DCCD region. Then, the pressure inside the pipe will return to the operating pressure.

The loading scenario considered in this study and applied to the FE model is as follows:

1. Indenting the pipe with the spherical rigid indenter to the initial DD.
2. Indenter removal.
3. Metal loss application (as shown in Fig. 6.2(c)).
4. Apply internal pressure (P) in the pipe equal to the MAOP.
5. Depressurize the pipe, then apply the inline pressure.

The metal loss is applied by deactivating the area where the corrosion is assumed to occur in the FE model. The internal pressure (P) inside the pipe is set to be equal to MAOP for an intact pipe, which is calculated based on Barlow's equation (2) provided in [13].

$$P = \frac{2 * DF * SMYS * WT}{OD} \tag{6.2}$$

Where DF is the design factor given by [13] and taken equal to 0.8 in this study and OD and WT are the outside diameter and the wall thickness of the pipe respectively. The inline pressure is assumed to be equal to 37.5% of the MAOP based on industrial partner recommendations in this study.

To test the created model sensitivity analysis are made and provided in subsection 6.5.1 to check the proper proportions of the part using solid elements to the part using shell elements, the number of elements in the solid part, the number of elements through thickness of the solid elements part, and the length of the pipe. All of these

aims to obtain stable results for the MEPSs using the FE model. To further verify the accuracy of the FE-predicted results, the MEPS results obtained from the developed FE model are compared, and provided in subsection 6.5.2, to strains obtained numerically in [115] and experimentally in [39].

Note that the number of FE models needed to be run in this study is large. Therefore, high performance computing, provided by Digital Research Alliance of Canada through their four computing clusters Cedar, Graham, Beluga, and Narval, is used to run the FE models in a timely manner and to collect the strain results from the models.

6.3. Reliability analysis and statistical data

In this section, the reliability problem is defined, and the reliability analysis technique considered in this study is presented together with the statistical data of the random variables (RVs) considered.

6.3.1. Limit state function (LSF)

The reliability analysis performed in this study is based on the MEPS generated in the pipe containing DCCD due to the indentation and the metal loss process then the pressurization of the pipe. The PoF in this study refers to the probability that the MEPS generated in the pipe due to the defects and the pressure exceeds the strain capacity (SC) of the pipe material. The LSF "$g_{MEPS}(X)$" provided in Eq. (6.3) is used for the reliability analysis.

$$g_{MEPS}(X_1, X_2, \dots, X_n) = SC - RS_{MEPS}(X_1, X_2, \dots, X_n) \tag{6.3}$$

Where $X_1, X_2, \dots, X_n$ are the n random variables considered in the study. $RS_{MEPS}(X_1, X_2, \dots, X_n)$ is a function representing the MEPS generated in the pipe depending on the values of the considered random variables. There is currently no reliable analytical or empirical equation available to predict the MEPS of various pipe, dent, and corrosion dimensions. As a result, the reliability analysis relies on the strain results obtained from the FE model rather than relying on analytical or empirical

equations. Therefore, an RS will be constructed for the MEPS function of the different pipe parameters. Then, the RSM will be applied to the generated RS to predict the probability of exceeding the SC of the pipe material.

6.3.2. Response surface (RS)

The RS [60] serves as a multivariable fitting surface with a number of terms that depend on the number of RVs considered and the required degree of the surface. In this study, a second-order RS, given in Eq. (6.4), will be employed to capture potential curvature within the MEPS as influenced by the considered RVs.

$$Y(X_1, X_2, \dots, X_k) = \beta_0 + \sum_{i=1}^{k} \beta_i X_i + \sum_{i=1}^{k} \beta_{ii} X_i^2 + \sum \sum_{i<j=2}^{k} \beta_{ij} X_i X_j + \varepsilon \qquad (6.4)$$

where Y is the response (i.e., the RS_{MEPS}), β_i and β_{ij} are the RS regression coefficients to be calculated from the regressor values X_i and the response value Y of several data points. ε is the random error component representing the difference between the predicted response value and the real response value for different parameters values. The random error is unknown and assumed to be negligible, thus not carried over in the RS equation during reliability analysis. Additionally, interaction terms are incorporated into the RS to investigate the effect of the interaction of an independent variable (factor or regressor) on the response. The RS is constructed around certain values of the RVs of the problem with a range for each RV equal to the central value $\pm\, \gamma$ times the standard deviation (STD) of the RV to represent the MEPS values. This implies that to construct the RS in this study, three values of each RV should be determined, which are a central value, a lower value, and a higher value (denoted by -1, 0, and 1 in this work) with a distance between them equal to $\gamma \times STD$. γ can be any arbitrary factor [64] that is often taken between 1 and 3.

6.3.3. Design of Experiment (DoE)

In order to construct the response surface for the MEPS of a certain defect several data points have to be collected. Each data point will consist of the MEPS generated in the

defect, which is the required response, together with certain model parameters, such as the pipe wall thickness, the yield strength (YS) of the pipe material, the dent depth, and the corrosion dimensions. The data points are preferred to be chosen in a matter that covers all the possibilities or combinations of the considered values of the considered parameters of the problem. In the dent combined with corrosion problem considered in this work, first, the reliability analysis will be performed on a plain dent problem, then it will be performed on the dent combined with corrosion problem.

In the plain dent problem, according to [101], only three problem parameters are considered, which are the pipe WT, the YS of the pipe material, and the dent depth (DD). Three values or levels are considered for each variable to construct the response surface at each iteration. To take all the possible combinations of the three values for the three parameters a full-factorial DoE will be used. Fig. 6.4 shows all the possible combinations of the three levels (-1, 0, and 1) of each parameter.

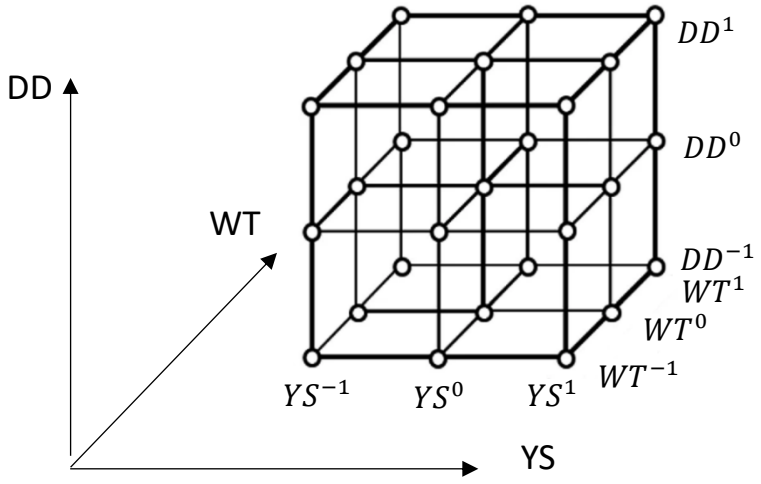

Figure 6.4. *Graphical representation of the full-factorial DoE of the three parameters WT, YS, and DD.*

The number of combinations considered in the full-factorial DoE for p number of parameters or problem RV and n number of levels or values for each parameter is

determined by n^p [67]. In this case, there exist three parameters in the problem and each parameter has three levels, which produces 3^3 =27 possible combinations or experiments to construct a local RS. For each combination, a FE model is generated and the MEPS is calculated, then the least squares regression equations are used to determine the regression coefficients in the RS equation.

To combine the corrosion defect with the dent defect, the parameters of the problem have to include the corrosion dimensions. In this study, only the corrosion longitudinal length and the corrosion depth are considered for the reliability analysis; therefore, they will be the only parameters describing the corrosion dimensions added to the reliability analysis. Therefore, the parameters of the dent combined with the corrosion problem are five parameters, which are WT, YS, DD, CLL, and CD.

According to the full-factorial DoE, the consideration of all the possible combinations of the three levels of each of the five problem parameters will produce 3^5 =243 combinations to produce only one local RS. A FE model has to be analyzed for each combination of the parameter value to calculate the MEPS; therefore, depending on the full-factorial DoE will be highly computationally consuming and impractical.

In this study, for the five-parameter RS equation, there exists one constant term, five linear terms, five quadratic terms and ten interaction terms, leading to a total of 21 regression coefficients. Instead of using full-factorial DoE, the following experiments or data points are formed to construct each RS considering three levels (the lower value "-1", the central value "0", and the higher value "1") for each of the five RVs:

1- One experiment has the central value of all the five RVs

2- Ten experiments consider the extreme levels ("-1" and "1") of each of the RVs while setting the remaining four of the RVs to their central value "0". Together with the first experiment, enough experiments are provided for the evaluation of the coefficients of the five quadratic terms in the RS equation.

3- Thirty-two experiments consider the combination of the extreme values of each RVs ("-1" and "1") to make sure that enough experiments are provided to evaluate the five linear terms and the ten interaction terms in the RS equation.

The above scheme produces 43 experiments that need to be analyzed to construct an RS for the reliability analysis.

6.3.4. Response surface method (RSM)

The RSM is used as the reliability method for calculating the PoF of the DCCD in this study. The steps for using the RSM to calculate the PoF in this study are as follows:

1- Using the mean value of the RVs and the DoE, the data points needed to construct the second-order RS are determined. The initial central values for the variables used to create the initial RS is the mean value of their corresponding RVs. However, in case of any extra iteration, the central values of the variables are set to the most probable point (MPP) values.

2- The RS is constructed by applying the least squares equations on the data points obtained from the DoE and the FE analysis.

3- Reliability analysis is performed using the FORM on the LSF "g_{MEPS} " to calculate the PoF and the estimated MPP.

4- The resultant estimated MPP is checked to be within the limits of the RS (central value $\pm\ \gamma$ ×STD) constructed in the second step and used to perform the FORM analysis.

5- The obtained PoF is the final PoF if the estimated MPP is within the RS limits.

6- A new RS is constructed with the RVs values of the estimated MPP $\pm\ \gamma$ ×STD if the estimated MPP is outside the range of the RS limits. Furthermore, the whole process starting from 1 to 5 is repeated until reaching convergence.

6.3.5. Statistical data

The random variables selected for the dent defect reliability analysis are the DD, WT, and YS according to [101]. For the corrosion defect, the corrosion depth (CD) and the

corrosion length in the longitudinal direction of the pipe, which we name the corrosion longitudinal length (CLL) are considered random variables in this study. The corrosion defect is also considered concentric under the indenter. The statistical data for the five RVs considered including the mean, the standard deviation (STD), and the probability distribution are provided in Table 6.1.

Table 6.1. *Statistical data for RVs.*

Random Variable	Unit	Mean	STD	Distribution	Reference
Wall thickness (WT)	mm	Nominal Value	2.35% of the mean value	Normal	[78]
Yield strength (YS)	MPa	386.55	21.63	Normal	[78]
Strain capacity (SC)	-	0.3	0.018	Normal	[46]
Dent depth (DD)	mm	See section 6.4	1.25*	Normal	-
Corrosion depth (CD)	mm	See section 6.4	0.078 WT*	Normal	-
Corrosion longitudinal length (CLL)	mm	See section 6.4	7.78*	Normal	-

∗ The STD of DD, CD, and CLL is obtained from the industry based on the accuracy of the used in-line inspection tool.

6.4. Study cases

To investigate the effect of corrosion on a dent defect, two different pipes with different OD/WT ratios, given in Table 6.2, are chosen. Several single plain dent defects, using the same indenter with different DD, are created on each pipe, then two different corrosion defects with different corrosion depths are created on each dent defect. Then, for each dent defect, the PoF is calculated in the case of plain dent and in the two cases when the corrosion defects are applied to investigate the effect of the corrosion defect on the dent defect.

Table 6.2. *Designations and dimensions for the two study pipes.*

Pipe designation	Outside Diameter (OD) (mm)	Wall Thickness (WT) (mm)	OD/WT ratio	Steel grade
NPS 30	762	7.14	106.7	X52 Vintage
NPS 12	323.85	6.35	51	X52 Vintage

According to [10], the pipe is indented by a spherical indenter having a radius that is bigger than five times the pipe wall thickness to make sure that the created dent is a smooth dent. Therefore, for each of the two pipes the indenter radius is calculated, provided in Table 6.3, to be equal to around five times the wall thickness of the pipe. For each pipe, three dent defects are created in a matter that when the mean of the random variables of the pipe parameters are used, the MEPS values generated in the dent defects are equal to 27%, 25%, and 23%. To create the dents that generate different MEPS values in the pipe, for each pipe size the indenter radius remains constant, and the indentation depth is changed to obtain the target MEPS. Table 6.3 shows the different DDs used to generate the three levels of the MEPS generated in the two study pipes.

Table 6.3. *Indenter radius and dent depth of dent defects for the two study pipes.*

Pipe designation	Outside Diameter (OD) (mm)	Wall Thickness (WT) (mm)	Indenter Radius (mm)	Generated MEPS	Initial dent depth
NPS 30	762	7.14	36	27%	56.5
				25%	44.9
				23%	34.0
NPS 12	323.85	6.35	32	27%	27.5
				25%	23.1
				23%	19.9

Two different corrosion defects are created to investigate the effect of different corrosion defects on the probability of failure of the same dent defect.

The corrosion defects are created using the RSTRENG equations by the following assumptions and procedures:

1- Assume that the created corrosion is a plain corrosion defect that will make the burst pressure of the pipe equal to 1.25 times the maximum allowable operating pressure of the pipe, where 1.25 is the minimum factor of safety provided by ASME B31G.

2- Assume that the two generated corrosion defects will have corrosion depths of 0.4×WT and 0.6×WT respectively.

3- Use the RSTRENG equation given in Eq. (6.5) to determine the length of the corrosion defect in the longitudinal direction of the pipe to set the burst pressure of the pipe as described in the first point,

$$P_f = 2\sigma_{flow}\left(\frac{WT}{OD}\right)\left(\frac{1-X_d}{1-\frac{X_d}{M}}\right) \tag{6.5}$$

where X_d is the normalized depth of the corrosion defect, σ_{flow} is the flow stress, and M is the Folias factor, and they are given by Eqs. (6.6–6.8), respectively:

$$X_d = \frac{CD}{WT} \tag{6.6}$$

$$\sigma_{flow} = SMYS + 10{,}000 \text{ psi} \tag{6.7}$$

$$M = \begin{cases} \sqrt{1 + 0.6275 \times X_L - 0.003375 \times {X_L}^2}, & X_L < 50 \\ 3.3 + 0.032 * X_L, & X_L > 50 \end{cases} \quad (6.8)$$

where CD is the corrosion defect depth, X_L is the normalized length of the corrosion defect given by Eq. (6.9),

$$X_L = \frac{CLL^2}{OD \times WT} \quad (6.9)$$

The corrosion defect dimensions for each pipe are only depending on the pipe dimensions. Therefore, for each pipe, there are two different corrosion defects whose dimensions are given in Table 6.4.

Table 6.4. *Corrosion defects dimensions for the two study pipes.*

Pipe designation	Wall Thickness (mm)	Corrosion depth to WT percentage (%)	Corrosion depth (CD) (mm)	Corrosion longitudinal length (CLL) (mm)
NPS 30	7.14	40	2.856	92.5
		60	4.285	52.5
NPS 12	6.35	40	2.54	56.6
		60	3.81	32.2

6.5. Results

6.5.1. FE model sensitivity

Sensitivity analysis is performed on the FE model developed to determine the appropriate length of the pipe, the dimensions of the part using solid elements compared to the part using shell elements, the mesh sizes for the solid and shell elements, the number of elements per thickness for the part using solid elements. DDs

of 60 mm and 30 mm is used for the NPS 30 and NPS 12 pipes respectively for the sensitivity analyses. The DDs are chosen to be higher than the DDs used in the study, provided in Table 6.3, to make sure that the sensitivity analyses are valid for the smaller DDs used.

Sensitivity analysis is performed on the two pipe configurations presented in Table 6.2. Absolute value of the approximate relative error (AVARE) is used to determine the convergence of the MEPS results. The MEPS results are considered valid and stable once the AVARE of a finer mesh or for a longer pipe is less than 1%, so that the inaccuracy in the MEPS results does not significantly affect the reliability analysis. In some of the presented cases, a finer mesh with much smaller AVARE value is reached; however, the coarser mesh, having an AVARE less than 1%, is used to make the numerical model computationally less expensive and suitable for the reliability analysis.

In Fig. 6.5, several pipe lengths are considered for both pipe configurations, and the AVARE in the MEPS values reached less than 0.039% at pipe length over OD ratio of 32.8 for the NPS 30, and 0.64% for NPS 12 pipe. The pipe length considered for the NPS 30 pipe and the NPS 12 pipe are 25000 mm and 10600 mm, respectively.

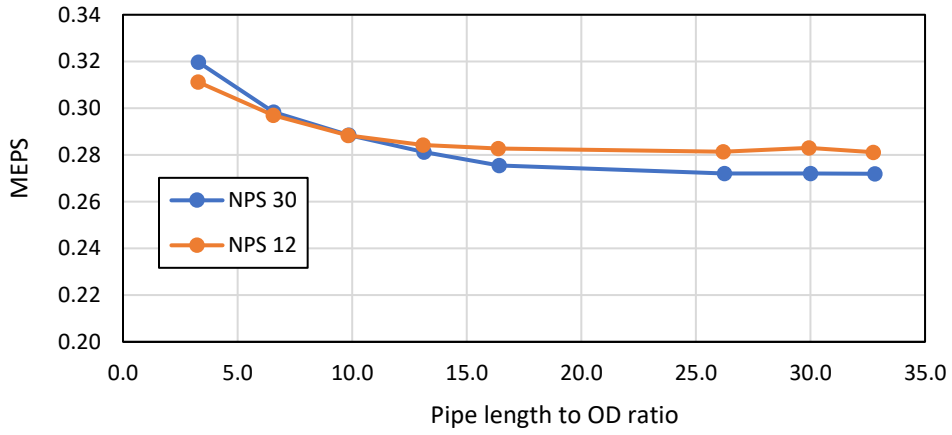

Figure 6.5. *MEPS results for different NPS 30 and NPS 12 pipe lengths to determine the suitable analysis length for both pipes.*

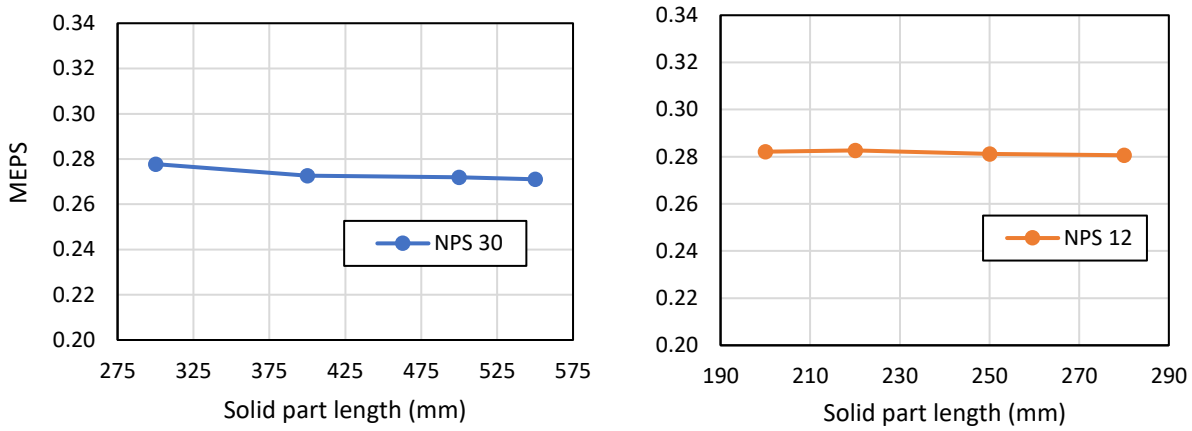

(a) (b)

Figure 6.6. *Effect of solid part longitudinal length on MEPS for the NPS 30 (a) and NPS 12 (b) pipes.*

Fig. 6.6 shows the variation of the MEPS in NPS 30 and NPS 12 models with different chosen solid part longitudinal lengths. The AVARE is less than 1% (0.28%) for the 500 mm solid part longitudinal length for the NPS 30, therefore 500 mm length is used as the longitudinal length. For the NPS 12, the AVARE values for all the used lengths in Fig. 6.6(b) are less than 1%, and the 250 mm longitudinal length is chosen for the solid part.

The change in the MEPS values against the circumferential length of the solid part (in degrees) of the pipes is presented in Fig. 6.7.

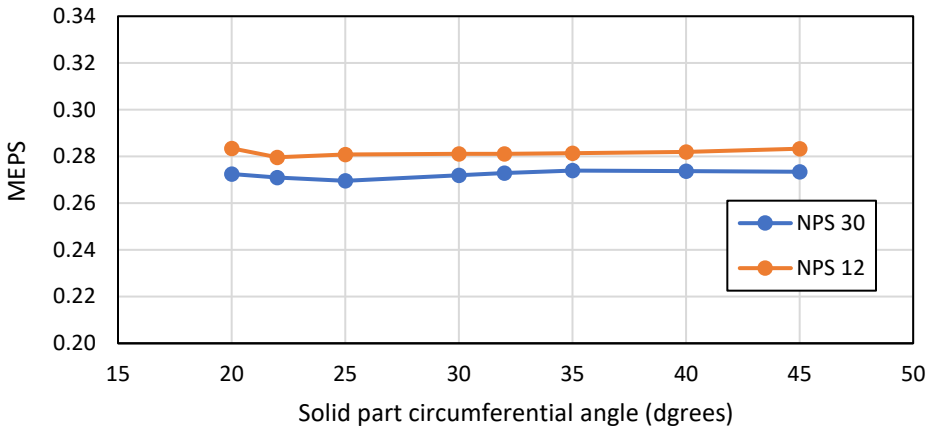

Figure 6.7. *Effect of solid part circumferential dimensions on MEPS for the NPS 30 and NPS 12 pipes.*

Different circumferential angles, ranging from 20 to 45 degrees, are used for the solid part circumferential dimensions. The AVARE in the MEPS values are fluctuating between 0.087% and 0.035% showing that the solid part circumferential dimension does not have a significant effect on the MEPS of both pipes. A circumferential angle of 30 degrees is used for both pipes to determine the circumferential dimension of the solid part.

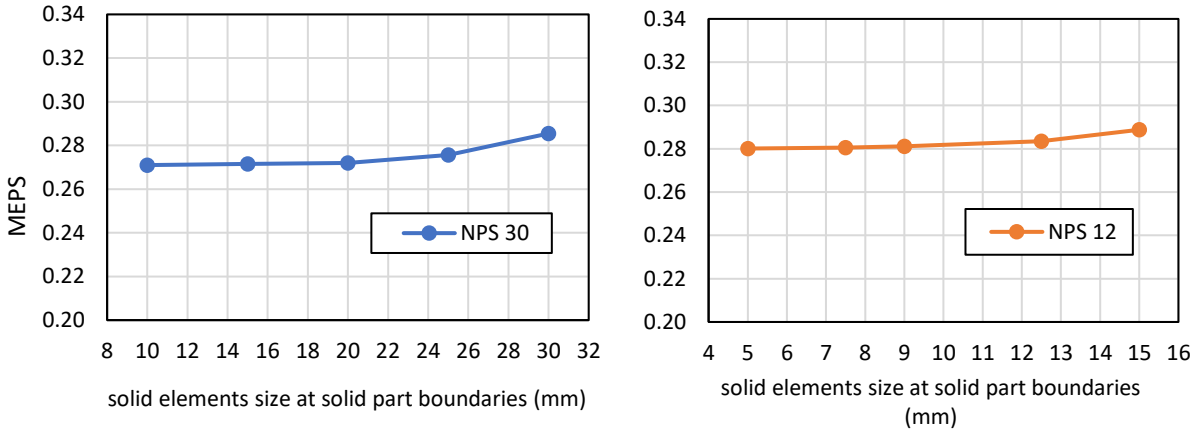

(a) (b)

Figure 6.8. *Effect of the solid element dimensions in the solid part on the MEPS in the dented region of the NPS 30 (a) and NPS 12 (b) pipes.*

The change in the MEPS values against the mesh size of the solid elements is shown in Fig 6.8. The 20 mm element size reached 0.14% AVARE in the MEPS values for the NPS 30 mesh and the 9 mm element size reached 0.24% AVARE in the MEPS values for the NPS 12, therefore, these element sizes are used in the developed model for the reliability analysis.

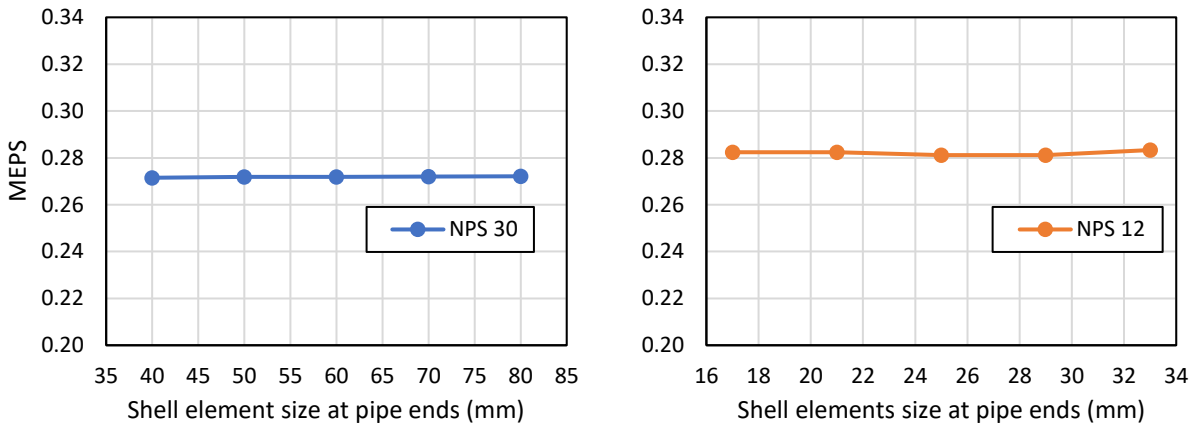

(a) (b)

Figure 6.9. *Effect of the shell element dimension at the pipe ends on the MEPS in the dented region of the NPS 30 (a) and NPS 12 (b) pipes.*

The change in the MEPS against the size of the shell elements at the pipe ends is shown in Fig. 6.9. The change in the shell elements' size at the pipe ends caused a fluctuation of the AVARE in the MEPS between 0.16% and 0.004% for the NPS 30 and between 0.75% and 0.002% for the NPS 12 showing a nonsignificant effect of the shell element size at the pipe ends on the MEPS in the dented region of both pipes. In this study, the shell element size is set to 60 mm for NPS 30 and 25 mm for NPS 12.

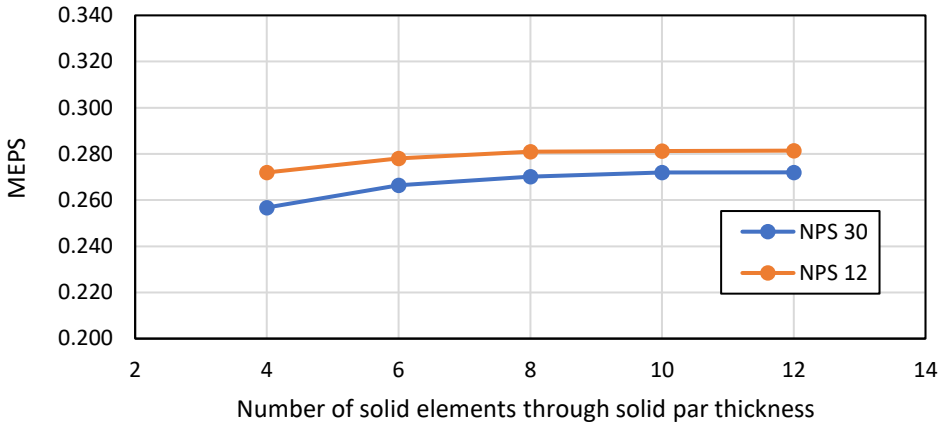

Figure 6.10. *The effect of the number of FEs through solid part thickness on the MEPS in the dented region.*

The change of the MEPS against the number of solid elements through the thickness of the solid element part is presented in Fig. 6.10. The values of the MEPS reached an AVARE of 0.64% for the NPS 30 and a value of 0.063% for the NPS 12 at 10 elements through the thickness, therefore, 10 elements per thickness are used in the FE models used in this study.

6.5.2. FE model verification

To verify the FE model results, the equivalent (vonMises) plastic strains (EPS) produced from the model is compared to the numerical results given in [115]. The pipe analyzed in [115] is based on the pipe experimentally tested by Shuai et *al.* [39] that has a length of 6988 mm, an outside diameter of 720 mm, and a wall thickness of 8.1 mm. The pipe is made of API 5L X52 steel with 375 yield strength, 468 MPa tensile strength, and 208 GPa modulus of elasticity. The spherical indenter used in the experiment has a 50 mm indenter radius and an initial indentation depth of 67 mm that is reduced to an indentation depth of 48.68 after the indenter removal and the elastic spring back of the pipe.

A pipe with the same dimensions and properties is created using the developed FE model to be validated. It has to be mentioned that the significant change in the EPS is within a 50 mm circle around the dent apex as shown in Fig. 6.11.

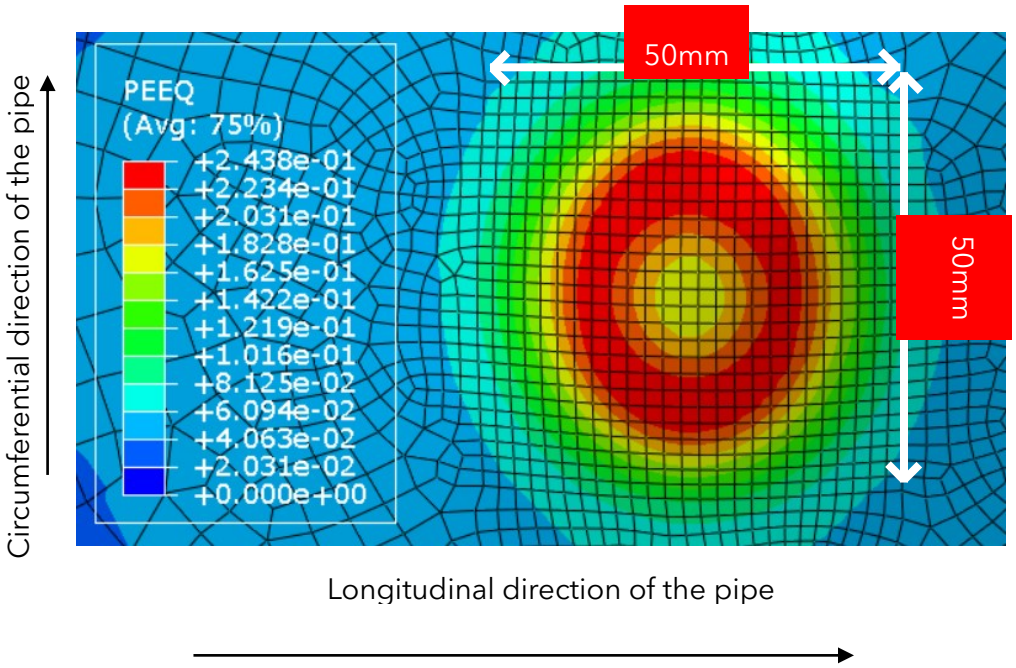

Figure 6.11. *A significant change in EPS in the area close to the dent apex.*

The nearest strain results to the dent apex provided in [39] are 50 mm away from the apex without providing results in the area at which the MEPSs are occurring. However, in [115], numerical results in the area near the dent apex are provided. Therefore, the circumferential and longitudinal EPS (vonMises strain) results provided in Fig. 6.9 in [115] are used to validate the model as shown in Figs. 6.12 and 6.13 respectively.

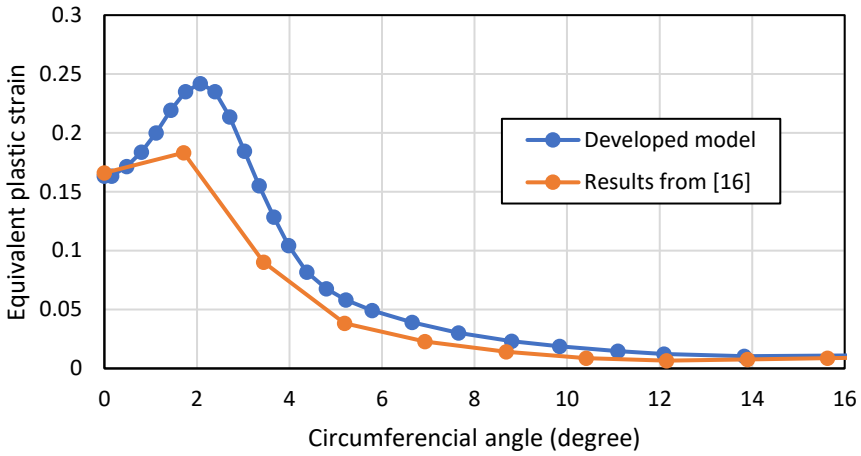

Figure 6.12. *Circumferential equivalent plastic strains in the pipe solid part at the pipe middle.*

It can be seen from comparing the results of the EPS in the longitudinal and circumferential directions around the dent apex that the results of the developed model have the same trend with the results provided in [115] for the EPS. However, for the part around the indentation apex, the developed model is predicting a higher EPS peak of 24.19% in the circumferential direction and 23.16% in the longitudinal direction compared to a maximum EPS of 18.32% in the circumferential direction and 17.24% in the longitudinal direction predicted by the model in [115]. It has to be mentioned that a finer mesh of an element size of 2 mm is used in the developed model compared to a coarser mesh size used in the reference model of 5 mm and the results are reported at almost each 10 mm. We therefore attribute the size of these differences to the difference in the mesh size between our models and the models reported in [16].

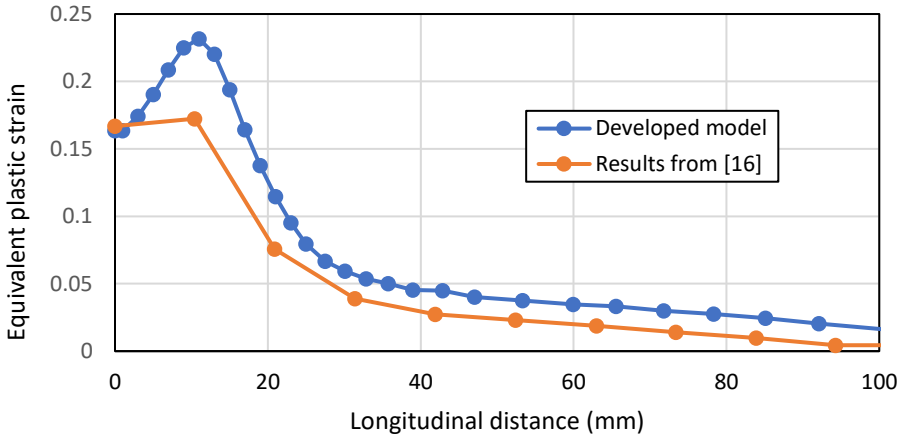

Figure 6.13. *Longitudinal equivalent plastic strains at the pipe solid part center from the dent apex.*

Also, the dent depth after the elastic rebound of the pipe of the developed FE model is 47.67 compared to 48.68 obtained from experimental results in [39] with an absolute relative error of 2.075% showing the good agreement of the developed model with the provided experimental results.

6.5.3. Deterministic dent and corrosion interaction

In this subsection, the deterministic effect of corrosion dimensions on the dent defect is investigated. For the two pipes, given in Table 6.2, a plain dent defect is created using a DD higher than the DDs used in the study and given in Table 6.3. A plain dent of 70 mm DD is created for NPS 30 and 33 mm DD is created for the NPS 12.

For each pipe, on the dent defect, several corrosion defects with different circumferential and the longitudinal dimensions on the pipe OD surface, and different corrosion depths are created to check deterministically the effect of the corrosion defect on the dent. For the NPS 30 pipe, three different corrosion surface dimensions are chosen: 20×20, 40×40, and 60×60 mm. And for the NPS 12 pipe, three different corrosion surface dimensions of 15×15, 25×25, and 35×35 mm are chosen. For each of these surface corrosion dimensions, a corrosion depth from 0.1×WT to 0.8×WT with an increment of 0.1×WT is created on the pipe to investigate its effect on the MEPS.

The corrosion's largest surface dimension is chosen such as when combined with the 0.8×WT corrosion depth, the failure pressure of the pipe, calculated using the RSTRENG equations, is 10% lower than the MAOP of the pipe.

Fig. 6.14 represents the MEPS of the NPS 30 pipe with different corrosion defects. As the figure implies, the MEPS is steady for different corrosion surface dimensions and for corrosion depths up to 60% of WT. However, For the 0.7 and 0.8% of WT corrosion depths, the MEPS increases for the three corrosion surface dimensions.

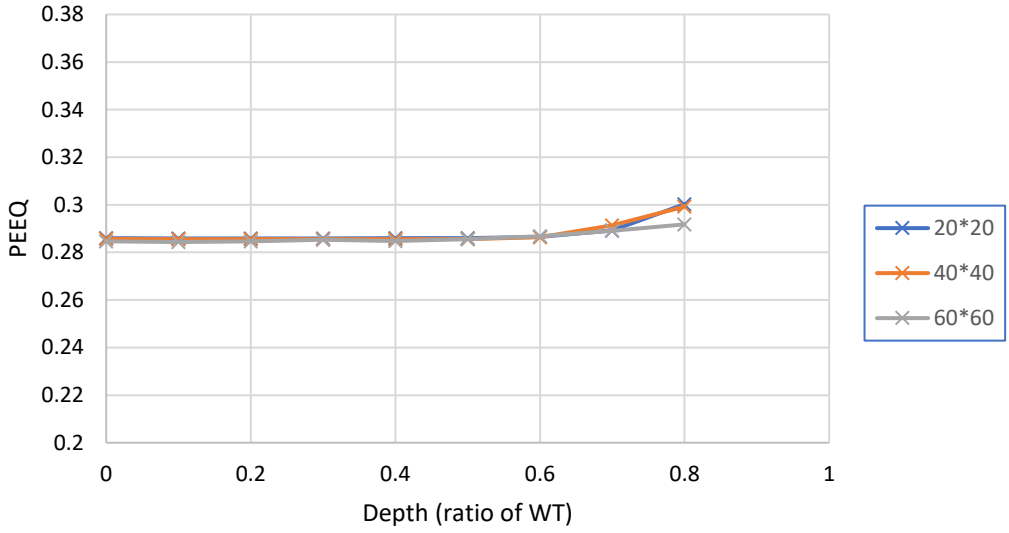

Figure 6.14. *Longitudinal equivalent plastic strains at the pipe solid part center from the dent apex.*

Fig. 6.15 represents the MEPS of the NPS 12 pipe. The MEPS remains steady up to 0.5×WT corrosion depth for all the corrosion surface dimensions. After 0.5×WT corrosion depth, the value of the MEPS for higher corrosion depth starts to increase for the different corrosion surface dimensions. The rate of increase of the MEPS for the NPS 12 in Fig. 6.15 for corrosion depths deeper than 0.6×WT is higher than MEPS in NPS 30 in Fig. 6.14.

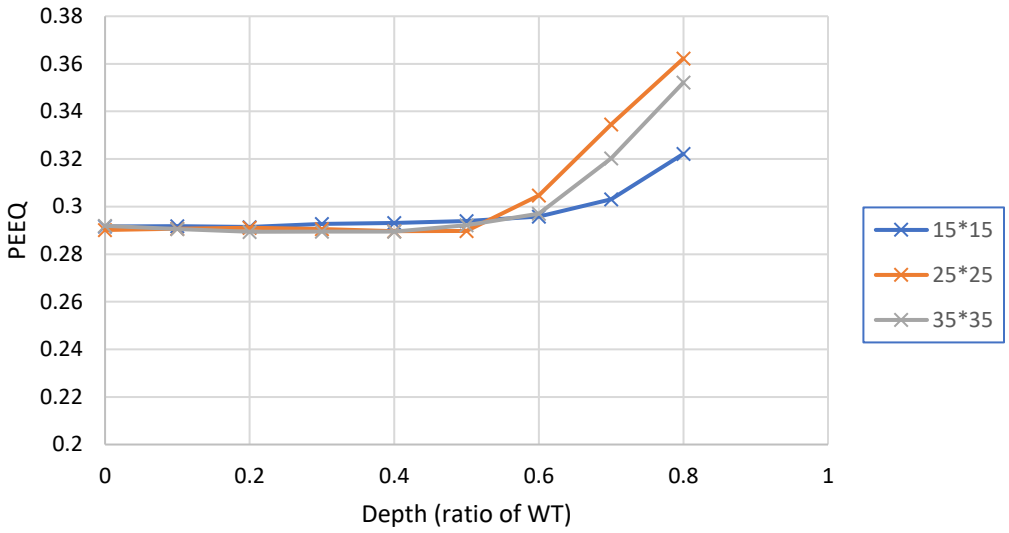

Figure 6.15. *Longitudinal equivalent plastic strains at the pipe solid part center from the dent apex.*

The DCCD with 25×25 mm corrosion surface dimensions and 0.8×WT is used to explain the peaking in EPS values for deep corrosion defects. The shape of the dent defect profile after the application of the corrosion defect at the final stage of loading is presented in Fig. 6.16.

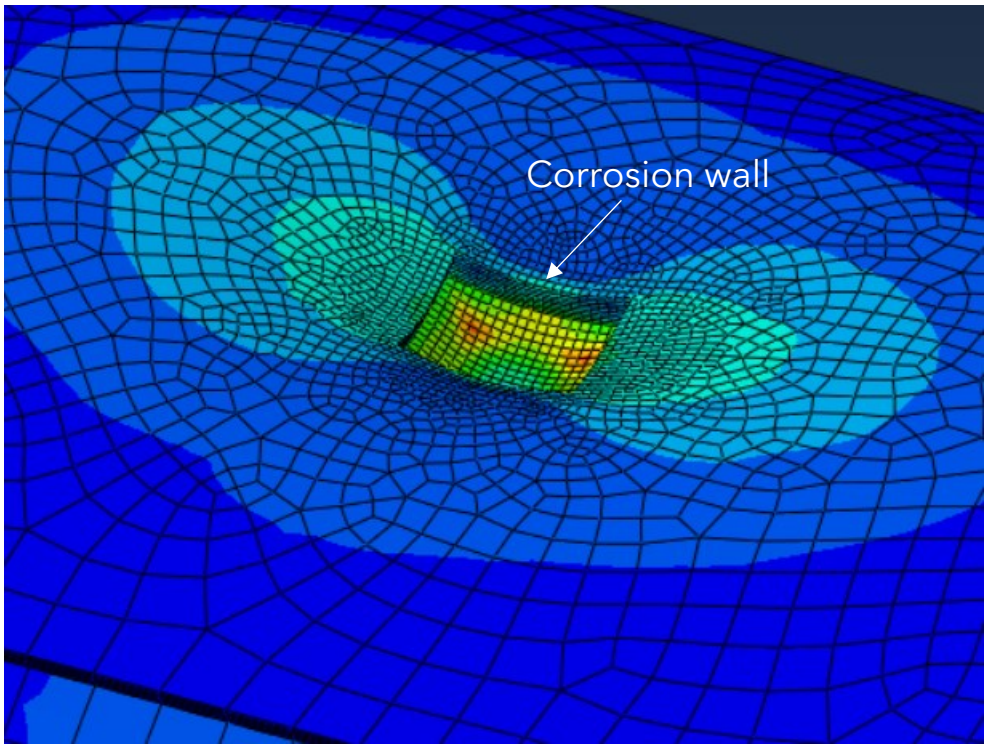

Figure 6.16. *The outside diameter profile for 25×25 mm corrosion surface dimensions with 0.8×WT corrosion depth given in Fig. 6.15 shows the corrosion defect orientation and depth.*

After indenting the pipe, removing the indenter, and applying the metal loss, the inside diameter profile of the dented area of the 25×25 mm with 0.8×WT corrosion depth, shown in Fig. 6.17(a), is similar to the DCCD with the same surface dimensions corrosion depth less than 0.5×WT before the application of the MAOP. Generally, with the increase of the internal pressure to reach the MAOP of the pipe, the inside surface starts to reround reducing the curvature created by the indentation and the DD decreases while maintaining a smooth profile for the dent, as shown in Fig. 6.17.

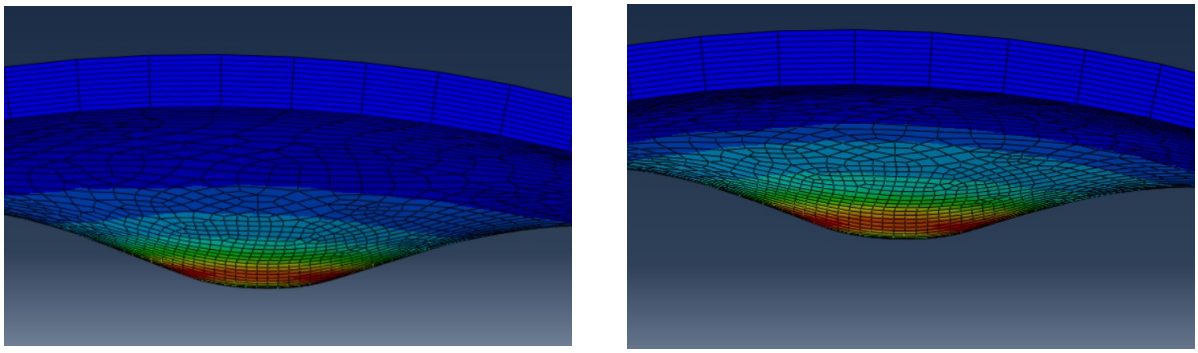

(a) (b)

Figure 6.17. *Inside diameter dent defect profile for 25×25 mm corrosion surface dimensions with 0.6×WT corrosion depth given in Fig. 6.15 (a) before and (b) after applying the MAOP.*

However, for the case where the corrosion depth is 0.8×WT, the remaining WT of the corroded area is only 20% of WT of metal material that is plastically strained from the indentation process while the WT around the corroded area is 100% of the WT, as shown in Fig. 6.16. During the rerounding of the pipe due to MAOP application, shown in Fig 6.18, the surface distance between the corrosion walls, shown in Fig. 6.16, decreases after being plastically increased during the indentation process, squeezing the 20% remaining WT in between the corrosion walls. The remaining thin part of the corrosion part bulges inwards (towards the center of the pipe) creating a different curvature from the remaining dented region. The generation of the bulge is shown with zero internal pressure in Fig. 6.18(a), 75% of MAOP in Fig. 6.18(b), and 100% MAOP in Fig. 6.18(c). The difference in curvature creates a concentration of strains at the region separating the corroded area from the remaining dented region, as shown in Fig. 6.19. In this situation, the edge of the corrosion area lies within the highly plastically strained region under the indenter.

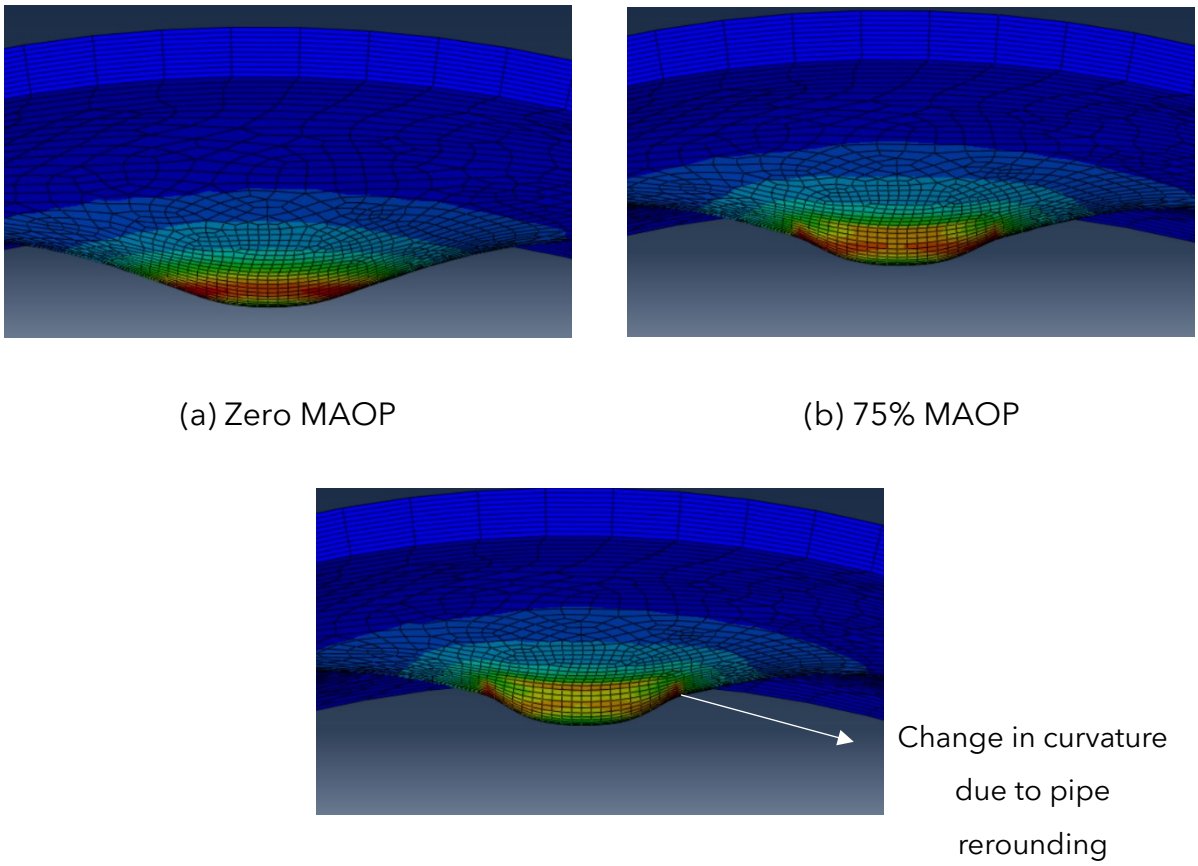

Figure 6.18. *Inside diameter dent defect profile for 25×25 mm corrosion surface dimensions with 0.8×WT corrosion depth given in Fig. 6.15 while applying the MAOP.*

With the increase of the corrosion surface dimensions, the corroded part becomes bigger than the plastically deformed region placing the corrosion edge away from the highly strained region. The difference in curvature between the remaining WT in the corroded area and the full WT decreases, which reduces the strain peaking caused by the curvature difference.

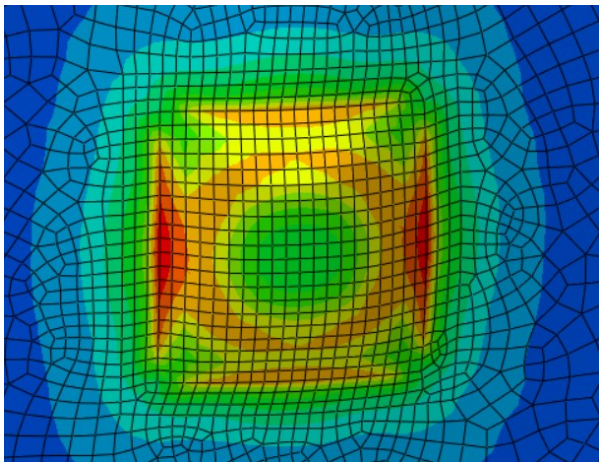

Figure 6.19. *Inside diameter view for the 25×25 mm corrosion surface dimensions with 0.8×WT corrosion depth provided in Fig. 6.16 showing the EPS concentration after the application of the MAOP.*

The radius of the indenter in both pipes is close (32 mm for NPS 12 and 36 mm for NPS 30), and the strained region under the indenter has a diameter of almost the same as the radius of the indenter. For the NPS 12, the corrosion dimensions needed to reach 90% of the MAOP is smaller than the corrosion dimensions needed to reach the same percentage of MAOP for the NPS 30. The dimensions of the corrosion for the NPS 12 make it interact with the strained region from the indentation causing the strain concentration and the difference between the curvature in the corroded and the full thickness part when applying the internal MAOP. However, for the NPS 30, the corrosion surface dimensions are relatively bigger with less interaction with the highly strained region from the indentation process, reducing the peaking in the strain values.

Huang et *al.* [116] performed a study on the investigation of different parameters on the failure pressure of DCCD. A FE models was created by Huang et *al.* using the C3D8R solid element in ABAQUS to model the pipe. In [116] the pipe was created and meshed with the dent defect, then the indenter was pushed against the pipe at the corrosion defect location. This loading procedure is different than the loading procedure followed in this work, as the corrosion metal loss is applied after the indentation of the

pipe. The failure pressure is reached in Huang et *al.* study when the MEPS in the DCCD region reaches the minimum elongation of the pipe steel material. Despite using curved edge for the corrosion defect to avoid stress and strain concentration in Huang et *al.* study, a strain concentration at the edge of the corrosion defects was observed when using a pipe with OD/WT ratio of around 50 similar to the strain concentration shown above in this study. The equivalent plastic strain concentration in [116] also occurs on the inside diameter surface of the pipe causing the MEPS to shift from the strained area under the indenter to the edges of the corrosion defect.

6.5.4. Reliability analysis results

Reliability analysis is performed on the defect cases provided in section 6.4. The reliability results (the PoF and the reliability index, beta) of the NPS 30 pipe are provided in Table 6.5. For the plain dent cases, the PoF increases with the increase of the DD. After the application of the corrosion defect in the three cases of different DD, the PoF remains almost the same indicating that the corrosion defect up to 60% of WT does not affect the PoF of the dent defect from a strain-based reliability analysis point of view. From the obtained results, during the indentation process, the metal part that is strained the most is the part around the center of the indenter with a diameter approximately equal to the radius of the indenter, which is equal to around 36 mm for the NPS 30. The circumferential length of the corrosion is chosen to be equal to 46.5 mm, which does not overlap with the most strained part from the indentation process. Regarding the longitudinal length of the corrosion, the RSTRENG equations resulted in a 52.5 mm corrosion longitudinal length for the 0.6×WT corrosion depth and 92.5 corrosion longitudinal length of the 0.4×WT corrosion depth, which makes the corrosion longitudinal length longer than the highly strained part from the indentation. Therefore, no peaking in the strain occurs for the NPS 30 pipe.

Table 6.5. *Reliability results for the NPS 30 pipe.*

MEPS	Defect	Reliability Results

		Beta	PoF
27%	Plain Dent	1.559	0.059491
	Shallow Corrosion (40% WT)	1.520	0.064206
	Deep Corrosion (60% WT)	1.377	0.084262
25%	Plain Dent	2.606	0.004584
	Shallow Corrosion (40% WT)	2.650	0.004028
	Deep Corrosion (60% WT)	2.605	0.004593
23%	Plain Dent	3.734	9.411E-05
	Shallow Corrosion (40% WT)	3.851	5.883E-05
	Deep Corrosion (60% WT)	3.912	4.573E-05

The probability distribution of the MEPS generated in the pipe is plotted against the strain capacity of the pipe steel material in Fig. 6.20 to show how the statistical distribution affects the PoF. The probability distribution are created by running a Monte Carlo Simulation on the RS obtained from the last iteration in the RSM analysis, then using the generated simulations to obtain the distributions.

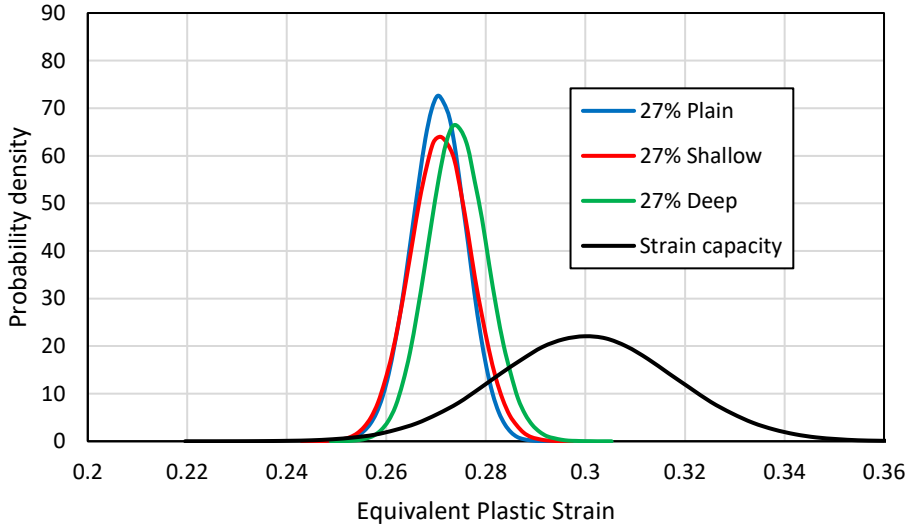

(a) 27% MEPS

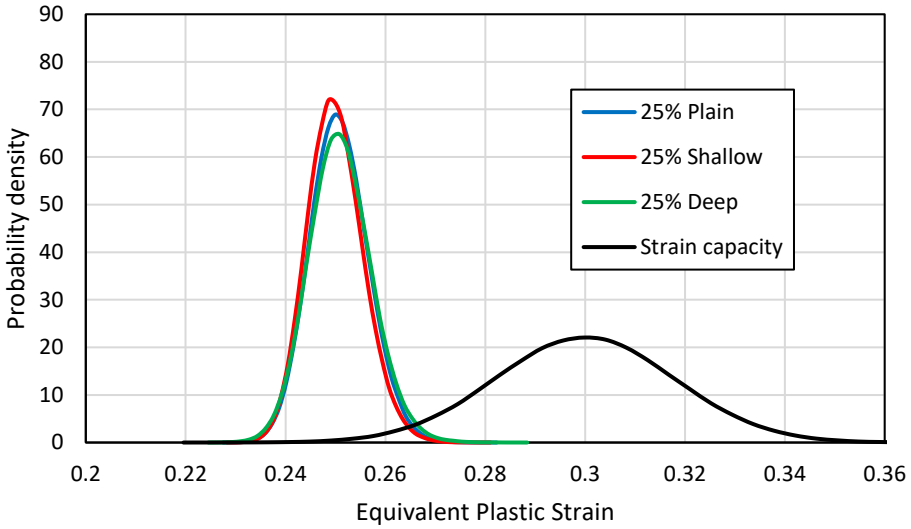

(b) 25% MEPS

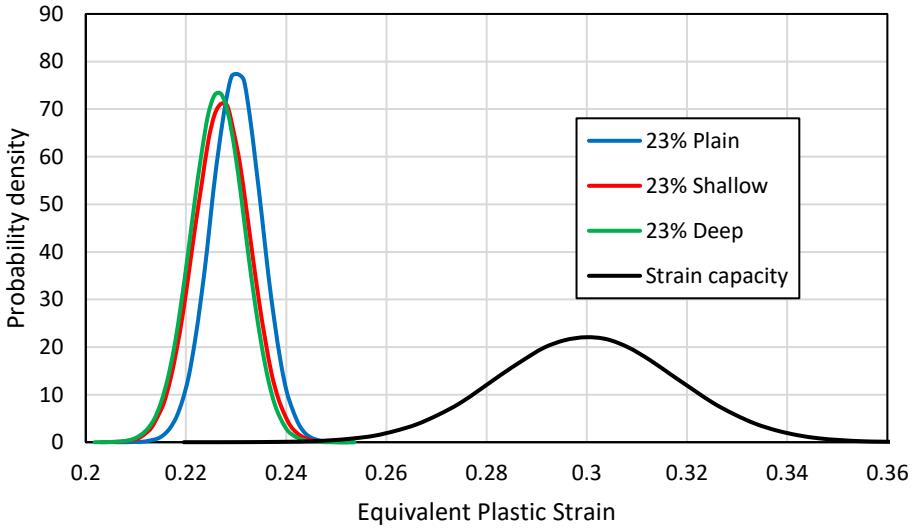

(c) 23% MEPS

Figure 6.20. *Probability distribution of the MEPS demand and the pipe material strain capacity at the different strain levels for the NPS 30 pipe.*

It can be seen from the distributions in Fig. 6.20 that with the increase of the MEPS level due to DD increase, the statistical distributions are shifted to the right increasing the

overlap with the strain capacity distribution and hence increasing the PoF. It can be also noticed that the peak of the probability density curve is slightly increasing with the decrease of DD, which makes the probability density of the higher DD flatter with higher STD. The flatter probability density will also contribute to the increase of the PoF due to the increase of overlap with the SC probability distribution. However, the main reason for the increase of the PoF with the increase of the DD is the increase of the MEPS probability density mean and the shift of the probability density curves to the right. For each strain level, the plain dent, the dent combined with the shallow corrosion, and the dent combined with the deep corrosion statistical distributions for the MEPS are almost matching with some slight differences, which resulted in a very close PoF for the three cases at the three MEPS levels.

The reliability results of the NPS 12 are given in Table 6.6. The effect of the corrosion defect on the PoF is negligible for the shallow corrosion defect, as the difference in the PoF between the plain dent and DCCD is insignificant. However, for all strain levels the PoF changes significantly for the 60% of WT corrosion defects.

Table 6.6. *Reliability results for the NPS 12 pipe.*

MEPS	Defect	Reliability Results	
		Beta	PoF
27%	Plain Dent	1.366	0.085915
	Shallow Corrosion (40% WT)	1.603	0.054521
	Deep Corrosion (60% WT)	0.979	0.163610
25%	Plain Dent	2.462	0.006913
	Shallow Corrosion (40% WT)	2.486	0.006460
	Deep Corrosion (60% WT)	1.651	0.049338
23%	Plain Dent	3.433	0.0002979
	Shallow Corrosion (40% WT)	3.658	0.0001270
	Deep Corrosion (60% WT)	2.485	0.0064759

For the NPS 12, the indenter radius is equal to 32 mm making the highly strained part under the indenter have a diameter approximately equal to the indenter radius. The corrosion circumferential length is chosen to be equal to 40 mm, which does not overlap with the highly strained part. However, the RSTRENG equations are producing a corrosion longitudinal length of 32.2 mm for the 60×WT corrosion depth making the corrosion overlap with the end of the highly strained part and producing plastic strain peaking at the outer radius of the highly strained part as shown in Fig. 6.21. However, for the 0.4×WT corrosion defect, the corrosion longitudinal length produced by the RSTRENG equations is equal to 56.6 mm making the corrosion defect edge not overlapping with the highly strained region.

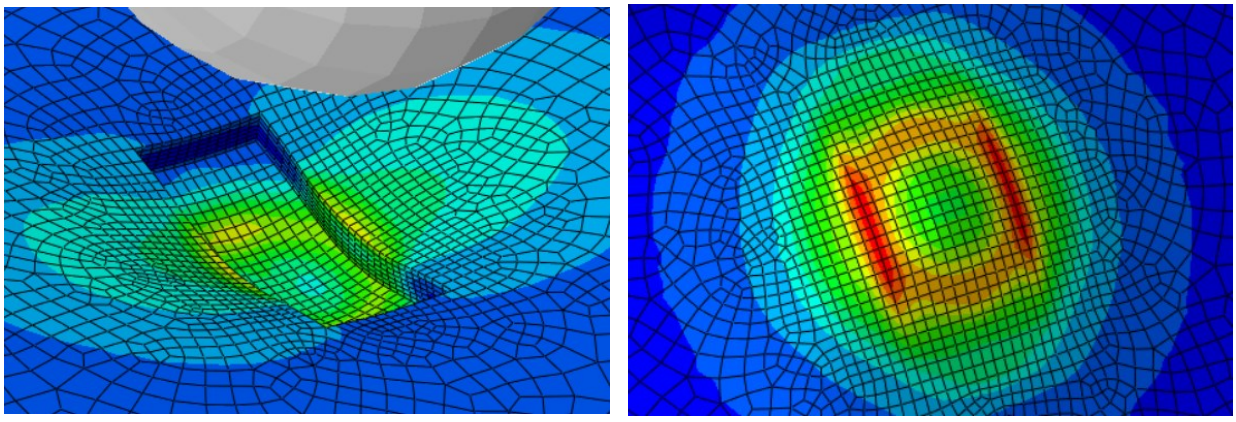

(a) (b)

Figure 6.21. *FE model results of deep corrosion in (a) showing the peaking of strains on the inside diameter surface of the pipe.*

The plastic strain peaking affected the PoF of the 0.6×WT corrosion depth. The statistical distributions of the MEPS generated in the pipe are plotted together with the strain capacity of the pipe material in Fig. 6.22 for the different strain levels to interpret the reliability analysis.

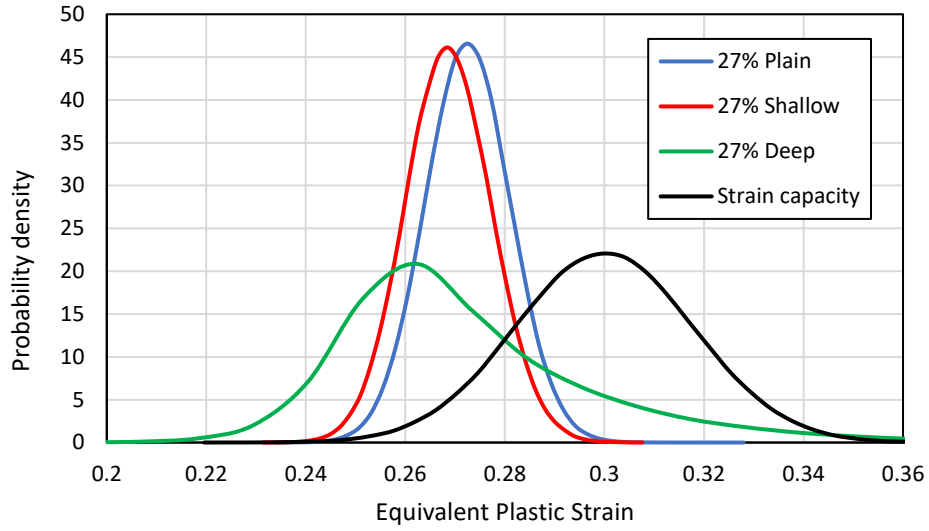

(a) 27% MEPS

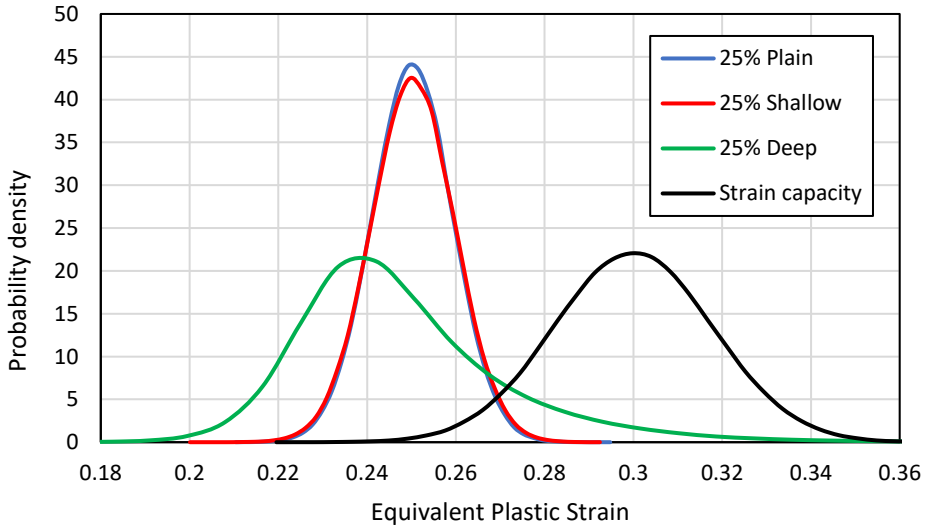

(b) 25% MEPS

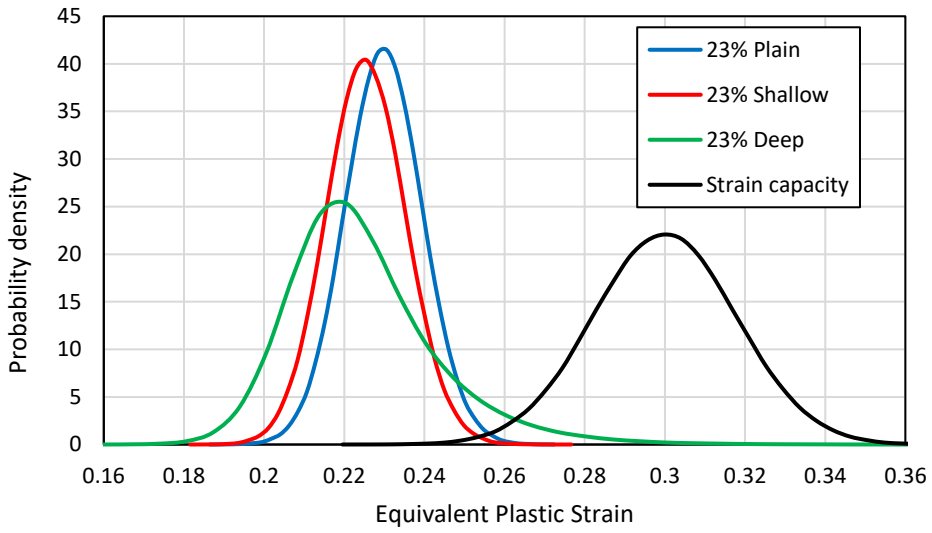

(c) 23% MEPS

Figure 6.22. *Probability distribution of the MEPS demand and the pipe material strain capacity at the different strain levels for the NPS 12 pipe.*

Generally, in Fig. 6.22, with the increase of the MEPS level, the statistical distributions of the MEPS are shifted to the right increasing the overlap with the strain capacity statistical distribution and increasing the PoF. The statistical distribution of the MEPS for the 0.4×WT corrosion defect almost matches the statistical distribution of the plain dent defect making the PoF of both cases close to each other, which was expected due to no overlapping of the corrosion edge with the highly strained region. However, for the 0.6×WT corrosion, the MEPS statistical distribution has a smaller mean and higher standard deviation compared to the other two distributions, increasing the overlap with the strain capacity distribution and, hence, increasing the PoF of this case.

A study by Gossard et *al.* [118] was conducted to determine the effect of the interaction between corrosion and dent defects on the burst pressure of the pipe. In the study, twenty DCCD were identified in the field from inline inspection, then were excavated and the DCCD were laser scanned to extract their profile. A FE model of the pipe having the DCCD profile obtained from the laser scan was created. A C3D4 element in

ABAQUS was used to model the pipe, and the pressure was increased gradually until failure for each of the twenty features. The metal loss depth (expressed as a % of the pipe WT) ranged from 10% to 31% in the tested cases and the dent depth (measured as a percentage of the pipe OD) ranged from 1.2% to less than 7.7%. Despite the difference in the failure assumption between [118] and the work provided in this study, as in [118] the failure is assumed to happen when the von Mises stress in the pipe reaches 80% of the ultimate tensile strength of the pipe material while in this study the failure is assumed to occur when the MEPS reached in the DCCD region reaches the strain capacity of the pipe material, the results in both studies have a common conclusion: The main parameter controlling the burst pressure of the pipe is the DD not the corrosion depth. This conclusion corresponds to the observations presented in this study in Figs. 6.14 and 6.15 showing no effect of corrosion depth on MEPS developed in the dent defect at CD less than 50% of pipe WT for both the 762 mm OD pipe and the 323.85 mm OD pipe. Also, the conclusion corresponds with the results provided in Tables 6.5 and 6.6 in this study showing that at low CD values, for different dent depth, the effect of the corrosion defect on the dent defect is almost negligible, and also showing that the main factor controlling the PoF is the DD.

6.6. Limitations

It has to be mentioned that the POF calculated in this chapter is a conditional one, as some other random variables of the problem are not included in the reliability analysis, such as the pipe outside diameter, the maximum operating pressure of the pipe, and the corrosion circumferential length.

6.7. Conclusion

In this paper, the effect of corrosion on dent defects was investigated using a strain-based reliability analysis. The maximum equivalent plastic strain (MEPS) generated in the defected region was used to represent the severity of the dent combined with corrosion defect (DCCD). A response surface method was used together with the first-order reliability analysis method as the reliability analysis to calculate the probability of

failure (PoF) of the DCCD. A finite element (FE) model was developed and validated to calculate the MEPS generated in the pipe due to the indentation and the pressurization of the pipe. Two different pipes, NPS 30 and NPS 12 with wall thicknesses of 7.14 mm and 6.35 mm respectively, were used for the study. Different dent defects were created on each pipe with two different corrosion metal loss created on each dent defect to investigate the effect of corrosion on the dent defect. The following is concluded:

- Upon investigating the deterministic effect of the corrosion on dent defect, it has been found that for corrosion depths (CDs) up to 50% of the pipe wall thickness combined with dent defects, the corrosion did not have a significant effect on the MEPS generated in the DCCD region. And, for the same pipe with the same indenter size, the MEPS increased with the increase of the dent depth.
- For CDs above 50 to 60% of the pipe wall thickness, for corrosion defects that have edges existing in the area that is most strained from the indentation process, an inwards bulging effect is observed causing the increase of the MEPS at the edges of the corrosion defect leading to a spike in the MEPS of the DCCD.
- The PoF of all the defect cases in the study was calculated. It was found that, generally, that for the same pipe and the same indenter size, the PoF of the DCCD is governed by the indentation depth. The corrosion defects did not have a significant effect on the PoF of the dent defect. However, for the cases of deep corrosion defect (60% of wall thickness) in the NPS 12 pipe at all strain levels, the PoF increased significantly due to strain concentrations occurring in the FE models used to construct the RS due to the inward bulge of the remaining wall thickness in the corrosion defect area.

7. Conclusions, contribution, and recommendations

7.1. Conclusions

This study presented structural reliability assessment, using different reliability methods, on:

1- design factors against yielding provided in the Canadian and US oil and gas pipeline design standards, and the safety factors provided in the US standard for the assessment of corrosion defects on pipelines (ASME B31G-2012).

2- plain dent defects using pipe material strain capacity to determine the main parameters affecting the probability of failure of the dents in pipe, and to verify the limitations provided by the Canadian and US oil and gas standards for accepting dent defects.

3- plain dent defects using the ductile failure damage indicator (DFDI) and the strain limit damage (SLD) ductile strain damage models provided in the assessment and management of pipeline dents standard (API 1183-2020) and ASME boiler and pressure vessels code (ASME BPVC.VIII.3-2021), respectively.

4- dent combined with corrosion defect to determine the effect of the corrosion defect on probability of failure of dent defects.

The key conclusions and findings of this study can be summarized in this subsection.

1- Assessment of the design and safety factors:

Reliability analyses were performed to determine the probability of failure (POF)s associated with the design and safety factors, which are used in the design of intact steel pipes against yielding, and the integrity assessment of corroded steel pipes against burst failure. Different design cases of pipes with various corrosion defects were considered, as representative cases in engineering practice. Two different reliability methods, i.e., the first order reliability method (FORM) and the weighted Monte Carlo (WMC), were used for cross-checking. The POF associated with the design factor of 0.72 for yielding of intact pipes is found to be in a very high safety class with the maximum POF of $5.3*10^{-8}$. The maximum POF associated with the safety factor of

1.25 for corroded steel pipe failure is found to be approximately $2*10^{-9}$ when using the RSTRENG modified area method without considering the model error (uncertainty). However, the model error (uncertainty) ME affects the POF significantly. The comparison between the POFs estimated considering ME shows that there is urgent need to improve the RSTRENG model or develop more accurate failure pressure prediction models. The maximum POF is found to be approximately $3.9*10^{-5}$ and $3.12*10^{-2}$, respectively, for pipes with long and short corrosion defects. This implies that the safety factor of 1.25 makes pipes with long and short corrosion defects fall in a high safety class and a low safety class, respectively. The inconsistence in the reliability levels (or POFs) shows a need to use different safety factors to achieve consistent reliability levels in the design and maintenance of pipelines under different scenarios (e.g., different pipe steel grades, long or short defects).

2. Reliability assessment of plain dents based on pipe material strain capacity:

Strain-based reliability analyses were performed on plain dent defects of pipelines using the response surface method (RSM) and the FORM as the reliability method. Different defected pipe parameters such as the pipe outside diameter (OD), the pipe wall thickness (WT), the pipe length, the indenter size, the dent depth (DD) are considered for the analyses to determine the main factors affecting the POF and the safety of the dented pipelines. It has been found that the nominal value of the maximum equivalent plastic strain can be used as a measure of the severity of the dent defect generated in the defect and it is the primary factor affecting the POF of the defect. Moreover, smaller indenter sizes and pipes with smaller ODs are found to produce higher POFs for the same nominal maximum equivalent plastic strain (MEPS) levels generated in the defects. However, only using the DD/OD percentage to predict the severity of the dent defect does not always lead to consistent POF of the dent defect from the perspective of strain-based reliability analysis.

3. Reliability assessment of plain dents based on ductile damage models:

Strain-based reliability analysis using SLD and the DFDI is conducted on two different pipes with 51 and 106.7 outside diameter to wall thickness ratio subjected to plain dent

defect. A finite element model was developed and verified to calculate the stresses and the strains developed in the pipes from the indentation and pressurization process. For each pipe, two spherical indenters with different indenter radiuses were used to indent the pipe with different indenter depths. A RSM including the FORM analysis was used to perform the reliability analyses. The reliability analysis results were compared to the MEPS-based reliability analysis provided in for the same defect cases provided in this paper. It can be concluded that using the strain damage models for the reliability analysis, the POF increases with the increase of the indentation depth and the that the POF significantly increases with the decrease of the indenter size. The SLD and DFDI strain damage criteria are more sensitive to the change of the indenter size and the increase of the dent depth than the MEPS criterion.

4- Reliability assessment of dent combined with corrosion defects:

The effect of corrosion on dent defects was investigated using a strain-based reliability analysis. The MEPS generated in the defected region was used to represent the severity of the dent combined with corrosion defect (DCCD). An RSM was used together with FORM as the reliability analysis to calculate the POF of the DCCD. A finite element (FE) model was developed and validated to calculate the MEPS generated in the pipe due to the indentation and the pressurization of the pipe. Two different pipes, NPS 30 and NPS 12 with wall thicknesses of 7.14 mm and 6.35 mm respectively, were used for the study. Different dent defects were created on each pipe with two different corrosion metal loss created on each dent defect to investigate the effect of corrosion on the dent defect. The POF of all the defect cases in the study was calculated. It was found that, generally, the corrosion defects did not have a significant effect on the POF of the dent defect. However, for the cases of deep corrosion defect (60% of wall thickness) in the NPS 12 pipe at all strain levels, the POF increased significantly due to strain concentrations occurring in the FE models used to construct the response surface.

7.2. Significance and contribution

This thesis mainly contributed to the improvement of the design and safety factors provided in the oil and gas design and safety standards and for the assessment of plain dents and dents combined with corrosion defects for oil and gas pipeline operators.

1. Chapter 3 shows that the design and safety factors provided in the design and assessment standards need change to achieve reasonable and consistent safety levels. Regarding the safety level of the design of pipe against yielding, the safety level is very high reflecting a non economic design of pipelines; hence, an adjustment to the design factor is recommended. Also, the reliability results provided in chapter 3 show that the safety factors for corroded pipes against failure needs to be a function of the corrosion length to achieve consistent safety levels for all corrosion lengths.

2. The results provided in chapter 4 can be potentially used by the industrial partner "Enbridge pipeline Inc." partially funding this study to assess the dent defects in their pipelines. The conclusion that using only one random variable (the dent depth) is always predicting higher probability of failure, compared to considering the three main random variables, for plain dent defects helped Enbridge to filter the high number of dent defects in their pipelines. Then, they used the detailed analysis including the three random variables to predict the probability of failure of the critical dent defects with higher accuracy, which helped them increase the safety of their pipelines.

3. The damage-based reliability analysis provided the probability of failure associated with using the ductile failure damage indicator (DFDI) that is shown experimentally to efficiently predict the cracking in the plain dent defect. Therefore, the DFDI damage-based approach provide a more reliable type of reliability analysis for the failure of plain dent defect.

4. The deterministic and probabilistic analysis of the dent combined with corrosion defects provided quantitative data on the probability of failure of this type of defect for the first time, which will help assessing this type of defects in the future and provide a limitation and allowable limits for this type of defects in the oil and gas standards.

7.3. Recommendations for future work

The finite element modeling and the reliability analysis presented in this thesis can benefit greatly from further improvements that can ameliorate its results. The following are suggestions for future work to extend the use of the finite element model and reliability analysis results to widen its application domain.

1. Extend the finite element models developed in chapter 4 and chapter 6 to model the burst of pipelines including plain dents and dents combined with corrosion defects. Then, compare and validate the obtained results with the experimental and numerical data provided in the literature about the same problem.

2. Include the maximum allowable operating pressure inside the pipe as a random variable in the reliability problem as the MAOP can fluctuate affecting the stresses and the strains generated in the pipe, which will possibly increase the probability of failure of the defects.

3. Evaluate the safety level of the design factor against the burst of intact pipes given in CSA Z662:19 Annex C and compare it to the safety level against the yielding of intact pipes provided in this thesis.

8. References

[1] Abdelmoety AK, Zheng Q, Li Y, Kainat M, Yoosef-Ghodsi N, Adeeb S. Probability of Failure Associated with Design and Safety Factors for Intact and Corroded Pipes under Internal Pressure. J Pipeline Syst Eng Pract 2021;12. https://doi.org/10.1061/(ASCE)PS.1949-1204.0000544.

[2] Amaya-gómez R, Sánchez-silva M, Bastidas-arteaga E, Schoefs F, Muñoz F. Reliability assessments of corroded pipelines based on internal pressure – A review. Eng Fail Anal 2019;98:190–214. https://doi.org/10.1016/j.engfailanal.2019.01.064.

[3] Bai Y. Chapter 14: Remaining strength of corroded pipes. Elsevier Ocean Engineering Series, vol. 3, 2001, p. 229–55. https://doi.org/10.1016/S1571-9952(01)80028-3.

[4] Chen Y, Zhang H, Zhang J, Li X, Zhou J. Failure analysis of high strength pipeline with single and multiple corrosions. Mater Des 2015;67:552–7. https://doi.org/10.1016/j.matdes.2014.10.088.

[5] Choi JB, Goo BK, Kim JC, Kim YJ, Kim WS. Development of limit load solutions for corroded gas pipelines. International Journal of Pressure Vessels and Piping 2003;80:121–8. https://doi.org/10.1016/S0308-0161(03)00005-X.

[6] Shuai Y, Shuai J, Xu K. Probabilistic analysis of corroded pipelines based on a new failure pressure model. Eng Fail Anal 2017;81:216–33. https://doi.org/10.1016/j.engfailanal.2017.06.050.

[7] Cronin DS, Pick RJ. Prediction of the failure pressure for complex corrosion defects. International Journal of Pressure Vessels and Piping 2002;79:279–87. https://doi.org/10.1016/S0308-0161(02)00020-0.

[8] Zhang YM, Tan TK, Xiao ZM, Zhang WG, Ariffin MZ. Failure assessment on offshore girth welded pipelines due to corrosion defects. Fatigue Fract Eng Mater Struct 2016;39:453–66. https://doi.org/10.1111/ffe.12370.

[9] Qian G, Niffenegger M, Li S. Probabilistic analysis of pipelines with corrosion defects by using FITNET FFS procedure. Corros Sci 2011;53:855–61. https://doi.org/10.1016/j.corsci.2010.10.014.

[10] Cosham A, Hopkins P. The effect of dents in pipelines—guidance in the pipeline defect assessment manual. International Journal of Pressure Vessels and Piping 2004;81:127–39.

[11] Cosham A, Hopkins P. The pipeline defect assessment manual. Proceedings of the International Pipeline Conference, IPC, vol. B, 2002, p. 1565–81. https://doi.org/10.1115/IPC2002-27067.

[12] Alexander CR, Kiefner JF. Effects of Smooth and Rock Dents on Liquid Petroleum Pipelines. Final Report to The American Petroleum Institute 1997:1–13.

[13] National Standards of Canada. Oil and gas pipeline standard, Z662:19. National Standards of Canada 2019.

[14] The American Society of Mechanical Engineers. Pipeline transportation systems for liquids and slurries, ASME B31.4-2019. The American Society of Mechanical Engineers 2019.

[15] The American Society of Mechanical Engineers. Guide for gas transmission and distribution piping systems, ASME B31.8-2018. The American Society of Mechanical Engineers 2018.

[16] Kale A, Ben HT, Sridhar N, Chris JW. A probabilistic model for internal corrosion of gas pipelines. Proceedings of IPC 2004 International Pipeline Conference, 2004, p. 1–9.

[17] The American Society of Mechanical Engineers. Manual for determining the remaining strength of corroded pipelines, ASME B31G-2012. The American Society of Mechanical Engineers 2012.

[18] Maxey, W. A., Kiefner, J. F., Eiber, R. J., Duffy AR. Ductile fracture initiation, propagation and arrest in cylindrical vessels fracture toughness. Proceedings of the 1971 National Symposium on Fracture Mechanics, 1971, p. 70–81.

[19] Hasford WF. Mechanical behavior of materials. Cambridge University Press; 2005.

[20] The American Society of Mechanical Engineers. Manual for determining the remaining strength of corroded pipelines, ASME B31G-1991. The American Society of Mechanical Engineers 1991.

[21] Zhou W, Huang GX. Model error assessments of burst capacity models for corroded pipelines. International Journal of Pressure Vessels and Piping 2012;99–100:1–8. https://doi.org/10.1016/j.ijpvp.2012.06.001.

[22] He Z, Zhou W. Fatigue reliability analysis of dented pipelines. Journal of Pipeline Science and Engineering 2021;1:290–7. https://doi.org/10.1016/j.jpse.2021.08.004.

[23] Garbatov Y, Guedes Soares C. Fatigue reliability of dented pipeline based on limited experimental data. International Journal of Pressure Vessels and Piping 2017;155:15–26. https://doi.org/10.1016/j.ijpvp.2017.07.001.

[24] Cunha SB, Pasqualino IP, Pinheiro BC. Stress-life fatigue assessment of pipelines with plain dents. Fatigue Fract Eng Mater Struct 2009;32:961–74. https://doi.org/10.1111/j.1460-2695.2009.01396.x.

[25] Rosenfeld MJ, Pepper JW, Leewis K. Basis of the new criteria in ASME B31.8 for prioritization and repair of mechanical damage. Proceedings of the International Pipeline Conference, IPC, vol. A, 2002, p. 647–58. https://doi.org/10.1115/IPC2002-27122.

[26] Okoloekwe C, Kainat M, Langer D, Hassanien S, Roger Cheng JJ, Adeeb S. Three-dimensional strain-based model for the severity characterization of dented pipelines. J Nondestruct Eval Diagn Progn Eng Syst 2018;1:1–11. https://doi.org/10.1115/1.4040039.

[27] Zhao J, Cheng YF. A new criterion based on strain determination for dent assessment of pipelines. Journal of Pipeline Science and Engineering 2021:0–38. https://doi.org/10.1016/j.jpse.2021.11.004.

[28] Adeeb SM, Horsley DJ. A numerical procedure to establish a safe working pressure during excavation of a pipeline in a rock ditch. International Journal of Pressure Vessels and Piping 2006;83:488–97. https://doi.org/10.1016/j.ijpvp.2006.03.007.

[29] Tian X, Zhang H. Failure pressure of medium and high strength pipelines with scratched dent defects. Eng Fail Anal 2017;78:29–40. https://doi.org/10.1016/j.engfailanal.2017.03.010.

[30] Tian X, Zhang H. Failure criterion of buried pipelines with dent and scratch defects. Eng Fail Anal 2017;80:278–89. https://doi.org/10.1016/j.engfailanal.2017.06.049.

[31] Allouti M, Schmitt C, Pluvinage G. Assessment of a gouge and dent defect in a pipeline by a combined criterion. Eng Fail Anal 2014;36:1–13. https://doi.org/10.1016/j.engfailanal.2013.10.002.

[32] Okodi A, Li Y, Cheng JJR, Kainat M, Yoosef-Ghodsi N, Adeeb S. Effect of location of crack in dent on burst pressure of pipeline with combined dent and crack defects. Journal of Pipeline Science and Engineering 2021;1:252–63. https://doi.org/10.1016/j.jpse.2021.05.003.

[33] Ghaednia H, Das S, Wang R, Kania R. Safe burst strength of a pipeline with dent-crack defect: Effect of crack depth and operating pressure. Eng Fail Anal 2015;55:288–99. https://doi.org/10.1016/j.engfailanal.2015.06.005.

[34] Ghaednia H, Das S, Wang R, Kania R. Effect of Operating Pressure and Dent Depth on Burst Strength of NPS30 Linepipe With Dent-Crack Defect. Journal of Offshore Mechanics and Arctic Engineering 2015;137:1–8. https://doi.org/10.1115/1.4029895.

[35] American Petroleum Institute. Assessment and management of pipeline dents, API recommended practice 1183. API 2020.

[36] Alashti RA, Jafari S, Hosseinipour SJ. Experimental and numerical investigation of ductile damage effect on load bearing capacity of a dented API XB pipe subjected to internal pressure. Eng Fail Anal 2015;47:208–28. https://doi.org/10.1016/j.engfailanal.2014.10.011.

[37] Ghaednia H, Gerard K, Bhattacharjee S, Das S. Behavior of NPS30 pipe subjected to denting load. Proceedings of the ASME 2014 International Mechanical Engineering Congress and Exposition, 2017, p. 1–9.

[38] Ong LS, Soh AK, Ong JH. Experimental and finite element investigation of a local dent on a pressurized pipe. J Mater Eng Perform 2012;21:161–6. https://doi.org/10.1007/s11665-011-9932-1.

[39] Shuai Y, Shuai J, Zhang X. Experimental and numerical investigation of the strain response of a dented API 5L X52 pipeline subjected to continuously increasing internal pressure. J Nat Gas Sci Eng 2018;56:81–92. https://doi.org/10.1016/j.jngse.2018.05.037.

[40] Pinheiro BDC, Pasqualino IP, Cunha S. Stress concentration factors of dented pipelines. Proceedings of IPC2006 6th International Pipeline Conference, 2016, p. 1–10.

[41] Tiku S, Semiga V, Dinovitzer A, Vignal G. Full scale cyclic fatigue testing of dented pipelines and development of a validated dented pipe finite element model. Proceedings of the Biennial International Pipeline Conference, IPC, vol. 2, 2012, p. 693–702. https://doi.org/10.1115/IPC2012-90427.

[42] Kainat M, Woo J, Langer D, Krausert T, Cheng JJR, Hassanien S, et al. Effects of loading sequences on remaining life of plain dents in buried liquid pipelines. J Pipeline Syst Eng Pract 2019;10:04019001. https://doi.org/10.1061/(asce)ps.1949-1204.0000366.

[43] Woo J, Kainat M, Adeeb S. Development of a profile matching criteria to model dents in Pipelines using finite element analysis. American Society of Mechanical Engineers, Pressure Vessels and Piping Division (Publication) PVP 2017;5:1–10. https://doi.org/10.1115/PVP2017-65278.

[44] Abdulhameed D, Cakiroglu C, Lin M, Cheng R, Nychka J, Sen M, et al. The effect of internal pressure on the tensile strain capacity of X52 pipelines with circumferential flaws. Journal of Pressure Vessel Technology, Transactions of the ASME 2016;138:1–18. https://doi.org/10.1115/1.4033436.

[45] Elyasi N, Shahzamanian M, Lin M, Westover L, Li Y, Kainat M, et al. Prediction of Tensile Strain Capacity for X52 Steel Pipeline Materials Using the Extended Finite Element Method. Applied Mechanics 2021;2:209–25. https://doi.org/10.3390/applmech2020013.

[46] Lin M. Characterization of Tensile and Fracture Properties of X52 Steel Pipes and Their Girth Welds. M.Sc. (2015). University of Alberta, Edmonton, AB, Canada, 2015.

[47] American Petroleum Institute. API Specification 5L. American Petroleum Institute 2018.

[48] Zhao J, Cheng YF. A new criterion based on strain determination for dent assessment of pipelines. Journal of Pipeline Science and Engineering 2022;2:18–28. https://doi.org/10.1016/j.jpse.2021.11.004.

[49] Arumugam U, Gao M, Krishnamurthy R, Wang R, Kania R. Root Cause Analysis of Dent with Crack: A Case Study. 2012.

[50] American Society of Mechanical Engineers. ASME Boiler and Pressure Vessel Code: SECTION VIII Rules for Construction of Pressure Vessels - Division 3. 2021.

[51] Li C, Dang S. Plastic damage analysis of oil and gas pipelines with unconstrained and constrained dents. Eng Fail Anal 2017;77:39–49. https://doi.org/10.1016/j.engfailanal.2017.02.009.

[52] Gao M, Krishnamurthy R, Tandon S, Arumugam U. Critical Strain Based Ductile Damage Criterion and its Application to Mechanical Damage in Pipelines. n.d.

[53] Wu Y, Xiao J, Zhang P. The analysis of damage degree of oil and gas pipeline with type II plain dent. Eng Fail Anal 2016;66:212–22. https://doi.org/10.1016/j.engfailanal.2016.04.004.

[54] Wu Y, Du Z, Li L, Tian Z. A new evaluation method of dented natural gas pipeline based on ductile damage. Applied Ocean Research 2023;135. https://doi.org/10.1016/j.apor.2023.103533.

[55] Wu Y, Li J, Li L. Damage and Springback Analysis of Two Typical Dented Pipelines with Different Parameters. Journal of Pressure Vessel Technology, Transactions of the ASME 2019;141. https://doi.org/10.1115/1.4043590.

[56] Melchers RE, Beck AT. Structural Reliability Analysis and Prediction. New Jersey: John Wiley & Sons; 2018.

[57] Rashki M, Miri M, Azhdary Moghaddam M. A new efficient simulation method to approximate the probability of failure and most probable point. Structural Safety 2012;39:22–9. https://doi.org/10.1016/j.strusafe.2012.06.003.

[58] Hasofer AM, Lind NC. An exact and invariant first order reliability format. J Eng Mech 1974;100:111–21.

[59] Der Kiureghian A, Lin H-Z, Hwang S-J. Second-order reliability approximations. J Eng Mech 1987;113:1208–25.

[60] Myers RH, Montgomery DC, Anderson-Cook CM. Response surface methodology - process and product optimization using designed experiments. New Jersey: John Wiley & Sons; 2016.

[61] Allaix DL, Carbone VI. An improvement of the response surface method. Structural Safety 2011;33:165–72. https://doi.org/10.1016/j.strusafe.2011.02.001.

[62] Rajashekhar MR, Ellingwood BR. A new look at the response surface approach. Structural Safety 1993;12:205–20.

[63] Gayton N, Bourinet JM, Lemaire M. CQ2RS: A new statistical approach to the response surface method for reliability analysis. Structural Safety 2003;25:99–121. https://doi.org/10.1016/S0167-4730(02)00045-0.

[64] Zhao W, Qiu Z. An efficient response surface method and its application to structural reliability and reliability-based optimization. Finite Elements in Analysis and Design 2013;67:34–42. https://doi.org/10.1016/j.finel.2012.12.004.

[65] Wei Y, Bai G, Wang B, Bai B. Reliability analysis on structures based on a modified iterative response surface method. Math Probl Eng 2018. https://doi.org/10.1155/2018/8794160.

[66] Kim SH, Na SW. Response surface method using vector projected sampling points. Structural Safety 1997;19:3–19. https://doi.org/10.1016/S0167-4730(96)00037-9.

[67] Montgomery DC. Design and analysis of experiments. 7th ed. New York: John Wiley and Sons; 2001. https://doi.org/10.1002/9781118147634.

[68] Dimitri V, Bljuger F, Yankelevsky D. Reliability evaluation in nonlinear analysis of reinforced concrete structures. Structural Safety 1997;19:203–17. https://doi.org/10.1016/s0167-4730(96)00025-2.

[69] Morp BY, Ellingwood BR. Reliability-based service-life assessment of aging concrete structures. Journal of Structual Engineering 1993;119:1600–21.

[70] Of S, Of E, Hong TBHP. Assessment of reliability of aging reinforced concrete structures. Journal of Structural Engineering 2000;126:1458–65.

[71] Szerszen MM, Nowak AS, Laman JA. Fatigue reliability of steel bridges. J Constr Steel Res 1999;52:83–92. https://doi.org/10.1016/S0143-974X(99)00015-2.

[72] Zhao Z, Haldar A, Breem FL. Fatigue-reliability evaluation of steel bridges. Journal of Structural Engineering 1994;120:1608–23.

[73] Valor A, Caleyo F, Hallen JM, Velázquez JC. Reliability assessment of buried pipelines based on different corrosion rate models. Corros Sci 2013;66:78–87. https://doi.org/10.1016/j.corsci.2012.09.005.

[74] Keshtegar B, el Amine Ben Seghier M. Modified response surface method basis harmony search to predict the burst pressure of corroded pipelines. Eng Fail Anal 2018;89:177–99. https://doi.org/10.1016/j.engfailanal.2018.02.016.

[75] Hassanien SSA, Adeeb S. Probabilistic-based assessment of Corroded Pipelines: A comparison between closed form and surrogate limit states. Proceedings of IPC 2006 International Pipeline Conference, vol. 3, 2006, p. 999–1004.

[76] Ahammed M. Probabilistic estimation of remaining life of a pipeline in the presence of active corrosion defects. International Journal of Pressure Vessels and Piping 1998;75:321–9. https://doi.org/10.1016/S0308-0161(98)00006-4.

[77] Teixeira AP, Soares CG, Netto TA, Estefen SF. Reliability of pipelines with corrosion defects. International Journal of Pressure Vessels and Piping 2008;85:228–37. https://doi.org/10.1016/j.ijpvp.2007.09.002.

[78] Hassanien S, Kainat M, Adeeb S, Langer D. On the use of surrogate models in reliability-based analysis of dented pipes. Proceedings of the 2016 11th

International Pipeline Conference, IPC, vol. 2, 2016, p. 1–9. https://doi.org/10.1115/IPC2016-64470.

[79] Green KP, Jackson T. Rail is quite safe, but pipelines are the safest way to transport oil and gas. National Post 2015.

[80] PHMSA (United States Department of Transportation). Pipeline failure causes: PHMSA. Https://Www PhmsaDotGov/Incident-Reporting/Accident-Investigation-Division/Pipeline -Failure-Causes 2020.

[81] Breton T, Sanchez-Gheno JC, Alamilla JL, Alvarez-Ramirez J. Identification of failure type in corroded pipelines: A Bayesian probabilistic approach. J Hazard Mater 2010;179:628–34. https://doi.org/10.1016/j.jhazmat.2010.03.049.

[82] Francis A, Espiner RJ, Edwards AM. Guidelines for the use of structural reliability and risk based techniques to justify the operation of onshore pipelines at design factors greater than 0.72. 21 World Gas Conference, 2000.

[83] British Standard Assosiation. Code of practice for pipelines, Part 2: Pipeline on land: Design, Construction & Installation, 1992.

[84] McLamp M, Hopkins P, Marley M, Nessim M. A justification for designing and operating pipelines up to stresses of 80% SMYS. Proceedings of the 2002 4th International Pipeline Conference., 2002, p. 745–57.

[85] Ahammed M, Melchers RE. Reliability estimation of pressurised pipelines subject to localised corrosion defects. International Journal of Pressure Vessels and Piping 1996;69:267–72.

[86] Netto TA, Ferraz US, Estefen SF. The effect of corrosion defects on the burst pressure of pipelines 2005;61:1185–204. https://doi.org/10.1016/j.jcsr.2005.02.010.

[87] Ziha K. Descriptive sampling in structural safety. Structural Safety 1995;17:33–41. https://doi.org/10.1016/0167-4730(94)00038-R.

[88] Olsson A, Sandberg G, Dahlblom O. On Latin hypercube sampling for structural reliability analysis. Structural Safety 2003;25:47–68. https://doi.org/10.1016/S0167-4730(02)00039-5.

[89] Ibrahim Y. Observations on applications of importance sampling in structural reliability analysis. Structural Safety 1991;9:269–81. https://doi.org/10.1016/0167-4730(91)90049-F.

[90] Au SK, Ching J, Beck JL. Application of subset simulation methods to reliability benchmark problems. Structural Safety 2007;29:183–93. https://doi.org/10.1016/j.strusafe.2006.07.008.

[91] Kiefner JF, Vieth PH. A modified criterion for evaluating the remaining strength of corroded pipes. 1989.

[92] The American Society of Mechanical Engineers. Welded and Seamless Wrought Steel Pipe ASME Standard, ASME B36.10M. The American Society of Mechanical Engineers 2018.

[93] Sotberg T, Leira BJ. Reliability-based pipeline design and code calibration. Proceedings of the thirteenth international conference on offshore mechanics and arctic engineering, vol. 5, 1994, p. 351–63.

[94] Zimmerman TJE, Cosham A, Hopkins P, Sanderson N. Can Limit States Design be Used to Design a Pipeline Above 80% SMYS (OMAE98-902). Proceedings of the Seventeenth International Conference on Offshore Mechanics and Arctic Engineering, 1998.

[95] Jiao G, Sotberg T, Bruschi R, Igland R. The SUPERB Project: Linepipe Statistical Properties and Implications in Design of Offshore Pipelines. Proceedings of the Sixteenth International Conference on Offshore Mechanics and Arctic Engineering, 1997, p. 45–56.

[96] Sotberg T, Moan T, Bruschi R, Jiao G, MCrk KJ. The SUPERB Project: Recommended Target Safety Levels for Limit State Based Design of Offshore

Pipelines. Pipeline technology: OMAE 1997; proceedings of the 16th international conference on offshore mechanics and Arctic engineering, vol. 5, 1997, p. 71–8.

[97] Abdelmoety AK, Zheng Q, Li Y, Kainat M, Yoosef-Ghodsi N, Adeeb S. Probability of Failure Associated with Design and Safety Factors for Intact and Corroded Pipes under Internal Pressure. J Pipeline Syst Eng Pract 2021;12:04021010. https://doi.org/10.1061/(asce)ps.1949-1204.0000544.

[98] Borri A, Speranzini E. Structural reliability analysis using a standard deterministic finite element code. Structural Safety 1997;19:361–82. https://doi.org/10.1016/S0167-4730(97)00017-9.

[99] Smith M. ABAQUS/Standard User's Manual, Version 2017. 2017. https://doi.org/https://www.3ds.com/products-services/simulia/products/abaqus.

[100] Okodi A, Li Y, Cheng R, Kainat M, Yoosef-ghodsi N. applied sciences Crack Propagation and Burst Pressure of Pipeline with Restrained and Unrestrained Concentric Dent-Crack Defects Using Extended Finite Element Method. Applied Sciences 2020;10:7554. https://doi.org/10.3390/app10217554.

[101] Abdelmoety AK, Kainat M, Yoosef-Ghodsi N, Li Y, Adeeb S. Strain-based reliability analysis of dented pipelines using a response surface method. Journal of Pipeline Science and Engineering 2022;2:29–38. https://doi.org/10.1016/j.jpse.2021.11.002.

[102] Wu Y, Du Z, Li L, Tian Z. A new evaluation method of dented natural gas pipeline based on ductile damage. Applied Ocean Research 2023;135. https://doi.org/10.1016/j.apor.2023.103533.

[103] Mcclintock FA. A Criterion for Ductile Fracture by the Growth of Holes. 1968.

[104] Rice JR, Tracey DA. ON THE DUCTILE ENLARGEMENT OF VOIDS IN TRIAXIAL STRESS FIET,DS*. vol. 17. Pergamon Press; 1969.

[105] Oyani M. Criteria of Ductile Fracture Strain. Bulletin of JSME 1972;15:1507–13. https://doi.org/https://doi.org/10.1299/jsme1958.15.1507.

[106] Hancock JW, Mackenzie AC. ON THE MECHANISMS OF DUCTILE FAILURE IN HIGH-STRENGTH STEELS SUBJECTED TO MULTI-AXIAL STRESS-STATES. vol. 24. Pergamon Press; 1976.

[107] Arumugam U, Gao M, Krishnamurthy R, Wang R, Kania R. Study of a Plastic Strain Limit Damage Criterion for Pipeline Mechanical Damage Using FEA and Full-Scale Denting Tests. n.d.

[108] Fischer ED, Kolednik O, Shan GX, Rammerstorfer EG. A note on calibration of ductile failure damage indicators*. vol. 73. 1995.

[109] Bao Y, Wierzbicki T. On the cut-off value of negative triaxiality for fracture. Eng Fract Mech 2005;72:1049–69. https://doi.org/10.1016/j.engfracmech.2004.07.011.

[110] Brünig M, Gerke S, Schmidt M. Damage and failure at negative stress triaxialities: Experiments, modeling and numerical simulations. Int J Plast 2018;102:70–82. https://doi.org/10.1016/j.ijplas.2017.12.003.

[111] Khan AS, Liu H. A new approach for ductile fracture prediction on Al 2024-T351 alloy. Int J Plast 2012;35:1–12. https://doi.org/10.1016/j.ijplas.2012.01.003.

[112] Kao AS, Spitzig WA, Richmond O, Kuhn HA. Tensile fracture and fractographic analysis of 1045 spheroidized steel under hydrostatic pressure. J Mater Res 1990;5:83–91. https://doi.org/10.1557/JMR.1990.0089.

[113] Li C, Dang S. Plastic damage analysis of oil and gas pipelines with unconstrained and constrained dents. Eng Fail Anal 2017;77:39–49. https://doi.org/10.1016/j.engfailanal.2017.02.009.

[114] Wu Y, Li J, Li L. Damage and Springback Analysis of Two Typical Dented Pipelines with Different Parameters. Journal of Pressure Vessel Technology, Transactions of the ASME 2019;141. https://doi.org/10.1115/1.4043590.

[115] Zhao J, Cheng YF. A new criterion based on strain determination for dent assessment of pipelines. Journal of Pipeline Science and Engineering 2021:0–38. https://doi.org/10.1016/j.jpse.2021.11.004.

[116] Huang Y, Qin G, Hu G. Failure pressure prediction by defect assessment and finite element modelling on pipelines containing a dent-corrosion defect. Ocean Engineering 2022;266. https://doi.org/10.1016/j.oceaneng.2022.112875.

[117] Sun J, Cheng ; Y Frank, Woo J, Muntaseer Kainat ;, Hassanien S. Assessment of Interaction Between a Dent and an Adjacent Corrosion Feature on Pipelines and the Effect on Pipeline Failure Pressure by Finite-Element Modeling 2021. https://doi.org/10.1061/(ASCE)PS.1949.

[118] Gossard J, Bratton J, Kemp D, Finneran S, Polasik SJ. Evaluating Dents with Metal Loss Using Finite Element Analysis, 2016.

[119] Zhao J, Cheng YF. Assessment by finite element modeling of corrosion in dent on X52 steel pipelines. International Journal of Pressure Vessels and Piping 2022;200. https://doi.org/10.1016/j.ijpvp.2022.104835.

[120] Zhao J, Lv Y, Cheng YF. A new method for assessment of burst pressure capacity of corroded X80 steel pipelines containing a dent. International Journal of Pressure Vessels and Piping 2022;199. https://doi.org/10.1016/j.ijpvp.2022.104742.

[121] Ramberg W, Osgood WR. Description of Stress-Strain Curves by Three Parameters 1943.